Environmental signal propagation, preservation and shredding in sedimentary systems

Thesis submitted in accordance with the requirements of the University of Liverpool for the degree of Doctor of Philosophy by

Stephan Christiaan Toby

October 2019

'The sediments are a sort of epic poem of the earth.

When we are wise enough, perhaps we can read in them all of past history.'

Rachel Carson, 'The Sea Around Us' (1951)

For my parents and sister.

Contents

List of tables

List of figures

Thesis abstract

Sediment flux is an important control on the morphology of sedimentary landscapes and stratigraphy as it sets the rates and scales of landscape dynamics. For example, sediment flux influences the shape and style of river channels, the avulsion frequency of rivers, and the position of shorelines. Over long timescales, the sediment flux through sediment routing systems relates to environmental forcing conditions such as climate and tectonics, which set rates of catchment erosion and sediment transport. This makes stratigraphy accumulating in sedimentary basins record a potential archive of past climatic and tectonic conditions that could inform our understanding of current and future environmental change. However, we may not always be able to identify environmental signals in the stratigraphic record because of stochastic processes in sedimentary systems (autogenics) that have the potential to obscure the transfer of environmental signals (allogenics) to landscapes and stratigraphy. Previous work demonstrates that autogenic landscape processes act as a low-pass filter on the transfer of environmental signals to the stratigraphic record, but signal amplitude must play a role too. A quantitative understanding of the conditions required to archive environmental signals is essential to underpin interpretations of these signals in the stratigraphic record.

The aim of this thesis is to develop a quantitative theoretical basis that can be used to assess the stratigraphic record as an archive for allogenic signals of varying sediment flux. First, I present a new theoretical framework that predicts a time-dependent magnitude threshold for the transfer of allogenic sediment supply signals to the stratigraphic record. The minimum signal amplitude is set by autogenic processes and decreases as an exponential function of signal duration. This new framework is supported by physical delta experiments specifically designed to test the framework. The threshold was constructed using an experiment forced with constant sediment supply rate and tested with four new experiments with similar forcing conditions, but cyclic sediment flux. Signals with a combination of cycle magnitude and duration that exceed the threshold are transferred to the stratigraphic record, while signals that fall below the threshold are not.

The threshold framework relies on high-resolution measurements of autogenic sediment fluxes, which are usually not available in stratigraphic studies. However, the exponential decay of the threshold can be approximated from long-term accumulation rates and an estimate of timescales at which autogenic processes level out. This approximation is applied to field-scale examples of the Pleistocene Kerinitis delta (Greece) and the Eocene Escanilla sediment routing system (Spain) to test whether Milankovitch-scale sediment supply cycles could realistically have been preserved in the stratigraphic record of these systems.

The delta experiments were also used to study how sediment supply cycles of different magnitudes and durations influence delta morphodynamics. The stochastic variability of autogenic processes obscures most theoretical relationships between sediment flux and morphodynamic processes. However, the experiments demonstrate that signals with a high rate of sediment supply change (acceleration) are likely to push existing morphology out of equilibrium, and thereby generate cyclicity in landscape evolution. Slowly accelerating signals increase channel depth, but do not affect floodplain morphology or the number of co-existing channels, like quickly accelerating channels do. Quickly accelerating high-frequency signals, however, may not leave thick enough deposits to withstand erosion prior to permanent burial, and so their preservation potential is limited.

The results of this thesis: (1) provide a theoretical framework that predicts the scales of sediment flux signals we may expect to find in the stratigraphic record; (2) detail how the threshold framework can be applied to the rock record, using datasets of limited temporal resolution; and (3) inform earth scientists of landscape response to sediment supply signals with different combinations of signal magnitude, duration and acceleration. As such, this work contributes to a more quantitative understanding of the effects of environmental signals on landscapes and the stratigraphic record.

Acknowledgements

First of all, I owe many thanks to Rob Duller, Silvio De Angelis and Kyle Straub. It has been a great experience having you as my supervisors and I have learned a lot from a team with such diverse expertise and approaches. I enjoyed Rob's never-ending enthusiasm in firing wild ideas at me, ranging from writing 18 *Nature*-papers in one PhD to climbing 18 mountains in one day. I had a great time working in Kyle's lab in New Orleans and particularly enjoyed our in-depth science talks, breaking and fixing the delta basin over and over again (on hindsight), and the team-spirit of the group. It is eye-opening seeing the experiments evolve, and it makes a very relaxing work environment hearing water flow in the lab while watching the experiments. Thanks, Silvio, for your guidance on more technical issues, and also for all our philosophical discussions about academia and life. I would also like to thank Jaco Baas and Chris Stevenson for interesting discussions during my examination and constructive comments on an earlier version of this thesis.

Thanks to my former supervisors John and Giovanni for triggering my interest in science and helping me in the search for a PhD position. To Rhodri Jerrett for joining Rob and me in the field. Your enthusiasm near interesting outcrops is only matched by Rob's general excitement after two doses of caffeine. Although the field data are not included in this thesis, there is no doubt my work benefited from our discussions in the field. I also thank Allard Martinius for his contributions to my fieldwork in Spain and our excursion to Roda. My 4th year project-student Adam was great company in the field and I thank him for all the hard work he put into his thesis. Also thanks to Isabella Masiero, Peter Burgess and Rob for our collaboration on the 'Big fan of signals' paper, and to Angel Bueno for his help with image analysis.

I am grateful to the sponsors of my PhD. Tuition fees and research expenses were paid for by the Natural Environment Research Council (NERC) through the Earth, Atmosphere and Oceans (EAO) Doctoral Training Partnership (DTP) between the University of Liverpool and the University of Manchester. I thank Julie Samson, the DTP administrator, in particular for all her efforts in making this DTP programme a great experience. I thank the University of Liverpool for funding my stipend. Experiments conducted for this thesis were funded through an NSF grant awarded to Kyle Straub.

The NERC DTP also funded my 3-month internship at Deltares in Delft. I thank Helena van der Vegt for our collaboration and a great summer in Delft, and Dirk-Jan Walstra and his unit at Deltares for hosting me and providing access to their facilities. I am grateful to Joep Storms, Hemmo Abels, Allard Martinius and their PhDs and postdocs for including

me in their group at the TU during my stay in Delft. I am also grateful to Nicoletta Leonardi for introducing me to Delft3D in Liverpool.

My PhD wouldn't be the same without my friends and officemates in the 'seismology research group'-office in Liverpool. My research might not quite fit that description, but it felt like I fit in right from the very first day. I found great friends in Sergio, James and Minxuan, and Pete and Isabella from the office next door. The office hasn't been the same after you all started leaving. Thanks for your short-courses in geophysics, coding and cooking. Also thanks to my newer office mates, for fun discussions and sharing some of your seismology knowledge. I enjoyed the friendly atmosphere among my colleagues in Liverpool and I would like to thank all my friends here for making these years in Liverpool such a nice experience. I fear forgetting anyone in an effort of naming you all (sorry Yael).

I thank everyone in the department at Tulane for being so welcoming. I was lucky to spend most of my first year with you and I look back on it as a great time, both because of the research environment and because of my friends in the department. In particular, I would like to thank my lab buddies Tushar, Ripul, Qi, Chris, Meg and Bobola for all their help with the experiments and sharing data of previous experiments. I could not have run the experiments without your support. I also thank Iain for the hard work he put into his undergraduate thesis on some of the experimental data, and Jim, the SEAD administrator, for swiftly solving all the problems I ran into while uploading datasets to the server.

I would like to thank my parents, my sister, and my friends at home for their support. It always puts a smile on my face to see you when I visit home and it is even better to see yours when we meet or call. I very much appreciate the times my parents, Sandra, Luuk, Sander, Hans, Marco, Vince, Tamara, Frans and Flavio came to visit Liverpool. Finally, thank you Cris for all your support while I have been working on this thesis, and for ridiculing my excitement when I see nice rocks on just about any of our trips.

1. Introduction

1.1. Motivation

Understanding the processes that give rise to clastic sedimentary rocks and strata has been a core discipline of geology for decades (Ager, 1973; Vail et al., 1977; Miall, 2015). Not only do sedimentary rocks host valuable natural resources such as water and hydrocarbons (Flint and Bryant, 1993; Van Dijk et al., 2016), but they house unique information related to past surface conditions on Earth and other planetary bodies (Allen, 2008a; Duller et al., 2015). Clastic strata form as a result of sediment accumulation in the landscape over shorter timescales, followed by progressive burial, compaction and lithification over longer timescales (Schumer and Jerolmack, 2009; Lai et al., 2018). The detrital sediment grains that constitute clastic sedimentary rocks originate from mountain catchments where weathering breaks down exposed rocks into loose material (West et al., 2005; von Eynatten and Dunkl, 2012). Once mobilised by gravity, water, wind or ice, these grains start a journey that could take them through hillslopes, rivers and seas until permanently deposited (e.g. Allen (2017); Garzanti et al. (2019)).

Stratigraphy may be a physical record of Earth surface conditions because the transport and deposition of sediment depend on climatic and tectonic conditions (e.g. review by Romans et al. (2016)). The spatial and temporal extend of the stratigraphic record is unmatched, given that approximately 75% of the Earth's surface is currently covered by sedimentary rocks (Wilkinson et al., 2009) and the oldest dated (metamorphosed) sedimentary rock is around 3.85 billion years old (Nutman et al., 1997). In perspective, other records such as ice cores, hold proxy records of Earth surface conditions up to about 2.7 million years old (Kehrl et al., 2018). This makes the stratigraphic record a unique long-term archive of information that could inform predictions of future environmental change.

It is well known that the architecture of stratigraphic successions is shaped by long-term climatic and tectonic forcing conditions (Castelltort et al., 2015), because they set both the volume of sediment delivered to landscapes and oceans (sedimentary basins), and the generation of space to accommodate that sediment (Jervey, 1988; Posamentier and Allen, 1993; Schlager, 1993). Tectonics control the volume and rate of sediment supply, and the calibre of grain size exported from mountain catchments (Whipple and Tucker, 2002; Bonnet and Crave, 2003; Whittaker et al., 2011). Catchment erosion rates, and so sediment flux to adjacent basins are also strongly dependant on rates of precipitation and temperature, and parent lithology (Syvitski and Milliman, 2007). The generation of accommodation, necessary

for sedimentary rocks to accumulate, ultimately comes down to base level, which is usually set by relative sea level (RSL). RSL is set by the combined effect of tectonic subsidence and climatically driven eustatic sea level oscillations (Posamentier et al., 1999).

Given that the balance between the rate of sediment supply and the rate of accommodation generation shapes large-scale stratigraphic architecture, numerous studies have attempted to reconstruct past surface conditions on Earth (Lopez-Blanco et al., 2000; Duller et al., 2012; Brooke et al., 2018) and other planetary bodies (Milliken et al., 2010; Anderson et al., 2019) from the stratigraphic record. However, the reconstruction of past environmental forcing (climatic and tectonic) from the stratigraphic record is complicated. Sediment transport and deposition buffer sediment flux signals of environmental forcing travelling through a sediment routing system (Paola et al., 1992; Castelltort and Van den Driessche, 2003; Allen, 2008b) (Figure 1.1), and landscapes are dynamic even in the absence of changing environmental forcing (Muto et al., 2016; Paola, 2016). For example, rivers move across the alluvial plain through a combination of lateral migration and by rapid wholescale relocations known as avulsions (Hudson and Kesel, 2000; Slingerland and Smith, 2004; Lauer and Parker, 2008). As the internal dynamics of landscapes (autogenic processes) constantly change the sediment transport configuration in the landscape, they also shape the stratigraphic record (Burgess et al., 2019). Although the emphasis of many stratigraphic studies is on reconstructing environmental signals, they may be indistinguishable from strata generated by autogenic processes. This is because timescales and magnitudes at which autogenic processes change the landscape overlap with changes expected from environmental signals (Muto et al., 2007; Hajek et al., 2012; Hajek and Straub, 2017; Trower et al., 2018). In fact, stochastic autogenic variations in landscape dynamics may completely destroy external signals, inhibiting signal transfer and preservation in the stratigraphic record (Peper and Cloetingh, 1995; Jerolmack and Paola, 2010; Van De Wiel and Coulthard, 2010). Understanding how and under what conditions environmental signals are transferred to the stratigraphic record is thus essential for accurately reconstructing past environmental signals and predicting future landscape dynamics.

In this thesis, I develop a quantitative theoretical basis that can be used to assess the stratigraphic record as an archive for signals of varying sediment flux, with a particular focus on channelized river and fan systems. In the remaining parts of this Chapter 1 I provide a brief overview of internal (autogenic) and external (allogenic) controls on landscape dynamics, and on our current understanding on the transfer of allogenic signals to the stratigraphic record. In Chapter 2, I present methods used to produce physical experiments of river deltas. These experiments support a new theoretical framework, presented in Chapter 3, that predicts the threshold condition necessary for sediment supply signals to be transferred

into the stratigraphic record. Chapter 4 builds on the theoretical framework and describes a workflow that enables its application to field-scale systems. Chapter 5 contains an in-depth analysis of morphodynamic processes in physical delta experiments that shows whether certain landscape characteristics may be used to identify sediment supply signals in the stratigraphic record. In Chapter 6 I combine the main points of each chapter in a discussion on the implications of my work on our ability to reconstruct sediment supply signals from the stratigraphic record.

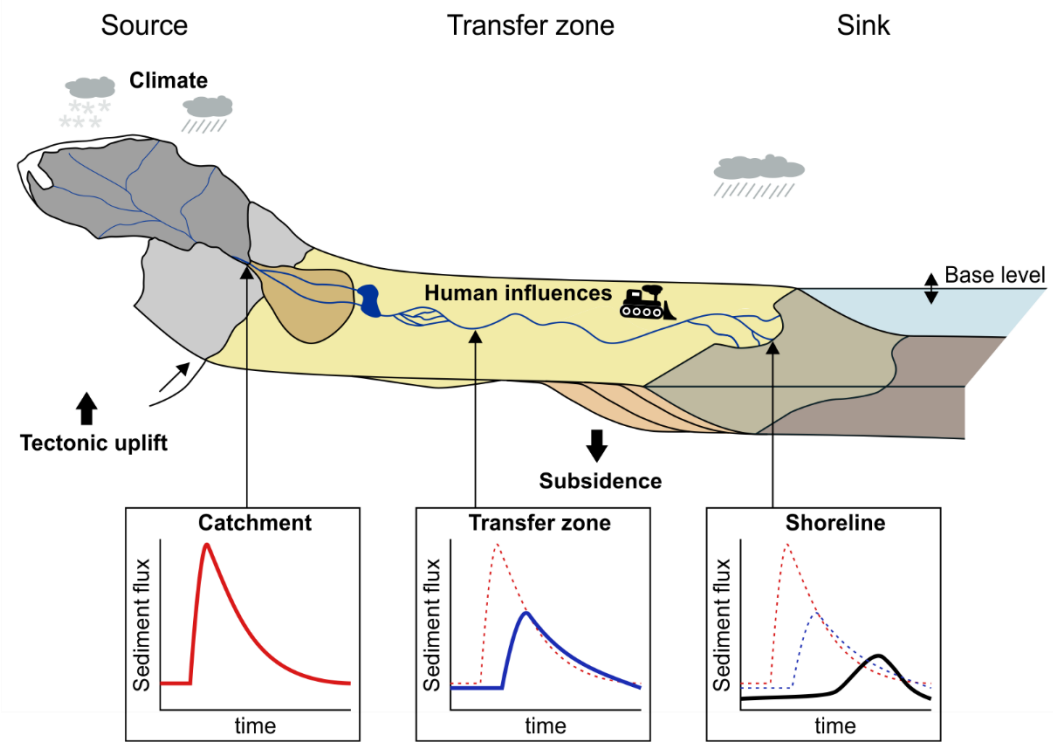

Figure 1.1. Source-to-sink sediment flux.

Schematic source-to-sink sedimentary system, where sediment is generated in an eroding catchment ('source') and transported through the landscape ('transfer zone') to a sea or ocean ('sink'). The sediment flux through the system depends on allogenic forcings such as climate, tectonics and human influences. The graphs below show a hypothetical sediment flux at three locations: when leaving the catchment, in the transfer zone, and at the sink. Sediment transport and deposition modifies and attenuates the signal. After Romans et al. (2016).

1.2. Origin of catchment-derived sediment supply signals

The etymological roots of the word allogenic come from ancient Greek and refer to things having an external source. In sedimentology it is commonly used for everything that originates externally to the environment of interest. Within the scope of this thesis, allogenic

forcing refers to all influences on landscape dynamics that originate externally to the environment of interest. These may produce signals that are also referred to as environmental signals given that they are generally a consequence of changing tectonic or climatic conditions (Romans et al., 2016). This thesis focuses on allogenic signals of temporally varying sediment supply rate over timescales up to 10^5 years. Although human-induced interventions in landscape development could be classified as an allogenic signal, the focus of this thesis is thus on much longer timescales.

Siliciclastic sediment is the erosional product of catchments and so the delivery of sediment depends on surface topography. The height of mountain ranges is given by the balance between rates of tectonic uplift and erosion. Over long timescales, tectonic uplift sets the sediment flux out of mountain catchments because it supplies the rock mass to be denuded (Bonnet and Crave, 2003; Schlunegger and Kissling, 2015). Numerical models of catchment erosion relate erosion rates to surface slope and water discharge, and consequently predict sediment supply signals in response to variations in precipitation (climate) and tectonic uplift (Humphrey and Heller, 1995; Allen and Densmore, 2000; Braun et al., 2015; Armitage et al., 2018). However, these models show that the response of catchments to varying uplift rates is buffered, which particularly inhibits the transfer of high-frequency tectonic signals as signals of varying sediment flux to basins (Whipple and Tucker, 1999; Li et al., 2018). This is due to a non-linear response of erosion rates to tectonic uplift. In addition, sediment can be temporally stored within a catchment, which delays and dampens signals of changing uplift rate (Lu et al., 2005). Catchments thus act as a low-pass filter on tectonic signals.

To some degree, signal buffering also applies to climatic signals. However, sediment supply signals of climatic origin are different from tectonic signals. Climatic signals are usually modelled as changes in precipitation rate, which tend to show faster responses than tectonic signals (Allen and Densmore, 2000), although the response timescale depends on the direction in which the forcing is changing (Tucker and Slingerland, 1997). Increasing precipitation rapidly leads to an increase in sediment flux, but after an initial peak this flux may drop when sediment reserves in the catchment are depleted. Decreasing precipitation rate on the other hand causes a gradual decrease in erosion rates, and thus in sediment flux. Given the sensitivity of catchments to climate signals in particular, these may well lead to high-frequency (Milankovitch-scale) sediment supply signals to basins (Tucker and Slingerland, 1997; Castelltort and Van den Driessche, 2003; Braun et al., 2015). Another source of cyclic sediment flux signals leaving a catchment may result from a resonance of catchments to a perturbation, caused by aggradation-incision feedback cycles between a catchment and adjacent fan (Humphrey and Heller, 1995).

Although environmental forcing may generate sediment flux signals from catchments to sedimentary basins, the reconstruction of sediment fluxes from basin stratigraphy is difficult (Allen et al., 2013b; Tipper, 2016). One reason for this is that measurements of vertical aggradation rate decrease with a power-law function of the time window measured over, known as the Sadler-effect (Sadler, 1981; Paola et al., 2018). This is because local sedimentation rates vary (Schumer et al., 2011) and are interrupted by phases of no deposition or erosion (Sadler and Strauss, 1990a; Schumer and Jerolmack, 2009; Tipper, 2015). At the scale of a depositional system, local variations average out over long timescales (Jerolmack and Sadler, 2007), so with sufficient spatial coverage, long-term mean deposition rates can be estimated. Another indicator for supply signals is a change in sediment properties (Marr et al., 2000; Fedele and Paola, 2007; Armitage et al., 2011). Landscape dynamics drastically change by differences in sediment properties such as cohesion (Edmonds and Slingerland, 2010; Straub et al., 2015) and grain size (Caldwell and Edmonds, 2014; Burpee et al., 2015), and so the type of supplied sediment, in addition to the supply rate, is an important control on stratigraphic architecture.

The empirical BQART equation (Syvitski and Milliman, 2007) may serve as an alternative to sediment fluxes estimated directly from the stratigraphic record. This equation provides an estimate of suspended sediment flux to river mouths based on a multiregression analysis of present rivers using input parameters of water discharge, catchment area, maximum relief and temperature, and parameters such as lithology or human influences. Estimates of ancient sediment fluxes using BQART seem to correspond well with other independent methods in the field and suggest roughly 30% change in sediment supply between glacial-interglacial cycles (Hidy et al., 2014; Watkins et al., 2018), even though this approach lacks a fundamental theoretical relation between forcing conditions and sediment flux.

1.3. Base level signals

In addition to allogenic signals of varying sediment supply, which often coincide with changes in water discharge, allogenic forcing also sets the rate of accommodation generation. In fact, base level variations have been attributed as the major control on large-scale stratigraphic architecture. There is overwhelming evidence in the geological record of relative sea level variations. This has led to the sequence stratigraphic framework, which relates large scale stratigraphic architecture to RSL oscillations (Vail et al., 1977; Van Wagoner et al., 1988; Catuneanu et al., 2009). The amplitude of eustatic sea level cycles ranges up to approximately

200 m (Miller et al., 2005) and fluctuates at timescales that overlap timescales of autogenic processes. For example, the most recent glacial – interglacial cycles can be correlated to orbital forcing on a 100 ky timescale, while Early to Middle Pleistocene sea level oscillations seem to correlate to 41 ky scale cycles (Clark et al., 2006). Tectonic processes may contribute to RSL signals. For example, basin-wide subsidence rates vary over longer timescales by regional tectonic processes such as fault linkage (Gupta et al., 1998) or glacial rebound (Lambeck and Chappell, 2001). For the scope of this thesis, I isolate the problem of allogenic sediment flux signals by assuming constant RSL rise to generate accommodation.

1.4. Autogenic processes

Sediment transport depends on the threshold for sediment motion. This threshold relates to sediment properties (grain size, density, cohesion), which vary spatially in landscapes. The flow velocity of water, or other media, also varies spatially because of topographic gradients or turbulence (Jerolmack, 2011). As a consequence, sediment transport is not spatially uniform. Topography, and thus morphology, is constantly reorganised by local sediment transport and deposition. These morphodynamic processes that occur as a consequence of crossing sediment transport thresholds and distributing energy within a sediment transport system are referred to as autogenic (Beerbower, 1964; Ventra and Nichols, 2014). Autogenic processes include large-scale dynamics such as lateral river channel migration and avulsion, and drive the formation of bedforms, channels, bars and crevasses. These autogenic changes in the landscape occur even under constant allogenic forcing conditions (Paola, 2016; Burgess et al., 2019) and create a full spectrum of autogenic frequencies in landscape evolution (Jerolmack and Paola, 2010; Postma, 2014). As such, autogenic processes play an important role in modifying the landscape and stratigraphic architecture, and in the buffering and modification of allogenic signals.

Landscape dynamics are always a consequence of both allogenic forcing and autogenic processes, and thus the two cannot be seen independently from each other. This is because allogenic forcing influences water discharge, topographic gradients, and the type of sediment available in a landscape. An allogenic change in supplied sediment properties, such as grain size and cohesion, strongly influences system behaviour and morphology (Edmonds and Slingerland, 2010; Caldwell and Edmonds, 2014; Li et al., 2017). Avulsion frequency increases with increasing rates of accommodation production, because accommodation production drives slope changes and enables superelevation of channels (Tornqvist, 1994; Martin et al., 2009b; Wickert et al., 2013). The lateral migration rate of channels (Wickert et

al., 2013) and avulsion frequencies (Bryant et al., 1995; Ashworth et al., 2004; Reitz et al., 2010) both show a positive correlation with sediment supply rate, because morphodynamic processes occur faster when there is more sediment in flux. The transport slope of sedimentary systems is a function of water discharge and sediment supply, where higher sediment concentrations produce steeper slopes (Parker et al., 1998; Whipple et al., 1998; Guerit et al., 2014). The feedback between transport thresholds and water discharge causes river channel geometry to reorganise to changing water discharge (Nicholas et al., 2016; Phillips and Jerolmack, 2016). Understanding the link between autogenic processes and allogenic forcing is important, because it is the rates and scales of autogenic processes, set by allogenic forcing conditions that determine landscape morphology and the architecture of the stratigraphic record, and therefore also the transfer of environmental signals to stratigraphy.

Although autogenics often have no set periodicity (Paola, 2016), several studies show that stratigraphy formed under constant allogenic forcing conditions can show cyclicity. For example, experimental studies (Kim and Jerolmack, 2008; van Dijk et al., 2008, 2009; Clarke et al., 2010) demonstrated how autogenically driven alternations between sheet flow and channel incision can cause cyclic stratigraphy. Kim and Paola (2007) showed that constant slip along a normal fault can create autogenic cycles of lake development and disappearance. Autogenic processes such as avulsion may cause periodic trends in stratigraphy, as observed in experimental studies (Kim and Jerolmack, 2008) and interpreted from field data (Stouthamer and Berendsen, 2007). Without prior knowledge on allogenic forcing conditions, cyclic stratigraphic architecture created by autogenic processes may easily be mistaken for periodic allogenic forcing.

Autogenic processes thus generate significant 'noise' in stratigraphy even in the absence of variable allogenic forcing (Karamitopoulos et al., 2014; Hajek and Straub, 2017). The distinction between stratigraphy formed by allogenic forcing and autogenic processes is still a major challenge. Although autogenics are often assumed to produce small-scale, non-correlatable stratigraphic architecture (Einsele, 2000; Ventra and Nichols, 2014), autogenic stratigraphic architecture could resemble periodic allogenic forcing (Kim and Jerolmack, 2008; Hajek et al., 2012; Hampson, 2016). Autogenic processes may also obscure allogenic forcing on stratigraphy (Jerolmack and Paola, 2010; Van De Wiel and Coulthard, 2010). Whereas a fundamental principle of sequence stratigraphy is that stratigraphic architecture is largely driven by allogenic forcing, and RSL in particular, there is considerable debate on the role of allogenic versus autogenic forcing on stratigraphy (Rodriguez-Tovar and Pardo-Iguzquiza, 2003; Muto et al., 2007; Vaughan et al., 2011; Hilgen et al., 2015; Muto et al., 2016; Paola, 2016).

Although stratigraphic studies often aim to decipher past tectonics and climate, it has become increasingly clear that these signals cannot be inferred from the stratigraphic record without a thorough understanding of their interaction with local intrinsic processes in sedimentary systems. In order to accurately interpret the stratigraphic record, we must work towards quantitative frameworks that predict under what conditions sediment supply signals are transferred to the stratigraphic record. In the next section I review existing concepts and methods that are used to assess signal propagation through sediment routing systems, and predict their preservation in strata.

1.5. Environmental signal propagation

The dynamic sedimentary systems that connect eroding catchments with depositional basins are referred to as sediment routing systems (SRS; Allen (2017)). Section 1.2 and 1.3 discussed how allogenic forcing may lead to sediment flux signals travelling through a SRS as they adapt to tectonic and climatic conditions. Just like tectonic and climatic signals can be buffered by catchment dynamics, depositional landscapes also buffer environmental signals as they propagate across sedimentary basins (Humphrey and Heller, 1995; Dade and Friend, 1998; Romans et al., 2016; Pizzuto et al., 2017). The concept of landscape buffering was born out of the response of 1D models of diffusional landscapes, as presented in Paola et al. (1992). Over long time scales, this model forms an equilibrium with forcing conditions as topography reaches a steady state between supply and accommodation. After a change in allogenic forcing, it takes time for a signal to propagate through the landscape, which buffers the signal. Mathematically, the time it takes for a signal to propagate downstream depends on the diffusivity (ν) of a river system. Consequently, for a system with length L, the time for the system to reach a new equilibrium is approximated by:

$$T_{eq} = \frac{L^2}{\nu},$$

which was reformulated to more measurable quantities in landscapes as (Metivier and Gaudemer, 1999):

$$T_{eq} = \frac{L w H}{q_s},$$

where H is the elevation difference between the start and end of the system, w is the width of the floodplain and q_s is the sediment yield in m^2/s. A prediction of this diffusional model is that when the forcing period is much longer than T_{eq}, the basin will reach an equilibrium with forcing conditions; however forcing periods much shorter than T_{eq}, will only influence a part of the basin that is proportional to the square root of the signal's periodicity. Estimates of an equilibrium timescale for river systems are generally in the order of 10^3-10^6 yrs (Paola et al., 1992; Dade and Friend, 1998; Marr et al., 2000; Castelltort and Van den Driessche, 2003; Armitage et al., 2013). What this means for the propagation of signals through SRS is that when the period of environmental forcing (T_s) is less than T_{eq}, the signal is substantially buffered by the depositional system (Paola et al., 1992; Humphrey and Heller, 1995; Metivier and Gaudemer, 1999).

As a consequence of the buffering of high-frequency signals, the transport system (Figure 1.1) may not carry environmental signals to the depositional sink (Metivier, 1999; Metivier and Gaudemer, 1999; Hoffmann, 2015). Castelltort and Van den Driessche (2003) clearly demonstrated that the amplitude of Milankovitch-scale sediment supply signals of 20 ky and 40 ky, and potentially 100 ky cycles too, attenuate with distance, making allogenic signal transfer to the landscape most likely in proximal areas or short systems. However, field evidence suggests climatic signals may propagate, even in large systems (Blum and Tornqvist, 2000; Goodbred, 2003; Clift et al., 2008; Allen et al., 2013a; Allen et al., 2014). A range of studies attributed this to the feedback between water discharge and river equilibrium slope, which may amplify sediment supply signals to basins (Forzoni et al., 2014). Coeval sediment and water supply cycles lead to proximal aggradation during low supply, and this sediment may be scoured and remobilised when water supply goes up again (Van Den Berg Van Saparoea and Postma, 2008; Simpson and Castelltort, 2012). A similar feedback exists because of proximal aggradation during glacial times, when large volumes of sediment are generated in the catchment that will only be transported during wetter interglacials (Malatesta et al., 2018; Watkins et al., 2018). Climatic and tectonic signals may also lead to a distinctly different spatial and temporal distribution of grain sizes over the landscape (Horton et al., 2004; Armitage et al., 2011). Coulthard and Van de Wiel (2013) predicted that climate change leads to signals of variable sediment flux, but this effect is limited in tectonics. However, tectonic signals cause an increase in grain size. The interaction of sediment supply and water discharge in climatic signals thus determines our ability to distinguish and reconstruct tectonic and climatic signals in the stratigraphic record.

The idea of environmental signal propagation through SRSs and their attenuation with distance is now widely accepted in numerical and conceptual models (Romans et al., 2016). However, diffusional models do not typically include stochastic autogenic processes.

The importance of this is pointed out in a landscape evolution model that developed a state of self-organized criticality (SOC; Van De Wiel and Coulthard (2010)), which results in nonlinear variations in sediment flux caused by autogenic processes. Part of the autogenics in this model are caused by topographic gradients that generate local differences in flow and sediment transport conditions. In addition, riverbeds may develop an armour layer caused by the preferential entrainment of fine grains. Sediment transport rates through the model vary significantly depending on whether the armour layer is breached. As a result, Van De Wiel and Coulthard (2010) stated that it is impossible to relate individual pulses of sediment flux either to allogenic signals or autogenic processes.

This work was followed by Jerolmack and Paola (2010), who used a model of an avalanching pile of granular material (rice) to illustrate a concept they named signal shredding: the destruction of sediment flux signals by storage and release events of sediment travelling over the surface. In their model, sediment is added at the top of the pile and collected at the bottom. As every grain added to the pile can cause an avalanche of any size, sediment leaves the piles in pulses of different size. The largest pulse is equal to the largest possible avalanche on the pile, given by the difference between the minimum and maximum surface slope. Given this, signals of varying sediment feed rate to the avalanching pile may not lead to correlatable signals of sediment flux leaving the pile. The transport of grains by avalanching may destroy periodic signals by smearing the signal's frequency out over a range other frequencies, given by avalanches on the surface. Signal shredding, or SOC, thus obscures the transfer of sediment flux signals to landscapes and into the stratigraphic record.

Importantly, Jerolmack and Paola (2010) also predicted and tested two scenarios in which sediment flux signals can survive signal shredding. The first option is when signals exceed a threshold duration (T_x), which is set by the recurrence interval of the largest avalanches:

$$T_x = \frac{L^2}{q_0},$$

where q_0 is the input sediment flux. For river channels, this timescale equates to the time it takes to elevate a channel to the avulsion threshold height. Alternatively, signals survive shredding when the amplitude far exceeds the size of the largest avalanche. The magnitude (M_{max}) of such an event is approximated by:

$$M_{max} \sim L^2 \cdot S_c,$$

where L is the length of the 1D system, and S_c is the threshold failure slope. As this exceeds the storage capacity of the avalanching pile, such a signal must be transferred to the bottom of the pile. This magnitude is approximated by $M_{max}=L \cdot h$ in river systems, where h is river depth.

The above examples demonstrate that stochastic autogenic processes obscure allogenically forced signals of varying sediment flux. It is the limits of autogenic timescales and magnitudes that determine the transfer potential of environmental signals to landscapes. Other models and field observations also demonstrate that autogenic processes destroy allogenic signals (Edmonds et al., 2010; Lazarus et al., 2019). However, these models generally focus on the propagation of signals over the surface, and not to the subsurface and the stratigraphic record. This is important because the storage of environmental signals in stratigraphy necessarily requires burial and permanent storage of sediment, 'permanent' meaning that sediment has been buried to sufficient depth that it is beyond the reach of the maximum autogenic scour depth of the system (i.e. incision by channels). The next section summarises recent work on the limits of environmental signal preservation in the stratigraphic record.

1.6. Preservation of allogenic signals in stratigraphy

The signal shredding theory of Jerolmack and Paola (2010) predicts that signals exceeding a temporal threshold will influence sediment fluxes in a landscape. However, this framework requires modification to deal with questions of signal preservation in stratigraphy. To store a signal in stratigraphy it must be buried below the active layer where sediments can be reworked, and so the timescale of burial is important for the preservation of signals in the stratigraphic record (Beerbower, 1964; Wang et al., 2011). This timescale is the stratigraphic equivalent of the autogenic saturation timescale T_x (Jerolmack and Paola, 2010). In sedimentary systems, autogenic processes cause spatial variations in topographic elevation as they passively fill in accommodation generated at a constant rate. An important point is that these variations level out at long timescales (Sheets et al., 2002; Lyons, 2004; Straub et al., 2009). In other words, sedimentation fills accommodation more evenly when the time window over which the measurement is averaged is increased (T_w; Figure 1.2).

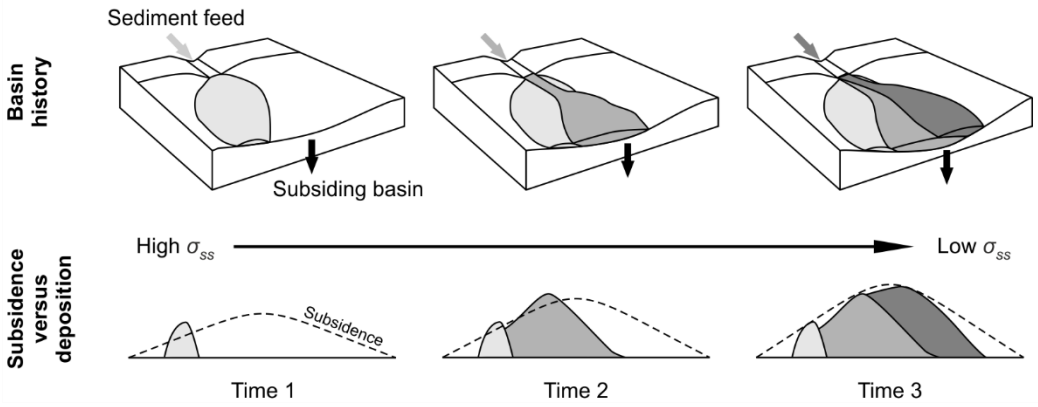

Figure 1.2. Accommodation/subsidence.

Schematic diagram of a subsiding basin being filed in by lobes. When analysed over short time windows, sedimentation is local, while accommodation is generated basin-wide. Over increasingly long timescales, sedimentation fills in subsidence more evenly. This is quantified by the standard deviation of sedimentation/subsidence (σ_{ss}). Figure modified from Lyons (2004) and Straub et al. (2009).

Straub et al. (2009) quantified this by measuring the standard deviation of sedimentation/subsidence (σ_{ss}) in stratigraphic cross-sections:

$$\sigma_{ss}(T_w) = \left(\int_{L_x} \frac{r(T_w,x)}{r(x)} - 1 \right)^{\frac{1}{2}}$$

where $r(T_w,x)$ is the local sedimentation rate measured over T_w at distance x along the section, $r(x)$ is the long-term average sedimentation rate at this point in the basin and L_x is the length of the cross-section. The decay of σ_{ss} follows a power-law function of T_w (Straub et al., 2009):

$$\sigma_{ss} = aT_w^{-\kappa}$$

where a and κ are coefficients. The value of κ quantifies to what degree sedimentation fills in topographic lows, a process known as compensational stacking (Straub et al., 2009). Anti-compensation occurs where $\kappa<0.5$, which may occur at short timescales where the transport system is stable, for example by levees. This may cause sedimentation on topographic highs. Completely random stacking is marked by $\kappa=0.5$. Over increasingly long time windows, however, lateral migration of the feeding system makes sediment spread more and more evenly, and so κ approaches 1. The timescale at which this occurs is named the compensation timescale (T_c), because stratigraphy follows a predictable pattern of compensational stacking when discretised over sufficiently long time windows. Wang et al. (2011) find that T_c, i.e. the

time window at which $\kappa \approx 1$ first occurs, is well approximated by dividing the maximum topographic roughness of the surface (H_c) and the long-term aggradation rate (r): $T_c = \frac{H_c}{r}$. Field estimates that quantify compensational stacking suggest that larger topographic features such as lobe-scale roughness and basin depth may better approximate T_c, which could extend stochastics autogenic timescales to 3 to 6 times channel-aggradation timescales (Trampush et al., 2017).

In a study on the transfer of RSL signals to the stratigraphic record, Li et al. (2016) predicted that RSL cycles with a periodicity $< T_c$ are destroyed, or stratigraphically shredded, by autogenics, unless the magnitude of sea level cycles overwhelms autogenic dynamics. They tested this hypothesis with a series of physical delta experiments in the Tulane University Delta Basin (TDB). First, they used an experimental stage characterised by constant allogenic forcing to quantify autogenic dynamics. T_c was estimated by measuring the depth of the larger channels on the delta (H_c) and the long-term steady base-level rise in this experiment sets r. Next, they conducted a series of experiments similar to the control stage, but with RSL cycles superimposed on the long-term base level rise. Each of the experiments had a different combination of signal periodicity and peak-to-peak amplitude (magnitude). The duration of these signals was scaled to be either longer or shorter than T_c, and the magnitude was scaled to be larger or smaller than H_c. Indeed the experiments demonstrated that sea-level variations with a periodicity $> T_c$ were transferred to the stratigraphic record. Sea level signals with a periodicity $< T_c$ were shredded, unless the magnitude of the sea level variations exceeded H_c.

Stratigraphic completeness, the fraction of time that is recorded in a stratigraphic dataset also relates to T_c, as T_c gives the maximum time window over which channels can rework previous deposits. Straub and Foreman (2018) demonstrate that basin-wide stratigraphic sections are complete when discretised at a time window of T_c. For proxy-records (isotopes, etc.), a time window of $2T_c$ serves as a Nyquist frequency for the resolution of the stratigraphic record (Foreman and Straub, 2017). This means that proxy signals can only be reconstructed from stratigraphic sections if they exceed a duration of $2T_c$, which has significant implications for the preservation potential of geologically short-lived events. For example, even strong climatic signals expressed by isotope excursions during the Paleocene-Eocene Thermal Maximum are distorted by autogenic processes (Trampush and Hajek, 2017).

Channel depth-based estimations of T_c in field-scale river systems are usually of the order of 10^4-10^5 yrs (Straub and Wang, 2013; Li et al., 2016). Given that a timespan of T_c may produce 10s of metres of stratigraphy, autogenic influence on stratigraphy extends to scales typically linked to allogenic forcing. This scale is also relevant for water or hydrocarbon

reservoirs. Interpretations of the stratigraphic record should thus account for stochastic autogenics as a potential explanation for stratigraphic patterns (Straub and Wang, 2013). Predictive frameworks such as the work by Li et al. (2016) and Foreman and Straub (2017) may thus help defining a null hypothesis of stratigraphy formed by autogenics without transfer of allogenic signals. Given that numerous studies aim to resolve allogenic signals that may have similar temporal and/or spatial scales as autogenic processes (Abels et al., 2013; Hilgen et al., 2015), these theoretical frameworks could provide a step in the direction of quantitative and objective interpretation of environmental signals in the stratigraphic record.

The buffering of environmental signals by catchments and sediment transport, the modification and shredding of allogenic signals by autogenic processes and the existence of thresholds on the transfer of allogenic signals to stratigraphy make stratigraphic successions an incomplete representation of Earth's history, and maybe we should not expect to '*read in them all of past history*' (Carson, 1951). In fact, recent work summarized above demonstrates that we should only expect to find the longest or largest of signals in the stratigraphic record, together with a range of autogenic signals. However, exact thresholds for the preservation of periodic sediment supply signals in the stratigraphic record are currently unknown.

Even when sediment supply signals exceed thresholds for signal propagation and preservation, their interpretation is difficult given difficulties in quantifying sediment supply (Allen et al., 2013b) and the range of other coeval allogenic and autogenic forcings on stratigraphy (Allen et al., 2013a). Significant challenges lie in the integration of model-based theories with field stratigraphy (Paola, 2000). Testing models with field data is complicated by the limited temporal resolution typical for stratigraphic datasets, and spatial restrictions because of outcrop extent and the resolution of seismic data. Defining the conditions necessary to store sediment supply signals in stratigraphy would be a first step towards interpretations of the stratigraphic record based on quantitative, testable hypothesis. Significant progress could be made by linking such theories to metrics measurable from the stratigraphic record, keeping in mind the limitations of field stratigraphy.

1.7. Environmental signals in laboratory experiments

Theory for the propagation and preservation of environmental signals is largely developed using numerical models and physical scale models. This thesis utilises physical experiments of deltas to test hypotheses on the transfer of sediment supply signals to landscapes and the stratigraphic record. An overview of experimental work on fan successions is given in Schumm et al. (1987), Paola et al. (2009), and Clarke (2015). Physical experiments are widely

used in studies that test concepts of environmental signal transfer. This is because they form self-organised sedimentary systems under precisely defined boundary conditions (allogenic forcing) while data are collected at high spatial and temporal resolution.

Inspired by the sequence stratigraphic framework and the importance attributed to base level signals on stratigraphy, many experimental studies have focused on the effects of sea level variations. Where conceptual representations of sequence stratigraphy often do not account for autogenic influences, delta experiments illustrate how RSL signals change landscapes in the presence of autogenic processes and, for example, influence the diachroneity of stratigraphic surfaces (van Heijst and Postma, 2001; Martin et al., 2009a). Experiments also show how cyclic RSL variations of different duration produce distinctly different stratigraphic architecture (Heller et al., 2001; van Heijst and Postma, 2001). However, part of the variability in stratigraphic architecture is caused by autogenic processes of sediment storage and release (Kim et al., 2014). Yu et al. (2017) showed that high amplitude RSL signals exceed autogenic variability on deltas while signals of low amplitude but long duration not necessarily exceed autogenic limits, but shift the mean state of delta morphodynamics. These same experiments were used to validate the RSL signal shredding framework by Li et al. (2016)

In a study on the effects of constant sea level rise on delta morphodynamics, Martin et al. (2009b) found that avulsion frequency on deltas shows a positive linear correlation with the rate of accommodation creation. However, lateral channel migration rate seems not to be correlated with aggradation rate (Wickert et al., 2013). Avulsions cause autogenic transgressions, where inactive parts on the delta transgress while active lobes prograde or aggrade, even during constant accommodation generation (Martin et al., 2009b; Hajek and Straub, 2017). Autogenic transgressions may also occur by autoretreat (Muto and Steel, 1992; Muto, 2001; Muto et al., 2007), which is a consequence of increasing foreset height during RSL rise. In addition to uniform base level change, often modelled as RSL rise, some facilities allow variable subsidence on an adjustable basin floor, which enables testing the effects of spatially variable subsidence. For example, Kim and Paola (2007) showed a cyclic development and disappearance of lakes in the hanging wall of a normal fault with constant slip. Strong et al. (2005) used experiments to demonstrate that much of the variation caused by subsidence patterns can be removed by replacing system length scales by a mass balance. This led to the development of a mass-balance framework that can be used to compare down-dip basin processes such as grain-size fining between basins of different scales and geometry (Paola and Martin, 2012).

Experiments agree with model predictions that changes in water discharge trigger a much faster response than changes in sediment flux under constant water discharge (Van

Den Berg Van Saparoea and Postma, 2008). Sediment supply signals influence large-scale stratigraphic architecture by modifying shoreline migration (Kim et al., 2006) or channel mobility. Lateral migration of a channel strongly depends on sediment supply rate (Wickert et al., 2013). Avulsion frequency is also positively correlated with sediment supply rate, although the exact relationship differs between experiments. Bryant et al. (1995) found an increase in avulsion frequency with sediment flux until a maximum frequency is reached where fluvial transport becomes saturated. Ashworth et al. (2004) also observe an initial increase in avulsion frequency, but saw a drop at high supply rates as the transport system switches to sheet flow. Ashworth et al. (2007) found that while increases in sediment feed rate led to a close to linear increase in avulsion frequency, slope changes were strongly buffered, presumably because changes in channelization and channel dimensions influenced sediment bypass.

Numerical models show that different types of allogenic signals interact (Armitage et al., 2011; Simpson and Castelltort, 2012). Few experiments have varied different forcing conditions at the same time. Van Den Berg Van Saparoea and Postma (2008) demonstrated how river gradients can be used to identify changes in sediment or water supply, and distinguished these changes from RSL signals. Bijkerk et al. (2014) showed that for signals of the same frequency, water discharge, and associated changes in sediment yield, is a secondary control on the architecture of stratigraphic successions to RSL variations. The effect of discharge variations depends on the phase difference with RSL signals, where transgressions are more significant when discharge is low, and regressions are more extensive when high discharge increases sediment transport to the shoreline. Mikes et al. (2015) used the same experiments and concluded that discharge variations in phase with RSL signals attenuate shoreline signals, while out of phase signals amplify shoreline migrations.

Laboratory experiments have played a significant role in the development of theories related to stratigraphic completeness (Cazanacli et al., 2002; Straub and Esposito, 2013; Foreman and Straub, 2017; Straub and Foreman, 2018) and signal shredding (Jerolmack and Paola, 2010; Wang et al., 2011; Li et al., 2016). Although scaling issues may exist (Chapter 3), experiments are particularly useful to test hypotheses in real-world small-scale sedimentary systems (Postma et al., 2008; Paola et al., 2009; Kleinhans et al., 2014). This thesis makes use of the self-organised nature of channelized landscapes that form both in field-scale systems and in fan experiments to study propagation and preservation of allogenic sediment flux signals in sedimentary systems.

1.8. Thesis aim and structure

1.8.1. Aims and objectives

The introduction above gave an overview of sedimentary systems and the different forcing mechanism that shape the stratigraphic record. Specifically, this chapter introduced how environmental signals can be buffered and obscured by the internal dynamics of landscapes. There is a clear need to quantitatively underpin interpretations of the stratigraphic record that invoke past signals of environmental change. The aim of this thesis is to develop a quantitative theoretical basis that can be used to assess the stratigraphic record as an archive for allogenic signals of varying sediment flux. To achieve this, I split the general aim up into three objectives discussed separately in Chapters 3 to 5. The results of these chapters are integrated in Chapter 6.

The first objective of this work is to develop a theoretical framework that quantifies which sediment supply signals are transferred and preserved into the stratigraphic record. The work of Jerolmack and Paola (2010) conceptually shows how signals of different magnitude and duration are shredded in a pile of avalanching material. However, this framework requires modifications to deal with sediment flux signals in three-dimensional subsiding landscapes. A starting point is to test T_c as a temporal threshold for the transfer of sediment supply signals to stratigraphy and integrate into this a magnitude threshold, which is as yet undefined. A theoretical understanding of the conditions necessary for signal transfer to the stratigraphic record allows quantitative predictions of the signals that may be archived in the stratigraphic record. Chapter 3 introduces a new theoretical framework that predicts the conditions necessary for sediment flux signals to transfer to the stratigraphic record. The minimum magnitude of sediment flux signals to be stored in stratigraphy is a function of the duration of the supply signal. This threshold magnitude function is supported by physical experiments of river deltas.

A second objective of this work is to develop methodology that will allow stratigraphers to predict the conditions for sediment supply signal shredding or preservation for sedimentary successions in the field. Our understanding of the stratigraphic record has hugely benefited from physical and numerical models, but we can only fully make use of these studies if they can guide quantitative predictions in field studies. Field data are typically of low spatial and temporal resolution, which limits our ability to make high-resolution paleo-environmental reconstructions, rendering stratigraphic interpretations subjective and debateable. The quantitative theoretical framework developed in Chapter 3 enables the formulation of testable hypothesis when collecting and analysing ancient field successions. In

Chapter 4 I outline a procedure to approximate the theoretical framework as applied to ancient field successions. This approximation works around the lack of high-resolution temporal data.

A third objective is to explore which measurable quantities in the landscape or stratigraphy could be used to identify sediment supply signals. As estimates of deposition rates are usually impossible to constrain from field data at a high temporal resolution, other metrics may prove better proxy records of sediment supply signals. This is because sediment flux signals may change landscape structure by setting the rate and scales of autogenic processes. However, we currently do not know whether periodic sediment supply signals generate deterministic patterns in these processes and their products. Chapter 5 contains a detailed analysis of morphodynamic processes in the physical experiments. The experiments simulate aggrading deltas formed under conditions of cyclic sediment flux, each with a different combination of cycle amplitude and periodicity. The experiments show how relative changes in sediment supply, water discharge, and generation of accommodation control morphodynamic processes and thereby the stratigraphic record.

Chapter 6 contextualizes the main results of Chapters 3-5 with the overarching aim of the thesis. Together, these chapters tell a full story on the interaction of allogenic sediment supply signals with autogenic processes, from a theoretical perspective and a practical perspective. Chapter 3 to 5 are written in the format of stand-alone papers and so motivations and key concepts are inevitably repeated throughout the thesis. The paper status and author contributions are stated below. Chapter 3 has been accepted for publication, and has been slightly modified to use consistent numbering and symbols throughout the thesis.

All references have been grouped into one reference list at the end of this thesis. Experimental metadata are given in Appendix 1. These metadata, together with the full datasets is available from the SEAD data repository (Li and Straub, 2017a, b; Toby and Straub, 2019a, b; Toby et al., 2019b). A list of all acronyms and symbols is provided in Appendix 2.

1.8.2. Publication status of the chapters

Chapter 3: Toby, S. C., Duller, R. A., De Angelis, S., & Straub, K. M. (2019). A stratigraphic framework for the preservation and shredding of environmental signals. Geophysical Research Letters, v. 46 (11), p. 5837-5845, doi.org/10.1029/2019GL082555.

Status: Published.

Submitted: 21 February 2019.

Accepted: 7 May 2019.

Published online: 11 May 2019.

The author contributions to this paper are as follows:

Stephan Toby – lead author, developed theory, conducted experiments, data analysis.

Rob Duller – conceived study, discussions, manuscript revisions.

Silvio de Angelis – data analysis, discussions, manuscript revisions.

Kyle Straub – conceived study, conducted experiments, discussions, manuscript revisions.

Chapter 4: Quantifying the limits of environmental signal propagation and preservation across ancient sedimentary systems

Status: in preparation.

The author contributions to this chapter are as follows:

Stephan Toby – PI, developed theory, data analysis, primary author of the manuscript.

Rob Duller –discussions, manuscript revisions.

Silvio de Angelis – discussions.

Kyle Straub –discussions, manuscript revisions.

Chapter 5: Delta morphodynamics and stratigraphy in the presence of environmental signals

Status: in preparation.

The author contributions to this chapter are as follows:

Stephan Toby – PI, conducted experiments, data analysis, primary author of the manuscript.

Rob Duller –discussions, manuscript revisions.

Silvio de Angelis – discussions.

Kyle Straub –discussions, data analysis.

1.8.3. Published datasets

Toby, S. C., Straub, K. M., 2019. TDB_16_1, SEAD data repository, doi.org/10.26009/s0iorjdx.

Toby, S. C., Straub, K. M., 2019. TDB_16_2, SEAD data repository, doi.org/10.26009/s0xtyi86.

Toby, S. C., Straub, K. M., Dutt, R., Akintomide, A., 2019. TDB_16_3, SEAD data repository, doi.org/10.26009/s0c20606.

Status: Each of these experimental datasets has been published and can be accessed through the links above. Metadata to the experiments are included in the appendix to this thesis.

The following people have contributed to the experiments:

Stephan Toby and Kyle Straub – conducted experiments.

Ripul Dutt and Akinbobola Akintomide – assisted in running experiment TDB-16-3.

Additional support from members of the Tulane Sediment Dynamics and Stratigraphy group, all contributors are listed in Appendix 1.

1.8.4. Additional work

Burgess, P. M., Masiero, I., Toby, S. C., & Duller, R. A. (2019). A Big Fan of Signals? Exploring Autogenic and Allogenic Process and Product In a Numerical Stratigraphic Forward Model of Submarine-Fan Development. Journal of Sedimentary Research, 89(1), 1-12. doi.org/10.2110/jsr.2019.3

The above paper is not included as a separate chapter, but I made significant contributions to the contents. The numerical model described in this work is developed by Isabella Masiero in collaboration with Peter Burgess. The application of this work to questions of sediment supply signals follows from discussions between Peter Burgess, Rob Duller and Stephan Toby. I contributed by performing model runs, data analysis and writing the initial manuscript.

2. Methods

2.1. Background to the experiments

In order to study delta morphodynamics and stratigraphy under controlled and closely monitored conditions this project makes use of physical experiments that produce self-organised sedimentary systems on a laboratory scale. These experiments provide a unique opportunity to study autogenic processes and their interaction with user-defined allogenic forcing, given by boundary conditions such as water discharge, sediment supply rate and properties, and RSL. The work by Li et al. (2016) forms a blueprint for the experiments used in this thesis. Their work identified thresholds on the shredding of cyclic RSL signals by autogenic processes. To quantify the scales of autogenic processes, Li et al. (2016) first ran an experimental stage with constant allogenic conditions of water discharge, sediment supply and base level rise. This stage covered the final 900 run hours of experiment TDB-12-1 (Li and Straub, 2017a) and is referred to as the 'control stage'. They used this stage to measure H_c and T_c. Next, they ran experiments with a similar setup, but forced with RSL oscillations superimposed on the long-term steady base level rise. The periodicity of these RSL signals was scaled relative to T_c and the magnitude of the signal was scaled to H_c. They found that periodic RSL signals are only transmitted to the stratigraphic record if either or both the amplitude and duration exceed H_c and T_c respectively.

A similar approach is used for the experiments presented in this thesis, but with the aim of scaling sediment flux signals to autogenic dynamics. To make effective use of the laboratory time, experiments were carefully scaled to systematically test the effect of sediment supply signal amplitude and periodicity. Following Li et al. (2016), sediment supply signal duration was scaled relative to T_c. However, signal magnitude, defined here as peak-to-peak amplitude, cannot be adopted from their work. Details on scaling a new threshold magnitude for sediment supply signals are provided in Chapter 3. This scaling is based on autogenic volume changes. To avoid confusion, volumes are converted to mass excluding porosity, using a density of 2650 kg/m^3 (quartz) and porosity measurements of the deposits (porosity = 53%). Porosity was estimated by measuring the volume of water that can be evaporated from water-saturated sediment cores taken from the experimental stratigraphy.

Chapter 4 makes use of two additional experimental stages. These stages used a similar setup to the control stage of experiment TDB-12-1, except for the cohesiveness of the sediment mixture. Cohesion is an important parameter in the autogenic behaviour of the experiments, which was detailed in Straub et al. (2015) and Li et al. (2017). We use those

stages in Chapter 4 for a calculation of the threshold magnitude in a system with different morphodynamic scales.

2.2. Design of the facility

Experiments presented in this thesis were run in the Tulane University Delta Basin (TDB) in the Tulane University Sediment Dynamics and Stratigraphy Laboratory. The rectangular basin is 4.2 m long, 2.8 m wide and 0.65 m deep (Figure 2.1). The concept behind these experiments is fairly simple. Water and sediment enter the basin from a point source after which sediment deposits in the basin as flow decelerates (Figure 2.2a-c). Water level in the basin can be precisely controlled to simulate sea level. Rising the water level creates space to be filled in with sediment, analogous to relative sea level rise. This allows sediment to accumulate vertically to form a stratigraphic succession (Figure 2.2d-e).

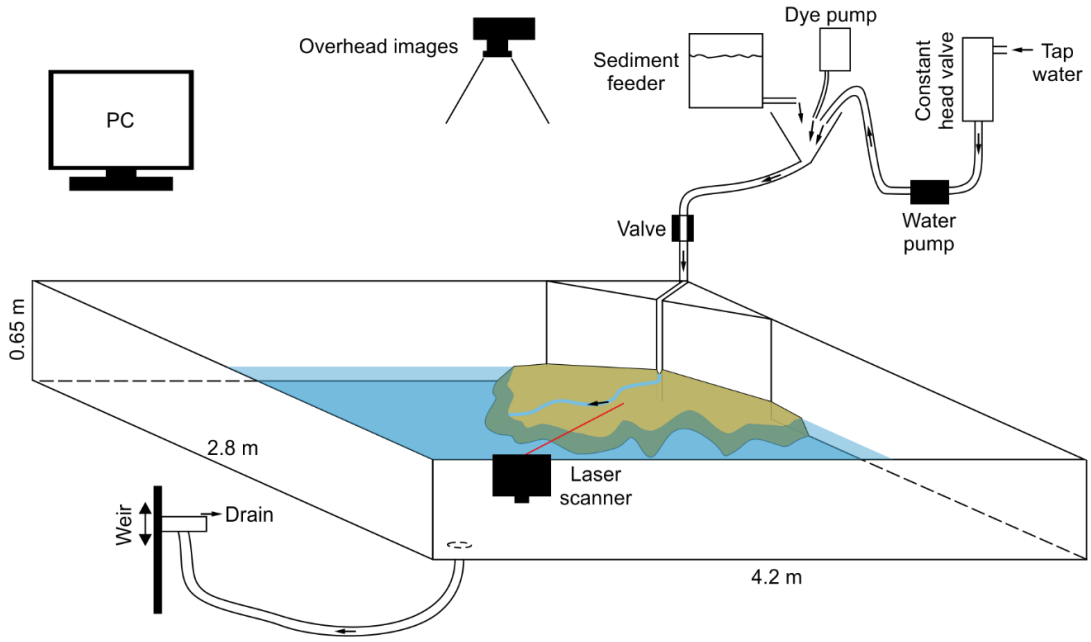

Figure 2.1. Schematic view of the Tulane Delta Basin (TDB).

Tap water is pumped into a funnel, where it is mixed with sediment and, at set times, blue dye. A series of valves ensures constant water pressure. The mixture flows through a narrow feeding channel into the main basin. Water level in the basin is controlled by a hydraulic connection with a manoeuvrable weir. Topography of the delta is mapped with a laser scanner and overhead photographs provide a plan-view image of the delta. Water level, sediment flux, water discharge and the timing of data collection are automated and can be controlled through a computer interface. Figure not to scale.

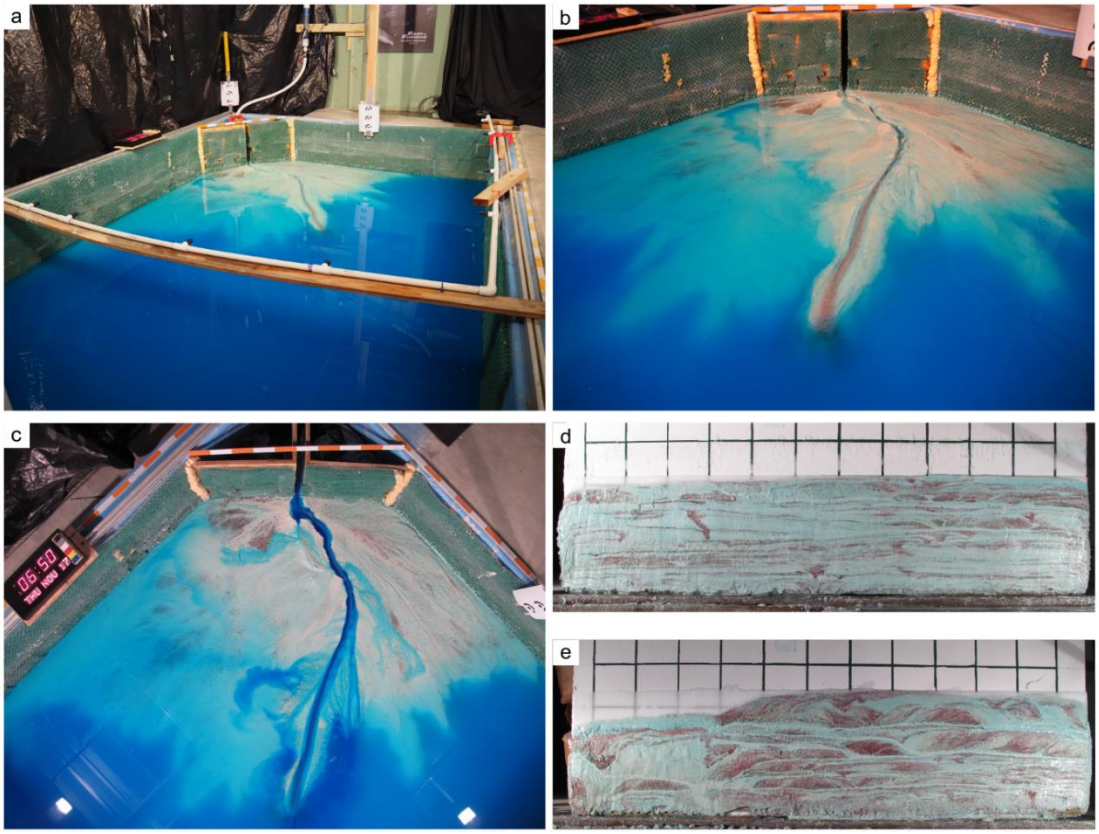

Figure 2.2. Photos of the Tulane Delta Basin and deposits.

(**a**) Overview of the basin at run hour 502 of experiment TDB-16-3. Sediment enters the basin through the white hose in the top left corner of the basin (Figure 2.2a). The drain is located on the basin floor in the bottom right corner, but is not visible here. The frame crossing the basin in the front of the picture is a misting system, which is used regularly in combination with soap to sink any floating sediment that may obscure topography scans. (**b**) Close-up view of the same time step as Figure 2.2a. Red sediment marks the coarsest grain size fraction. (**c**) Overhead image of the same time step as Figure 2.2a-b, with blue dye added to the water to visualise flow paths. The orange-white scale bar along the edge of the basin marks steps of 0.1 m. (**d**) Stratigraphic cross-section at 0.7 m from the delta apex. These cuts were made by freezing sediment onto a metal panel. Each of the squares on the panel is 0.1x0.1 m. (**e**) Stratigraphic cross-section at 1.1 m from the delta apex.

The setup of the TDB experiments is illustrated in Figure 2.1. The basin receives water and sediment from a point source that was situated in one corner of the basin. Before water enters the basin, it is routed through a constant head tank, which consists of a small reservoir and a float valve. This constant head ensures constant water pressure on a pump which moves water from the constant head tank to a funnel where it is mixed with sediment. Sediment is delivered to the funnel from a dry particle feeder (AccuFeed Vibrascrew). At set times, blue dye is pumped into the funnel to aid visualization of flow paths on the delta (Figure 2.2c). The mixture then flows through a hose with a valve that again ensures constant pressure in the last part of the feeding system (Figure 2.1). From here, the mixture flows into a narrow

feeding channel in a corner of the basin. This feeding channel is filled to the top with very coarse gravel to create a gentle flow path for the sediment-water mixture to flow down to basin level. The feeding channel extends 0.4 m from the basin corner, after which flow reaches the open basin.

Sediment may deposit in the feeding channel and open basin. Boundary conditions (allogenic forcing) to the basin can be precisely controlled via a computer connected with the sediment feeder, water pump, and dye pump. This allows user-defined and time-variable feeding rates into the basin. Sediment transport and deposition in the basin are self-organised and give rise to a wide range of autogenic processes and morphologies (Figure 2.2a-c). Water leaves the basin from a drain in the opposite end of the basin. This drain is connected with a computer-controlled weir that can move up and down. The hydraulic connection between water level in the basin and the height of the weir allows water level control in the basin to sub-millimetre precision. Water flowing out of the weir leaves the experiment through the sewage system.

To ensure accurate sediment feed rates into the basin, the sediment feeder was recalibrated approximately every 100 hr. The water pump and dye pump were calibrated before the start of each experiment. The experiments use tap water that was dyed blue with food colouring at set times. The sediment mixture used in these experiments was first introduced by Hoyal and Sheets (2009) and has since been used in several other studies and at different laboratories (e.g. Kleinhans et al., 2014; Li et al., 2016). The ingredients of the mixture are listed in the experimental metadata (Appendix 1). The grain size distribution of the sediment ranges from 1 to 1000 μm with a mean grain size of 67 μm (Figure 2.3). A quarter of the coarsest grain size class was coloured red to visualise grain size trends on the delta (Figure 2.2b) and in the stratigraphy (Figure 2.2d-e). The sediment was cohesive because of the clay fraction, but also because of a small amount of a polymer in the sediment mixture that becomes adhesive when water is introduced.

The evolution of the deltas was closely monitored with a FARO Focus3D-S 120 laser scanner, which scanned topography of the subaerial and submerged delta down to a water depth of approximately 50 mm with a vertical resolution of less than 1 mm. The scanner co-registered elevation data with RGB colour data. Two of these scans were collected for each run hour. The first scan was made towards the end of each run hour, with active flow on the delta. At the end of each run hour, the experiments were paused to make a scan of the delta without flow. The point clouds collected by the scanner were gridded on a grid with 5x5 mm cells. Topography caused small shadows for the laser scanner. Missing datapoints on the delta were interpolated as the mean of surrounding cells.

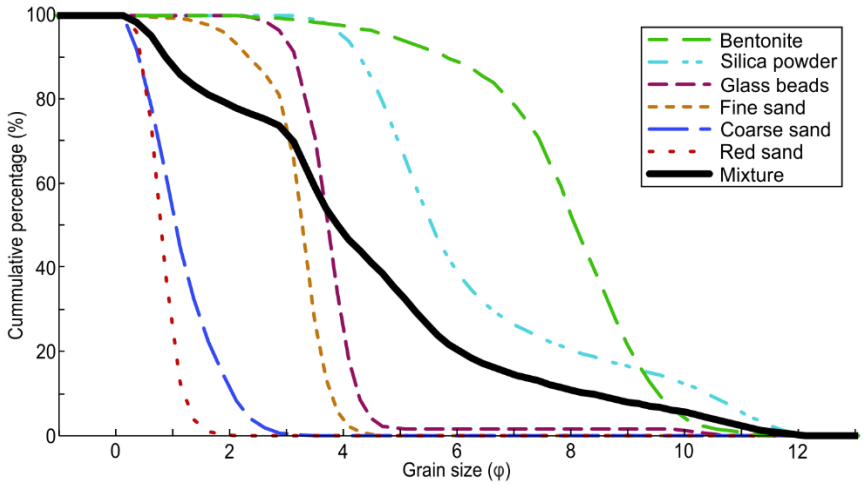

Figure 2.3. Grain size distribution of the sediment mixture.

Grain size distribution of the sediment mixture (solid black line) and each of the ingredients of the mixture. The mixture mimics earlier experimental work (Hoyal and Sheets, 2009). Figure modified from Li and Straub (2017a).

A second source of data comes from a Canon G10 digital camera mounted right above the experiments. This camera took images of the delta every 15 minutes, plus one in the break between each run hour. These images were used to create time-lapse videos of the experiments. Blue dye was added to the sediment-water mixture at the time photographs or scans were taken with flow switched on. After each experiment, stratigraphic cross-sections were made by lowering a 1.2 m wide hollow metal wedge into stratigraphy created by experiments. A cold mixture of dry ice and methanol in the wedge froze wet sediment onto the outside of the wedge. These sections were photographed before sediment melted off the wedge.

Most procedures in the TDB experiments were automated, allowing the experiments to run non-stop. Nonetheless, including inevitable technical problems, each of the experiments conducted for this work took between 1.5 and 4 months to run (Appendix 1). Several safety measures were installed to ensure water and sediment feed are working, sea level was accurate, and data were collected. In case of occasional errors, such as equipment failure or power cuts, these checks should pause the experiment by shutting down water and sediment supply to the basin. Unfortunately, a few data gaps exist in the experiments (Appendix 1). Where no data had been collected for short periods of time (1-5 hr), time series were interpolated linearly.

2.3. Morphodynamic processes on a laboratory scale

In broad terms, two approaches to scaling physical experiments were used in studies of sediment transport and basin morphodynamics. The first is dynamical scaling, which aims to scale some aspects of the physics of a field-scale system down to laboratory scale. Dynamic scaling is done by calculating dimensionless numbers that describe flow and sediment transport. Experiments are then designed for the scale model to match the field-scale number to replicate field conditions (Yalin, 1971; Ashworth et al., 1994; Peakall et al., 1996; Kleinhans et al., 2014). Most commonly, experiments are Froude-scaled. The Froude number (*Fr*) is a dimensionless number given by the ratio of inertial force and gravitational force, and a value of $Fr=1$ gives the limit between subcritical and supercritical flow. The Reynolds number (*Re*) gives the ratio between inertial force and viscous force, which describes whether flows are laminar or turbulent. Given that gravity, water density and viscosity are not changed in scale models, it is not possible to scale down *Fr* and *Re* at the same time (Ashworth et al., 1994; Peakall et al., 1996). Most field-scale systems are fully turbulent (Kleinhans et al., 2014), and so this problem is usually addressed by allowing lower *Re* in the scale model as long as flow is still turbulent. Another problem in scaling field systems arises from the scaling of bed shear stress (τ) with flow velocity (u). Bed shear stress cannot be scaled down at the same rate as *Fr* because τ depends on u^2 and *Fr* depends on u (Postma et al., 2008; Kleinhans et al., 2014). The critical bed shear stress, in dimensionless form given by the critical Shields number, sets the onset of grain motion. Given that τ also depends on water depth, scale models generally require a steep slope to reach a critical bed shear stress and mobilise sediment. Alternatively, sediment with a lower density such as plastic or walnut shell are used (Paola et al., 2009).

Kleinhans et al. (2014) argued that the ability of experiments to replicate field-scale morphology can be quantified, but concluded that experimental morphology cannot be scaled perfectly by adjusting experimental conditions. However, many experimental studies aim to answer general questions of sediment transport and deposition, and are therefore not necessarily scaled to one particular field-scale system. This introduces a second approach to experiments, where scale models are treated as individual, small-scale systems (Hooke, 1968). These types of experiments, which include models of alluvial fans, fan deltas and submarine fans, may violate some conventional scaling laws for hydrodynamics, but have proven useful in studies on morphodynamic processes because of the self-similarity of processes that form field-scale stratigraphy and reduced-scale laboratory stratigraphy over at least seven orders of magnitude (Hickson et al., 2005; Postma et al., 2008; Paola et al., 2009; Kleinhans et al., 2014). It follows from the scale-independence of morphodynamic processes that experiments form stratigraphy analogous to field-scale stratigraphy (Paola et al., 2009; Kleinhans et al., 2014).

An overview of experimental work on fan successions was given by Schumm et al. (1987), Paola et al. (2009), and Clarke (2015). Non-cohesive sediment mixtures in flumes often form alluvial fans or fan deltas with unconfined flow or braided channels and high Froude numbers. These mixtures usually consist of quartz sand, sometimes mixed with coal to simulate fine grains with a lower density that also provide a strong colour contrast e.g. (Sheets et al., 2002). Deposition in these experiments occurs through bars that migrate laterally (Hoyal and Sheets, 2009). Aggradation is inversely proportional to flow occupation because channels act as conduits, while short-lived flow events effectively deposit sediment (Sheets et al., 2002). The cohesive sediment mixture used in this thesis was introduced by Hoyal and Sheets (2009) and is known for forming stable channels, often with $Fr < 1$. Kleinhans et al. (2014) compared a range of different sediment mixtures, including this mixture. They observed that the cohesive mixture produces morphodynamics similar to those of deltas in cohesive substrates, but the properties of the polymer were difficult to quantify. They also found that the polymer fixates deposits over time, inhibiting later migration of rivers. However, these effects were limited in aggrading delta settings, making this mixture particularly suitable for studies on delta stratigraphy.

Compared to non-cohesive experiments, the strongly cohesive mixture creates a different style of autogenic processes, where channels fill because of backwater dynamics. Hoyal and Sheets (2009) described avulsion cycles in cohesive delta experiments that started with the progradation of a channel far into the basin. After the initial progradation, a mouth bar developed around which flow bifurcated. The bifurcations progressively moved upstream, shifting the location of the mouth bars, until the main channel avulsed and a new cycle started. This process formed a lobe, and lobes stacked compensationally, in contrast to non-cohesive deltas that stack compensationally by lateral bar migration. As a consequence of increased cohesion, autogenic processes occur over larger time and spatial scales (Straub et al., 2015; Li et al., 2017). As channel length and depth increase with increasing cohesivity, so does the time channels reside in one location. Consequently, autogenic flooding surfaces by RSL rise become more significant and more fine sediment bypasses the delta top and foresets. Given that strongly cohesive laboratory deltas show strong autogenic variations, these experiments are particularly well-suited for the scope of this thesis.

3. A stratigraphic framework for the preservation and shredding of environmental signals

This chapter has been published as: Toby, S. C., Duller, R. A., De Angelis, S., Straub, K. M., 2019: A Stratigraphic Framework for the Preservation and Shredding of Environmental Signals, Geophysical Research Letters, v. 46 (11), p. 5837-5845, doi: 10.1029/2019GL082555.

Abstract

The stratigraphic record contains unique information about past landscapes and environmental change. Whether landscapes faithfully transmit signals of environmental change to stratigraphy is unknown because autogenic processes, such as river avulsion, can obscure signals prior to long-term stratigraphic storage. We develop a theoretical framework that predicts when a sediment flux signal will be transferred from the landscape to stratigraphy. This threshold magnitude is a function of signal duration. The magnitude is set by the maximum rate of autogenic volume change of the landscape, which decreases with increasing time window. Physical delta experiments, specifically designed to test our theory, demonstrate that only sediment supply signals with a magnitude greater than the threshold are stored in stratigraphy, supporting our theory. This framework allows us to assess the fidelity of the stratigraphic record to archive past signals of environmental change and predict the short- and long-term impact of current Anthropogenic forcing on landscapes.

Plain Language Summary

We generate and validate a theory that predicts by how much sediment supply needs to vary in order to modify a landscape and store that signal in sedimentary deposits accumulating in the landscape. This theory predicts which ancient climatic or tectonic signals we can potentially reconstruct from geological data, and whether human activity leaves a trace in the landscape that will be preserved in the geological record.

3.1. Introduction

The stratigraphic record is a unique archive of past environmental change (Ager, 1973; Allen, 2008a) but this database is still underutilized because of difficulties distinguishing controls on stratigraphic architecture. Stratigraphy is traditionally interpreted in terms of a volumetric balance between the rate of sediment supplied to a sedimentary basin and the rate of accommodation generated by tectonic subsidence and eustatic sea level change. Within this framework, changes in climate and/or tectonics can alter the production and flux of sediment through sediment routing systems (SRS; Allen (2017)). These "allogenic" supply signals then propagate to a sedimentary basin and influence basin-wide deposition rates (Paola et al., 1992; Overeem et al., 2001; Duller et al., 2010; Armitage et al., 2011; Hampson et al., 2014) and the structure of stratigraphic sections (Duller et al., 2012; Allen et al., 2013b; Scotchman et al., 2015). Stratigraphic patterns linked to changes in this volumetric balance operate at timescales $>10^6$ yrs (Paola et al., 1992; Duller et al., 2010; Armitage et al., 2011). At timescales $<10^6$ yrs it is often difficult, but sometimes possible (Blum et al., 2018), to distinguish allogenic stratigraphic structure from structure generated by processes internal to a SRS (autogenic processes), which occur over similar time scales (Li et al., 2016; Hajek and Straub, 2017).

Autogenic processes constantly reorganize the transport system, resulting in local sediment storage, bypass, and release (SSBR) (Paola and Foufoula-Georgiou, 2001; Kim and Jerolmack, 2008; Paola, 2016), which causes 'noise' in landscape structure (Jerolmack, 2011), the effect of which is to potentially "shred" (*sensu* Jerolmack and Paola (2010)) allogenic signals within landscapes prior to stratigraphic transfer. Matters are complicated further when we consider not only the horizontal propagation of allogenic signals across the surface, as described above, but also the vertical propagation through the Earth's surface and into the stratigraphic record (Li et al., 2016; Foreman and Straub, 2017). This very real 'Earth Surface Barrier' has inhibited our ability to accurately glean past allogenic information from the stratigraphic record.

A clear and natural avenue to a generic solution set that can be used to discriminate between allogenic and autogenic stratigraphic structure is to bridge the gap that exists between Earth-surface morphodynamics and stratigraphy. Here we develop and test a new theoretical framework that delineates a threshold, set by morphodynamics, that must be surpassed if sediment supply signals are to be transferred to the stratigraphic record.

3.2. Theoretical framework

Concepts that originated in the field of fluid mechanics (von der Heydt et al., 2003) and were later applied to granular avalanching systems (Jerolmack and Paola, 2010) suggest two parameters must be considered when developing a threshold for sediment supply signal transfer to stratigraphy: a timescale of autogenic saturation; and a magnitude of autogenic SSBR. We recognize that the magnitude of autogenic SSBR is dependent on the timescale over which it is measured (Sadler, 1981) and so therefore the magnitude of a sediment supply cycle (SSC) necessary for stratigraphic storage is dependent on the duration of the cycle.

Previous studies suggest that the largest autogenic fluctuations set signal propagation and storage thresholds (Paola and Foufoula-Georgiou, 2001; Jerolmack and Paola, 2010; Li et al., 2016). This should also hold for stratigraphic storage of allogenic sediment supply signals. The maximum rate of autogenic change relates directly to the ability of an individual system to dissipate or accumulate an allogenic sediment supply signal. Here, an autogenic sediment flux change is defined by changes in terrestrial sediment volume over time, for systems experiencing constant forcing (Figure 3.1a-c). As such, we define a derivative threshold, Q_a, as the maximum autogenic change in sediment volume stored in a system per unit of time. Q_a decreases with the measurement time window, with smaller values expected for longer time windows until autogenic variations approach zero over very long timescales (Figure 3.1d). This stratigraphic storage threshold is novel as we recognize that the magnitude of a sediment supply signal necessary for sediment storage is dependent on the periodicity of the signal, which is in contrast to earlier studies that propose independent magnitude and periodicity thresholds (Jerolmack and Paola, 2010; Li et al., 2016).

To enable comparison between laboratory and field scale sedimentary systems, we define two normalization parameters that encapsulate autogenic dynamics. The time window of measurement is normalized by the compensation timescale, T_c, while Q_a is normalized by a new autogenic cycle derivative, M. T_c is an estimate of the maximum timescale of autogenic organization in stratigraphy (Sheets et al., 2002; Wang et al., 2011). It also approximates the maximum time necessary to bury a particle to a depth that is no longer susceptible to erosion from autogenic processes (Straub and Esposito, 2013; Straub and Foreman, 2018). It can be estimated as H_c/r, where H_c equals a maximum channel depth and r equals the long-term aggradation rate. T_c has been used as a temporal threshold for the transfer of relative sea level (RSL) and climate proxy signals (Foreman and Straub, 2017). We use T_c to define a dimensionless time, $T^*=t/T_c$.

M represents the maximum rate of change in sediment volume stored in an environment over a full period of sustained autogenic volume growth or loss (Figure 3.1c). In other words, M equates to the maximum observed rate of volume change between a trough in a time series of sediment volume and the subsequent peak, or vice versa. M is used to

define a dimensionless sediment flux, $Q^*=Q/M$. We can express a dimensionless version of Q_a as $Q_A^*=Q_a/M$.

With the framework outlined above, we predict that an allogenic sediment supply signal with a duration or periodicity, T_s, will be transferred to stratigraphy when the magnitude, Q_s, exceeds Q_a, measured over a time window equal to T_s (Figure 3.1d-e). This can be restated in dimensionless form as: signal transfer will take place if the dimensionless change in supply rate Q_s^* exceeds the Q_A^* threshold, measured at $T^*=T_s^*$.

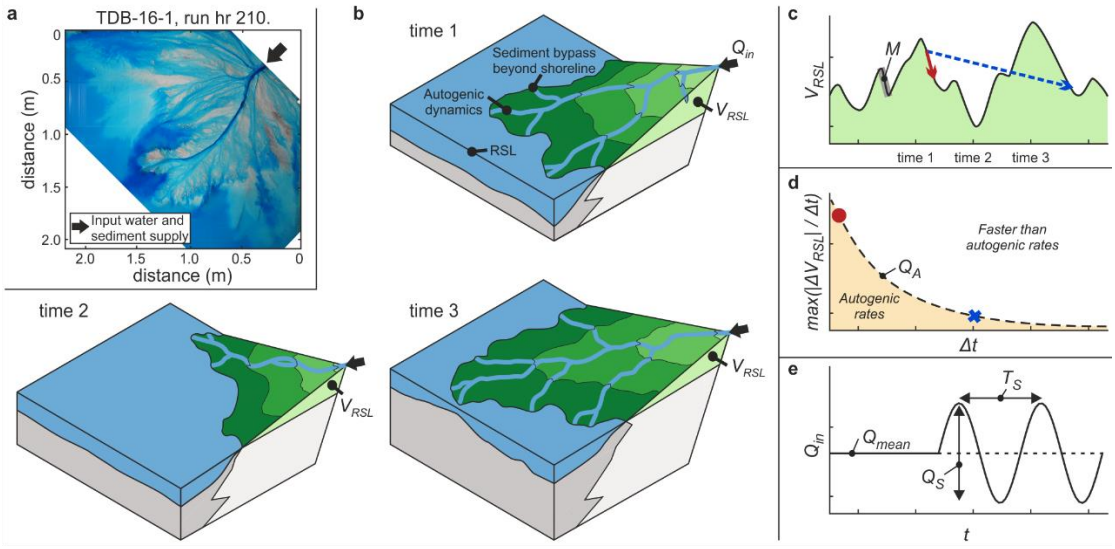

Figure 3.1. Schematic of autogenic volume changes.

(**a**) Overhead image of an experimental delta. (**b**) Schematic aggradational delta at three different time steps. Even under constant sediment supply rate (Q_{in}), the volume stored above sea level (V_{RSL}) continually adjusts in response to autogenic dynamics. (**c**) Schematic of autogenic changes in V_{RSL}. The rate of V_{RSL} change generally decreases with the time window measured over (e.g. red vs dashed blue arrow) and approaches zero over long timescales. (**d**) Schematic maximum rate of volume change (Q_a) for every possible time window of measurement. (**e**) Example of a cyclic sediment supply signal.

3.3. Methods

3.3.1. Set-up of the experiments

To test our theoretical framework, we explore the transfer thresholds for SSCs in a suite of physical laboratory experiments. In each experiment a delta developed in a basin that experienced a constant rate of accommodation generation through steady base-level rise, constant input water discharge and constant sediment mixture (Figure 3.1a). Topography was

measured at high temporal and spatial resolutions relative to system morphodynamics to monitor sediment volume changes on the delta.

Experiments were conducted in the Tulane University Delta Basin, which is 4.2 m long, 2.8 m wide and 0.65 m deep. Sea level was set to rise at 0.25 mm/hour and is controlled to submillimeter-scale resolution. Sediment (mean flux = 3.9 x 10^{-4} kg/s) and water (1.7 x 10^{-4} m^3/s) were mixed and fed from a point source. A cohesive sediment mixture with particles ranging from 1 – 1000 μm (D_{50} = 67 μm) mimics earlier experimental work (Hoyal and Sheets, 2009).

Steady base level rise initiated after the shoreline prograded 1.1 m from the source. In each experiment, the combination of sediment feed rate and base-level rise maintained the shoreline at an approximately constant location through the course of the experiment, with fluctuations associated with autogenic and allogenic dynamics. Topography in all experiments was mapped once an hour with a FARO Focus3D-S 120 laser scanner on a 5 mm horizontal grid in the down and cross basin directions with a vertical resolution < 1 mm.

3.3.2. Building a supply signal regime diagram

To characterize timescales and magnitudes of autogenic SSBR events we use a control stage of experiment TDB-12-1. During this stage the terrestrial delta volume was in dynamic equilibrium with the input sediment flux and rate of accommodation production (r=0.25 mm/hr). From a distribution of channel depths on the delta, we approximate H_c with the 95th percentile depth (12.2 mm) and estimate T_c=49 hr. In 900 run hours (18.4T_c) the experiment produced a deposit that was >18H_c thick. While no attempt was made at upscaling our results, extensive work demonstrates the "unreasonable effectiveness" (Paola et al., 2009) of experimental deltas due to the scale independence of many processes, including channelization.

Given our focus on the transfer of sediment supply signals to terrestrial stratigraphy, we quantify our hypothesized relationship between Q_A* and T* using a time series of deposit volume stored above sea level (Figure 3.2a). This terrestrial volume (V_{RSL}) varies because of changes of the surface slope and the location of the shoreline, which are dictated by autogenic SSBR on the delta top. We calculate Q_a for time windows that increase from 0.02T_c to 4T_c by steps of 0.02T_c (1 h). Autogenic episodes of V_{RSL} growth or loss are characterized by a range of durations that span up to 1.8T_c, but have a mean period of 0.4T_c. We measure M = 9.7x10^{-8} m^3/s ≈ 0.3Q_{in} from an autogenic V_{RSL} cycle with a duration of ≈0.3T_c (Figure 3.2a).

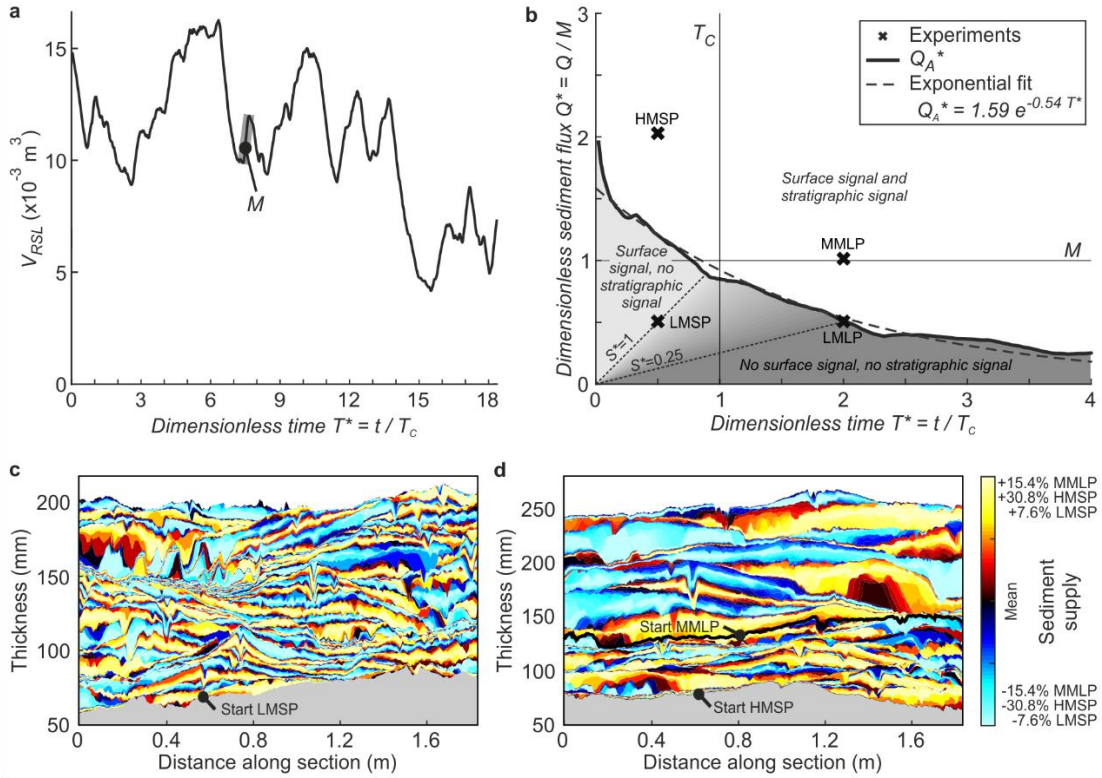

Figure 3.2. Construction of a regime diagram from autogenic volumetric changes.

(**a**) Plot of terrestrial volume (V_{RSL}) versus time for the control stage. Normalization parameter M is derived from the highlighted stage. (**b**) Q_A* versus measurement window (T*). For each time window, we calculate Q_A* from n=900-Δt samples. Q_A* is well approximated by an exponential fit (R^2=0.98). Crosses mark combinations of periodicity and peak-to-peak amplitude for cyclic experimental stages. We test Q_A* as a threshold for allogenic supply signals to be stored in stratigraphy. Acceleration parameter S* is discussed in the discussion section. (**c and d**) Semi-circular synthetic stratigraphic sections located at 0.7 m radius from the delta apex as if looking downstream. Stratigraphy is color-coded according to supply conditions during deposition. Panel c shows stratigraphy formed by signals of low magnitude and short period (LMSP) and panel d shows both high-magnitude short-period (HMSP) and low-magnitude long-period (LMLP) stages at the base and top, respectively.

We observe a decrease in Q_A* as a function of T*, which is well approximated by an exponential decay of the form $Q_A^*=ae^{bT^*}$ (Figure 3.2b). We hypothesize that allogenic sediment supply signals with a combination of periodicity and magnitude that plot well above the Q_A^* threshold will leave behind detectable evidence of allogenic signals in stratigraphy, while those that plot below Q_A^* will leave behind no detectable evidence in stratigraphy, i.e. the signals are shredded.

3.3.3. Testing the threshold

To test our proposed threshold, we explore the results from four additional experimental stages, each of which shared the same set of forcing conditions as the control stage with the exception of Q_{in}, which was varied following sinusoidal cycles (Figure 3.2b, Table 3.1). Periodicities of all cycles in any given stage was equal to either $2T_c$ or $0.5T_c$. Similarly, Q_s values were set to be either $2M$ or $0.5M$. While Q_{in} temporally varied, the mean supply rate (Q_{mean}) in each stage was equal to the control stage.

The allogenic SSCs were designed to systematically explore the joint influence of cycle period and magnitude relative to T_c and M, respectively (Figure 3.2b, Table 3.1). Natural sediment supply histories are more complex than our sinusoid, but we specifically use a simple experimental setup to leverage existing time series analysis methods. Our hope is that the concepts developed here can be easily modified for other classes of signals.

Table 3.1. Sediment supply characteristics for each experimental stage.

Experiment	Stage	Time(h)	Q_s (kg/h)	t_s (h)	Q_s^*(-)	T_s^* (-)	S^*(-)
TDB-12-1[1]	Control	385-1285	-	-	-	-	-
TDB-16-1[2]	Low Magnitude Short Period (LMSP)	140-630	0.22	24.5	0.5	0.5	1
TDB-16-2[3]	Low Magnitude Long Period (LMLP)	140-630	0.22	98	0.5	2	0.25
TDB-16-3[4]	High Magnitude Short Period (HMSP)	140-385	0.87	24.5	2	0.5	4
TDB-16-3[4]	Medium Magn. Long Period (MMLP)	385-875	0.43	98	1	2	0.5

[1]Li and Straub (2017a), [2]Toby and Straub (2019a), [3]Toby and Straub (2019b), [4]Toby et al. (2019b)

3.4. Results

We begin our signal hunt by exploring the time series of terrestrial sediment volume, equivalent to those used to define Q_a from the control stage. Theoretically, V_{RSL} is susceptible to supply signals by recording the combined effect of changes in transport slope and shoreline position. The equilibrium transport slope of a fan-delta is a function of the ratio of sediment to water supply (Parker et al., 1998; Whipple et al., 1998). Altering this ratio forces terrestrial transport slopes to adjust through deposition and/or incision, which may have a measurable impact on resulting stratigraphy (Sun et al., 2002). Altering the balance between sediment supply and accommodation generation can drive transgression or regression of shorelines (Muto and Steel, 1997). On short timescales these effects may be obscured by autogenic SSBR.

We construct periodograms by calculating the Fast Fourier Transform of a time series of V_{RSL} to explore when supply signals consistently produce measurable geomorphic responses (Figure 3.3a). This time series is extracted from surface topography scans taken at

a 1 hr resolution. All periodograms share a background structure characterized by power growth as a function of period, similar to that expected from time series with the presence of temporal correlation. Focusing first on short period signals, we observe spectral peaks that are significantly higher than spectral noise levels at the imposed period of the allogenic SSCs for both high and low magnitude experimental stages. The periodogram from the LMLP stage displays no significant peak at the imposed signal period. Interpretation of the MMLP stage is somewhat complicated as a broad peak is observed that centers at a timescale slightly below the imposed periodicity (Figure 3.3a).

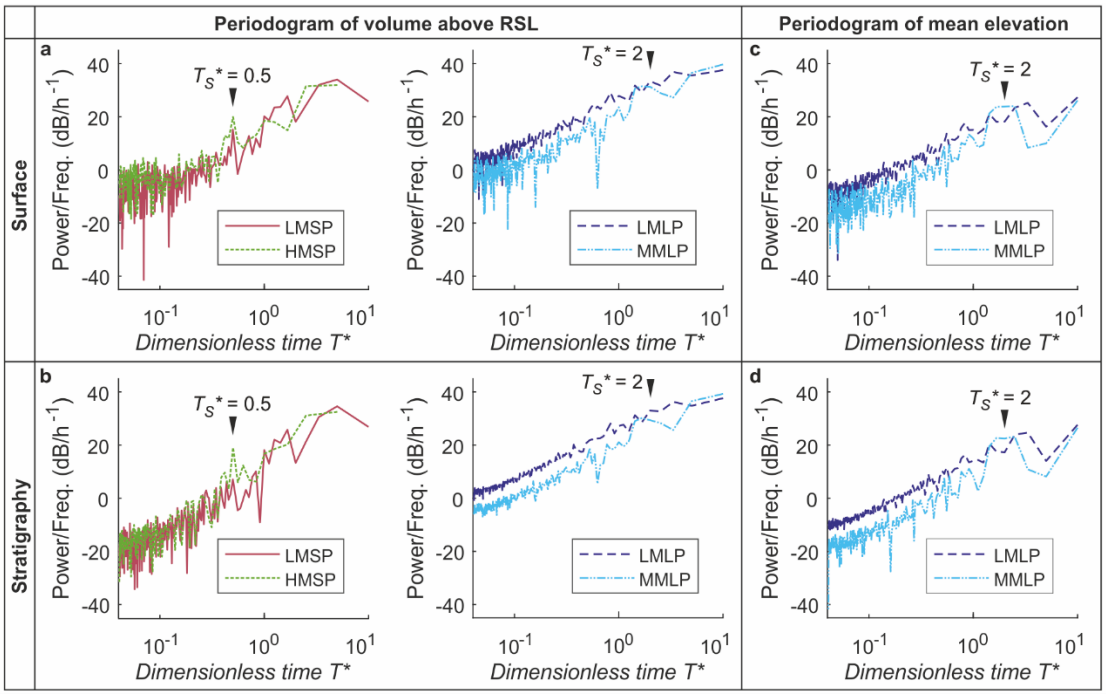

Figure 3.3. Time series analysis.

Periodograms of terrestrial volume (a-b) and mean elevation (c-d) for SSC experiments. Figure a and c are based on topography data, Figure b and d on synthetic stratigraphy. Peaks in the periodograms from the geomorphic surface datasets, at periodicities corresponding to those of imposed SSCs (black arrows), show signal transfer for all stages except LMLP. The stratigraphic data only shows signal transfer at the imposed SSC periodicities in stages HMSP and MMLP.

Next we document the transfer of signals to the stratigraphic record using stacked topographic scans clipped for erosion (Figure 3.3c-d), which we refer to as synthetic stratigraphy (Martin et al., 2009a; Li et al., 2016). Periodograms of paleo-terrestrial volume, generated from synthetic stratigraphy (Figure 3.3b), indicate that the observed peak in the surface data from the HMSP stage was transferred to the subsurface, while the observed LMSP peak is absent in the stratigraphic data. The spectra of stratigraphic data from the LP stages are similar to the geomorphic spectra.

The analysis of stages with SP supply cycles, outlined above, supports our hypothesized stratigraphic storage threshold, Q_A^*. While both SP stages exhibit allogenic signals in their geomorphology, only the HMSP signal, which plots above our transfer threshold, gets stored in the stratigraphy. To further test if the signals of LP stages are linked to the frequency of the SSCs, we perform an additional analysis on a time series of mean delta elevation relative to sea level. This is calculated by dividing V_{RSL} by the terrestrial area. We observed clear peaks at the imposed allogenic supply period in periodograms from both the geomorphology and stratigraphy of the MMLP stage, while no peaks in excess of spectral noise levels are observed in the LMLP stage (Figure 3.3c-d).

3.5. Discussion

3.5.1. Storage of geomorphic signals in stratigraphy

Our experimental results broadly support the existence of a stratigraphic transfer threshold of sediment supply signals based on time and space scales of autogenic processes. All experimental stages whose SSC characteristics place them above our Q_A^* threshold are recorded in the synthetic stratigraphy, while SSCs that fall below or on our Q_A^* threshold lack stratigraphic signals of supply cycles (Figure 3.2b).

One interesting observation is that some allogenic SSCs induce a geomorphic surface signal that is absent in stratigraphy (e.g. LMSP stage), while other allogenic cycles produce neither geomorphic surface nor stratigraphic signals (e.g. LMLP stage). These results suggest that the ability of an SSC, for a given magnitude, to produce a geomorphic surface response decreases as the cycle period increases. We propose that a signal acceleration term is governing this behavior. Acceleration is given by the temporal derivative of sediment supply, which here is a cosine function. Prior studies recognized the importance of an acceleration term for stratigraphic signals, specifically the completeness of the stratigraphic record (Sadler and Strauss, 1990b). The general idea is that a rapid change in sediment supply, even if small in total magnitude, can trigger a transient response at the Earth's surface as the system is unable to remain in equilibrium with forcing conditions (Postma, 2014). If the period of the signal is short, it might not produce a thick enough sedimentary response to withstand reworking prior to burial beneath the active surface. A longer signal of the same magnitude might not trigger a transient response as the system is able to remain in equilibrium with the forcing while the change in equilibrium states might not be large enough, relative to the stochastic dynamics, to produce a detectable signal.

Following Sadler and Strauss (1990b), we simplify acceleration by taking the ratio of signal magnitude and period and define dimensionless signal acceleration as $S^*=Q_s^*/T_s^*$ (Table 3.1). Given that LMSP produced a geomorphic response and LMLP did not, we suggest that a signal acceleration threshold value must exist between $0.25<S^*<1$ (Figure 3.2b), but more experiments are necessary to converge on a specific threshold.

Diffusional models of sediment transport indicate that the propagation of sediment flux signals attenuates with downstream distance (Paola et al., 1992). However, a critical aspect of our findings is that not all surface signals are stored within the stratigraphic record. While more proximal locations might have stronger signals propagating over the geomorphic surface, we note that archiving of these signals also depends on the long-term accommodation generation.

3.5.2. Field scale supply signal storage

Our theoretical framework could guide the interpretation of stratigraphy for sediment supply signals. Here we illustrate implications of our threshold for field scale allogenic cycles triggered by tectonic, climatic and anthropogenic influences. For simplicity purposes, we consider sediment supply signals of duration T_c, which are generally on the order of 10^4-10^5 yrs for sedimentary basins (Straub and Wang, 2013; Li et al., 2016). We note that T_c can vary with downstream distance as a result of changing channel depths and spatially varying accommodation production rates. We suggest utilizing an upper limit to T_c in the environment of interest for prediction of storage thresholds as it gives the most conservative prediction. Field estimates of T_c may follow from an analysis of compensational stacking patterns or channel unit thickness distributions (Trampush et al., 2017).

While our focus here is on signals close to T_c, estimation of storage thresholds at other timescales can be estimated by taking advantage of the exponential relationship between Q_A^* and T^*. The magnitude of Q_a likely depends on allogenic conditions such as landscape cohesion (Caldwell and Edmonds, 2014; Li et al., 2017) and flashiness of a system's hydrograph (Esposito et al., 2018; Fielding et al., 2018), amongst other physical variables and requires further exploration. At a timescale of T_c, Q_a for our control stage is approximately $1/3Q_{in}$.

Several recent studies highlight how the buffering of signals due to deterministic processes in erosional landscapes limits our ability to decode time series of sediment flux for the true timing and magnitude of tectonic signals (Armitage et al., 2013; Mudd, 2017; Li et al., 2018). For example, results from a suite of numerical experiments loosely scaled to Basin and Range catchments suggest that periodic changes in tectonic uplift rate by a factor of 10

are significantly buffered if the cycle period is much less than the landscape response time, $t_R > 10^6$ yrs (Li et al., 2018). As a result, the predicted magnitude of SSCs leaving the erosional catchment, for tectonic uplift periods between 10^4-10^5 yrs, is below 5% of the mean outlet sediment flux. The ratio of Q_a to Q_{in} from our experiments would suggest that signals exiting Basin and Range catchments should be prone to shredding in adjacent sedimentary landscapes prior to stratigraphic storage. As t_R in erosional landscapes scales with drainage area, signals from larger catchments will be more prone to stratigraphic shredding (Allen, 2008b).

Next we consider climate signals with durations between 10^4-10^5 years, the obvious choice for discussion being climate response to orbital forcings. Blum and Hattier-Womack (2009) calculate that a change in temperature due to Milankovitch-scale orbital forcing may result in 20-50% change in sediment yield according to the empirical BQART model (Syvitski and Milliman, 2007). The ratio of Q_a to Q_{in} at a timescale of T_c from our experimental dataset suggests that SSC characteristics might fall close to our proposed threshold. As such, signal transfer may (or may not) be possible. Here we stress that our regime diagram presents a theoretical threshold for signal storage. Practical limitations to field stratigraphic datasets challenge our ability to detect subtle signals.

Finally, our observation that a fast change in sediment supply is more effective at causing a landscape response implies that anthropogenic signals are a good candidate to trigger a response in the landscape. Current climate change is occurring at a fast rate (Zeebe et al., 2016), and, if continued for a sufficient amount of time, its signal will be transferred to stratigraphy. Likewise, sediment trapping by dams causes fast and significant changes in sediment yield (Blum and Roberts, 2009). Even though human influences emerged in the very recent past, the speed and magnitude by which the sediment supply changed is unlikely to be matched by autogenic processes, making stratigraphic storage of the Anthropocene ever more likely.

3.6. Conclusions

We developed a novel theoretical framework that successfully predicts the conditions necessary for the stratigraphic storage of sediment supply signals. The importance of this finding is two-fold: 1) it enables stratigraphers to quantitatively justify paleo-environmental interpretations and 2) offers a new direction for Earth scientists to explore time-dependent thresholds in landscapes.

Acknowledgments

We gratefully acknowledge support by the National Science Foundation (grant EAR-1424312), the NERC EAO Doctoral Training Partnership (grant NE/L002469/1) and the University of Liverpool. We thank members of the Tulane Sediment Dynamics and Stratigraphy Lab for help with the experiments and providing access to data from the control experiment. We thank an anonymous reviewer and editor Harihar Rajaram for constructive comments which greatly improved the manuscript. The data used are listed in the references.

4. Thresholds of environmental signal propagation through sediment routing systems and to the stratigraphic record

Abstract

The ability of strata to store information related to allogenic environmental forcing (climate and tectonics) is debatable because strata are also influenced by the internal dynamics of a system that operate at the Earth's surface (autogenics), and so overprint and remove evidence of environmental signals that also operate at the Earth's surface. We address this by reformulating and applying a theoretical framework that predicts an autogenic threshold function (ATF) that must be surpassed to ensure faithful transfer of allogenic sediment flux signals to the stratigraphic record. The calculation of an ATF can be approximated using input parameter values that are readily attainable from field systems, without the need for high temporal resolution datasets. To demonstrate the applicability of our approach we explore environmental signal propagation and transfer to the stratigraphic record of two ancient field systems: a small Pleistocene delta in Greece; and a large Eocene sediment routing system in the Spanish Pyrenees. This work integrates short-term system dynamics with long-term stratigraphic development and provides a much-needed procedure that enables field stratigraphers to quantify the capacity of sedimentary systems to store environmental signals.

4.1. Introduction

The ability of Earth Scientists to accurately deconstruct the stratigraphic record enables us to see beyond human observational timescales. This is crucial as it provides a unique perspective on the potential impact that climate and tectonics might have on our environment (Knight and Harrison, 2013). The impact of climate and tectonics on landscapes and the recent stratigraphic record is complex and unpredictable (Rygel and Gibling, 2006; Paola, 2016), but when viewed over long timescales the response of landscapes and the character of the stratigraphic record is predictable. This is because at longer timescales the morphology of landscapes and strata is governed by a balance between input sediment flux and accommodation generation (Van Wagoner et al., 1988; Posamentier and Allen, 1993; Schlager, 1993; Porebski and Steel, 2003; Carvajal et al., 2009; Catuneanu et al., 2009; Allen et al., 2013b). For this reason, diffusional models of sediment transport are used to conceptualize limits of signal propagation across the Earth's surface and to stratigraphic successions (Paola et al., 1992; Castelltort and Van den Driessche, 2003). Although informative and applicable, diffusional models imply that the ability of the stratigraphic record to store allogenic sediment supply signals can be evaluated through simple mass-balance or diffusional system response. However, we now know that any evaluation of strata for the presence of allogenic signals must incorporate the stochastic autogenic processes that are inherent to 3-dimensional sediment transport systems (Jerolmack and Sadler, 2007; Jerolmack, 2011; Schumer et al., 2011).

Given that autogenic processes operate at similar temporal scales to allogenic forcing, they can overprint and shred allogenic signals prior to stratigraphic transfer (Peper and Cloetingh, 1995; Jerolmack and Paola, 2010; Van De Wiel and Coulthard, 2010; Allen et al., 2013a; Burgess et al., 2019; Lazarus et al., 2019). Autogenic processes set a lower limit for the storage of allogenic signals in strata (Jerolmack and Paola, 2010; Li et al., 2016; Paola, 2016; Foreman and Straub, 2017; Trower et al., 2018). This autogenic limit was defined theoretically and captured experimentally by Toby et al. (2019a) who built on the theoretical framework of Jerolmack and Paola (2010) and demonstrated that the maximum rate of autogenic volume change at the surface of a system determines whether a particular allogenic sediment supply signal, which must also induce a volume change, will be successfully transferred to the stratigraphic record. Here we present a reformulation of the original autogenic threshold function (ATF) of Toby et al. (2019a) to overcome the requirement of high temporal resolution stratigraphic datasets that are not usually offered by ancient field systems. This new approach allows us to: (1) assess, to first order, the likelihood that a particular field site will contain evidence of particular environmental signals; and (2) predict whether these signals are

likely to have propagated through the sediment routing system (SRS, Allen (2017)). To demonstrate the workflow and applicability of our approach, we apply our new field approximation of the ATF to two ancient field scale systems.

4.2. Theoretical framework

The theoretical framework of Toby et al. (2019a) offers predictions about the autogenic threshold magnitude that sediment supply signals must overcome to ensure successful transfer to the stratigraphic record (Figure 4.1a). This threshold magnitude was calculated for a physical delta experiment (Figure 4.1b) and decreases exponentially as a function of signal duration.

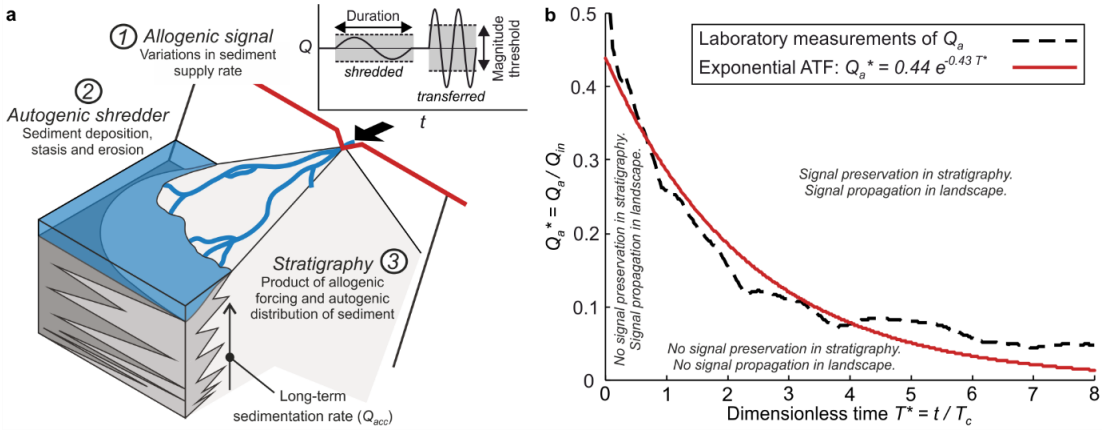

Figure 4.1. Autogenic thresholds for the transfer of sediment flux signals.

(**a**) Conceptual diagram of a subsiding delta receiving allogenic sediment supply signals of different durations and magnitudes. Toby et al. (2019a) predicted that the signal must overcome a time-dependent threshold magnitude, set by autogenic dynamics, in order to be transferred to stratigraphy. (**b**) Sediment supply signal transfer threshold magnitude as a function of signal duration for an aggrading experimental delta forced with constant rates of sediment supply, water discharge and sea level rise. Two lines show the measurements of Q_a^* from a time series of terrestrial volume (see supplementary material) and an exponential regression to the measurements for time windows up to $8T_c$ (Toby et al., 2019a). Notes on signal preservation and propagation are explained in the discussion section.

To enable direct comparisons between lab-scale and field-scale systems, dimensionless sediment flux (Q^*, using the asterisk consistently for dimensionless variables) is defined by dividing sediment flux (Q, units of volume per time) by the long-term mean sediment supply rate (Q_{in}, units of volume per time): $Q^*=Q/Q_{in}$. Similarly, dimensionless time (T^*) is defined as time (t) divided by the compensation timescale (T_c), which marks the transition from time

windows dominated by stochastic autogenic processes to time windows over which autogenics average out (Wang et al., 2011). T_c is given by dividing topographic roughness H_c (e.g. channel depth) by long-term aggradation rate r (Wang et al., 2011). The main result of Figure 4.1b is that any combination of signal magnitude and duration that plots above the AFT is preserved in stratigraphy, while signals that plot below the ATF are absent in the stratigraphic record as they are destroyed by autogenic dynamics. The ATF is described by the function $Q_a^*=Q_0^* e^{bT^*}$, where Q_a^* is the dimensionless threshold magnitude flux, Q_0 and b are scaling parameters of the exponential, and T^* is dimensionless signal duration. Although not all physical variables can be scaled down proportionally, experimental studies show that field scale processes generally scale down to laboratory systems (Paola et al., 2009; Kleinhans et al., 2014), including autogenic processes such as channelization that set the ATF. In the next section, we approximate the ATF for field-scale systems.

4.3. Field framework

To generate the ATF from a field dataset we make use of the exponential relationship $Q_a^*=Q_0^* e^{bT^*}$. Two or more combinations of Q_a^* and T^* are sufficient to constrain the parameter values Q_0^* and b, but a difficulty lies in finding these combinations given the limited spatial and temporal resolution of field systems. We approximate two points on the ATF using a mass balance, whereby the allogenic sediment flux into the environment of interest (Q_{in}^*) is split in two parts: a maintenance flux (Q_{acc}^*) and bypass flux (Q_{bp}^*). Maintenance flux is the sediment flux necessary to balance the rate of accommodation generated by subsidence or eustatic sea level rise. For simplicity we assume a constant rate of accommodation generation, so the maintenance flux can be calculated from the plan-view area (A) and long-term aggradation rate: $Q_{acc}=A \cdot r$.

Given constant accommodation generation, Q_{acc}^* is constant for all time windows of measurement. However, autogenic variations in sediment transport efficiency cause perturbations on this long-term accommodation rate. These are caused by different rates of sediment bypass and retention, which Toby et al. (2019a) identified as the exponential Q_a^* function, i.e. the ATF. To approximate parameter Q_0^*, we assume that at very short timescales ($T^* \rightarrow 0$) all sediment can be captured within the environment of interest (Esposito et al., 2017). This gives $Q_0^*=Q_{in}^*-Q_{acc}^*$. We compare this field-estimate to Q_0^* calculated by a regression through high-resolution measurements of Q_a^*. Supplementary Table 4.2 shows that these two independent methods give fairly similar results.

Next, we estimate b based on the assumption that sediment capture efficiency decays exponentially to a long-term mean, and so Q_a^* approaches an asymptote at zero. In the supplementary material, we use three different experimental stages to explore the timescales at which $Q_a^* \approx 0$. We approximate this by the time (T_{95}) it takes to reduce the magnitude of Q_a^* by 95% from the maximum value (Q_0^*). The experiments, each with different autogenic behavior, suggest that this timescale is approximately 6-8 times longer than T_c, which results in $b \approx 0.4$. However, this long timescale is largely due to avulsions occurring at timescales similar to T_c in the experiments, while T_c is usually orders of magnitude longer than autogenic avulsion cycles in field-scale systems. Where autogenic processes are much shorter than T_c, a lower limit for the ATF to approach zero is set by T_c. This is because on timescales shorter than T_c, autogenic processes influence morphology by definition. Using $T_{95}=T_c$ gives $b \approx 3$ (see supplement). Estimates of avulsion timescales could thus take away some of the uncertainty in an approximation of b and thereby the ATF.

The above workflow allows an approximation of the ATF in ancient field-scale systems given that parameter values can be estimated in the absence of high temporal resolution. Difficulty will always remain in estimating Q_{in} (Allen et al., 2013b), which can be approximated from a long-term basin-wide sediment mass balance or by empirical methods such as the BQART equation (Syvitski and Milliman, 2007; Watkins et al., 2018). Estimation of T_c from field-scale systems, usually of the order of 10^4-10^5 yrs, is straightforward and involves measurements of r and H_c (Li et al., 2016; Trampush et al., 2017). As these values are spatially variable within an environment, the maximum value of H_c and minimum value of r in a system are used as this combination generates the most conservative estimate of allogenic signal preservation.

4.4. Field application

We apply our field approximation to two different field systems: the Pleistocene Kerinitis Delta system (KDS) in Greece and the Eocene-Oligocene Escanilla sediment routing system (ESRS) in northern Spain. The KDS represents a Gilbert-type fan delta succession, which accumulated in the hanging wall of a normal fault in Lake Corinth (Barrett et al., 2019). The ESRS represents several, isochronous depocentres that can be traced laterally from the proximal area of the Tremp-Graus basin in the east, to the distal area of the Ainsa and Jaca basins in the west, a sediment transport distance of over 200 km (Michael et al., 2014). The ESRS provides an opportunity to demonstrate the application of our methodology to a

system that experiences considerable sediment by-pass between each single depocentre within the SRS (Michael et al., 2014).

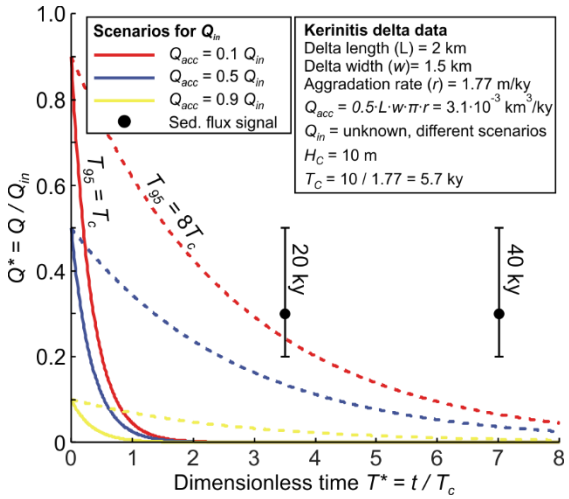

Figure 4.2. Threshold diagram for Kerinitis delta system (KDS).

Delta dimensions and subsidence rate are from Barrett et al. (2019) and channel depth from Backert et al. (2010). The total flux to the delta is unknown, so a range of Q_{acc}:Q_{in} values are explored. The lines show two scenarios for Q_a* to approach 0: a solid line for a scenario where T_{95}=T_c, and a dashed line for a scenario where T_{95}=8T_c. Black markers indicate hypothetical sediment supply signals of precession-scale (20 ky) and obliquity-scale (40 ky) with a magnitude of 0.3Q_{in}. Estimates of Milankovitch-scale supply variations range between 20% and 50% of Q_{in} (Blum and Hattier-Womack, 2009). Both signals exceed the threshold in most scenarios, except when long-term rates of sediment bypass are high and avulsion cycles on this Gilbert-type delta have a particularly long duration of the order of several ky.

We estimate the ATF for the KDS from published delta dimensions and accommodation rates (Figure 4.2). Barrett et al. (2019) speculated on obliquity-scale sediment supply signals, in addition to lake level oscillations at this periodicity. This allows us to predict whether sediment supply signals of this order exceed the stratigraphic transfer threshold using a hypothetical signal magnitude of 0.3Q_{in}, inspired by a 30% change in sediment supply in the area since the Last Glacial Maximum (Watkins et al., 2018) and estimates that Milankovitch cycles change sediment flux by 20-50% (Blum and Hattier-Womack, 2009). Because Q_{in} is unknown, we explore a range of different sediment retention scenarios (Figure 4.2). We also test two different scenarios for T_{95}, assuming that Q_a* approaches zero at timescales of T_c or 8T_c (b=3 and b=0.4 respectively). Regardless of the scenario, obliquity-scale (40 ky) cycles far exceed T_c. Precession-scale cycles (20 ky) exceed the threshold in most instances, except when sediment retention of the deltas is very low, and avulsion cycles are long, i.e. the order of T_c (5.7 ky). This is an unlikely scenario for this Gilbert-type delta. In fact, (Barrett et al., 2019) suggested avulsions on a decadal to centennial scale. Interpretations and models of the KDS

should thus account for signals of varying sediment flux, in addition to other allogenic forcings.

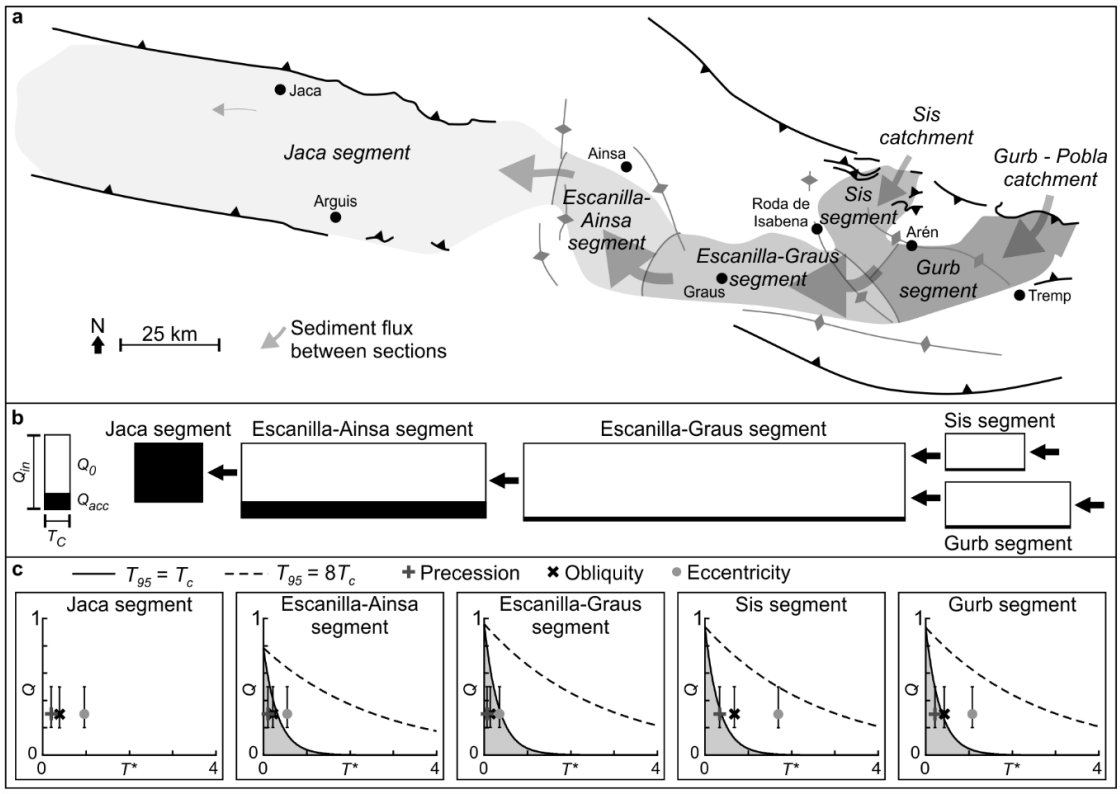

Figure 4.3. Escanilla sediment routing system between 39.1 and 36.5 Ma.

(**a**) Major structural features and sediment fluxes in the Escanilla SRS. Proximal to distal from right to left. Figure modified from Michael et al. (2014). (**b**) Schematic Escanilla SRS illustrates difference in T_c, Q_{in}, Q_{acc} and Q_0. Data in Table 4.1. (**c**) Field approximation of the stratigraphic transfer threshold function using data from Table 4.1 and examples of Milankovitch-scale signals (20ky, 40ky, and 100 ky), assuming a change in sediment supply rate of $0.3Q_{in}$ (range $0.2Q_{in}$ - $0.3Q_{in}$). Signals are transferred to the stratigraphic record if their combination of signal magnitude and duration plot above this line.

Table 4.1 Key data for calculations of transfer thresholds in the Escanilla sediment routing system, based on Michael et al. (2014).

	Gurb segment	Sis segment	Escanilla-Graus segment	Escanilla-Ainsa segment	Jaca segment
Member	Montsor 1 & 2	Sis 1 & 2	Middle Escanilla	Middle Escanilla	Upper Hecho
Environment	Alluvial fans	Alluvial fans	Fluvial	Fluvial	Shallow marine to deep marine lobes
Q_{in} (km³/My)	106	132	222	214	168
Q_{acc} (km³/My)	7	8	9	46	168
Q_{acc}* (-)	0.06	0.06	0.04	0.21	1
Z (m)	140	220	160	250	1000
r (m/ky)	0.054	0.085	0.062	0.096	0.38
H_c (m)	5 (assumed similar to Sis)	5 (typically 2-3 (Vincent, 1993))	17.5 (assumed similar to Ainsa)	17.5 (range 2.5-17 (Labourdette, 2011))	40 (estimates ~5-40 (Bayliss and Pickering, 2015))
T_c (ky)	93	59	284	182	104

The ESRS was divided into five individual segments (Figure 4.3a) by Michael et al. (2014) and these authors estimated the total flux into each segment (Q_{in}) and the flux retained within each segment (Q_{acc}, Table 4.1). This enables volumetric flux by-pass to be quantified at each segment boundary (Figure 4.3b). Using these estimates in combination with published aggradation rates (Michael et al., 2014) and channel depths (Vincent, 1993; Labourdette, 2011) we calculate the ATF for each segment of the ESRS for a time slice between 39.1-36.5 Ma (Figure 4.3C). We note that as there is no sediment flux out of the Jaca system the deposited volume faithfully matches the supplied sediment volume and the ATF for the entire Jaca system is effectively zero in this scenario.

We use the ATFs to evaluate the potential of each segment to store Milankovitch-scale signals with durations of 20 ky, 40 ky and 100 ky, again assuming a magnitude of $0.3Q_{in}$. For completeness, we plot two versions of the ATF. The highest threshold would occur if avulsion cycles are of a similar timescale as T_c, but this is unlikely for any of the segments. Therefore we discuss the more likely scenario where $T_{95} \approx T_c$. The thresholds predict that the 20 ky cycle will not be preserved in any of the segments, whereas the 40 ky and 100 ky cycles are transferred to the stratigraphic record of the Sis and Gurb segments (Figure 4.3C). The 40 ky cycles are not preserved in the Graus and Ainsa segments because T_c is much longer in these fluvial systems compared to the alluvial fans of Sis and Gurb (Figure 4.3B, Table 4.1). T_c is particularly long in the Graus segment, which may prevent stratigraphic storage of the 100 ky cycle.

4.5. Discussion

Our results demonstrate how the construction of ATFs for field successions provides an important, and unique, guideline for attempts to interpret of sediment supply signals from ancient field systems based on parameters readily obtainable from the field. A specific prediction of our framework, illustrated with the ESRS, is that the storage of supply signals is fundamentally influenced by both attenuation as signals propagate across the Earth's surface through SRSs, and by the spatial distribution of long term accumulation rates. The former is captured at the gross scale by diffusion models (Marr et al., 2000), and in terrestrial settings the latter is often set by regional subsidence gradients. So for passive margins, where subsidence often increases from source to sink, storage of signals in proximal settings might be difficult because of the limited accommodation production, whereas proximal accommodation production in foreland basins and hanging-wall basins enhances signal preservation.

The field-specific ATF can also be used for quantitative predictions of signal propagation from field data. This is because sediment flux signals travelling through a system are considered shredded if the sediment flux leaving a system does not preserve the input signal frequency (Jerolmack and Paola, 2010). For the Escanilla SRS, this means that a sediment flux signal that is shredded by one of the segments (e.g. precession cycles in the Sis and Gurb segments), cannot propagate through the landscape and influence more distal environments (e.g. the Jaca section). However, Toby et al. (2019a) showed that high-frequency signals that fall below the stratigraphic transfer threshold, and therefore would be considered stratigraphically shredded, are in fact transmitted through the geomorphic system prior to complete stratigraphic shredding. This means that although absent from the stratigraphy of a preceding segment, high-frequency allogenic sediment supply signals propagate to the next segment, where it may exceed the ATF and influence stratigraphy. As these signals travel through the SRS from source to sink, the original catchment signals will be increasingly modified by autogenic processes (Jerolmack and Paola, 2010) and attenuated (Paola et al., 1992). We suggest here that those landscapes affected by fast rates of supply change will tend to transmit these allogenic signals through SRS more effectively. Examples of landscapes that may facilitate fast rates of supply change, for example in response to glacial-interglacial cycles, are systems where links between catchment and basin are short and direct, such as the KDS. Given that larger catchments buffer high-frequency environmental signals (Castelltort and Van den Driessche, 2003), it is unlikely that high frequency sediment flux signals propagate through the sedimentary basins of large systems (e.g. Amazone, Mississippi), and such signals should thus not be expected in their stratigraphy.

The ATF is set by temporal differences in sediment capture efficiency. Sediment capture strongly depends on grain size, because fine grains have a longer advection length scale (Ganti et al., 2014). The assumption that all sediment can be trapped may thus not hold for the smallest grain sizes, which may bypass as wash-load even at very short timescales. Partitioning of grain-size could thus lead to overestimating the scaling parameters of the exponential. This could be accounted for in our approximation of the ATF by removing the sediment wash load component (Q_{wash}*) from Q_{in}* before calculating Q_0*: Q_0*= Q_{in}*-Q_{acc}*-Q_{wash}*. Estimating the wash load component is important for signal propagation through the landscape. Diffusional (Paola et al., 1992; Marr et al., 2000) and conceptual (Romans et al., 2016) models predict that sediment supply signals attenuate with distance. However, even when a sediment supply signal falls below our thresholds for signal propagation in a proximal segment, wash load grains could propagate the signal to more distal segments of the SRS system, where the same grains are no longer wash load. Here, fine grain

size classes may still hold significant flux signals exceeding the threshold for stratigraphic storage.

Validating the ATF with field data is difficult, because different allogenic forcings influence field systems simultaneously to sediment supply signals. In addition, the resolution of field data is limited, making the identification of sediment flux signals with a duration $\leq 10^5$ yr difficult. Field data for the KDS and the Gulf of Corinth indicates that the area has been particularly susceptible to climate cycles in the Pleistocene and later, and signals of varying sediment flux and relative sea level have been inferred from the stratigraphic record (Barrett et al., 2019; McNeill et al., 2019). This is in line with our prediction that Milankovitch-scale signals exceeded the ATF for the KDS (Figure 4.2). Field data for the ESRS suggest long-term change in sediment supply and subsidence rates related to regional tectonics (Whittaker et al., 2011). Superimposed on this, field evidence exists for precession and obliquity-scale sediment supply signals that propagated downstream to the submarine fans in the Ainsa and Jaca basins (Scotchman et al., 2015), even though our ATFs predict that such signals are stratigraphically shredded by upstream segments (Figure 4.3). The ATF thus suggests that these cycles may have been of autogenic origin. Alternatively, preserved sediment supply signals in these distal environments could indicate that the signals exceeded an acceleration threshold, enabling the propagation of signals. The propagation and preservation of these signals could also have been influenced by other types of signals (relative sea level, water discharge), which may have enhanced the propagation potential of sediment flux signals (e.g. Simpson and Castelltort, 2012). Although not conclusive, application of the ATF to the ESRS provides several hypotheses for the propagation and preservation of signals that may guide future field studies of the ESRS, and demonstrates a need for further research on the fate of environmental signals in sediment routing systems.

4.6. Conclusions

Our approximation of the ATF gives field stratigraphers a first quantitative basis to evaluate the role of sediment supply variation on the stratigraphic record. Numerical and physical models demonstrated the existence of autogenic thresholds on signal transfer, but application of these concepts to field systems is limited because of a lack of temporal and spatial resolution. Our work demonstrates how quantitative predictions on the transfer of sediment supply signals to the stratigraphic record can be made from field data of limited resolution. As such, this will improve our ability to test the stratigraphic record for the presence of environmental signals.

Acknowledgments

This study was supported by the National Science Foundation (grant EAR-1424312), the Natural Environment Research Council (NERC) EAO Doctoral Training Partnership (grant NE/L002469/1) and the University of Liverpool. We thank members of the Tulane Sediment Dynamics and Stratigraphy Lab for providing access to experimental data.

Supplementary information to Chapter 4

1. Experimental methods

We make use of three stages of physical delta experiments in the Tulane University Delta Basin (TDB). During each of these experimental stages an aggrading delta formed under constant conditions of sediment supply (3.91 x 10^{-4} kg/s), water discharge (1.72 x 10^{-4} m^3/s) and relative sea level (RSL) rise (0.25 mm/hr). The experimental stages all follow a similar layout, with one key difference between each of them: cohesion of the sediment mixture. Cohesion of the mixture is enhanced using a polymer that becomes adhesive when water is introduced (Hoyal and Sheets, 2009). Below and in Table 4.2 we describe key characteristics of the experiments based on analysis by Straub et al. (2015) and Li et al. (2017).

Table 4.2. Key experimental data.

	Experiment 1	**Experiment 2**	**Experiment 3**
Dataset name	TDB-12 stage 2	TDB-13 stage 2	TDB-13 stage 1
Run hours (hr)	385-1285	500-1000	75-300
Data source	(Li and Straub, 2017a)	(Li and Straub, 2017b)	(Li and Straub, 2017b)
Cohesion	Strongly cohesive	Weakly cohesive	Non-cohesive
H_c (mm)	12.2	7.0	2.3
T_c (hr)	49	28	9
Long-term mean sediment capture by delta (~Q_{acc})	53%	66%	73%
Empirical equation	$Q_a^* = 0.44\ e^{-0.43T^*}$	$Q_a^* = 0.47\ e^{-0.33T^*}$	$Q_a^* = 0.82\ e^{-0.40T^*}$
Empirical equation using only positive changes	$Q_a^* = 0.33\ e^{-0.49T^*}$	$Q_a^* = 0.46\ e^{-0.38T^*}$	$Q_a^* = 0.35\ e^{-0.18T^*}$
Empirical Q_0^*	0.33	0.46	0.35
Field approximation Q_0^*	0.47	0.34	0.27

Here we refer to experiment 1 for run hours 385-1285 of experiment TDB-12-1, which made use of a strongly cohesive sediment mixture (1.47 g polymer per kg sediment). This mixture produced channelized deposits which formed delta lobes that avulsed by backwater hydrodynamics (Hoyal and Sheets, 2009). Given H_c =12.2 mm and r=0.25 mm/hr, T_c is approximately 49 hr (Straub et al., 2015). This experiment served as the 'control experiment' in Toby et al. (2019a), which was used to construct the autogenic threshold function (ATF) of Figure 1B in the main text. Experiment 2 included run hours 500-1000 of experiment TDB-13-1 (Li and Straub, 2017b), which used a weakly cohesive sediment mixture (0.73 g polymer per kg sediment). Morphodynamic processes on this delta were similar to experiment 1, but T_c≈28 hr given that H_c=7 mm (Straub et al., 2015). Experiment 3 made use of a non-cohesive sediment mixture with no polymer. This produced a semi-circular delta dominated by sheet flow, but interrupted approximately every 50 to 100 hr by large incisional channels (Figure 4.4a). Experiment 3 consisted of run hour 75-300 of experiment TDB-13-1 (Li and

Straub, 2017b). We exclude the first 75 hr of experiment TDB-13-1 because the delta volume was low and may not have been in equilibrium with forcing conditions (Figure 4.4a). H_c, given by the 95th percentile channel depth, is 2.3 mm and so it follows that $T_c \approx 9$ hr (Straub et al., 2015).

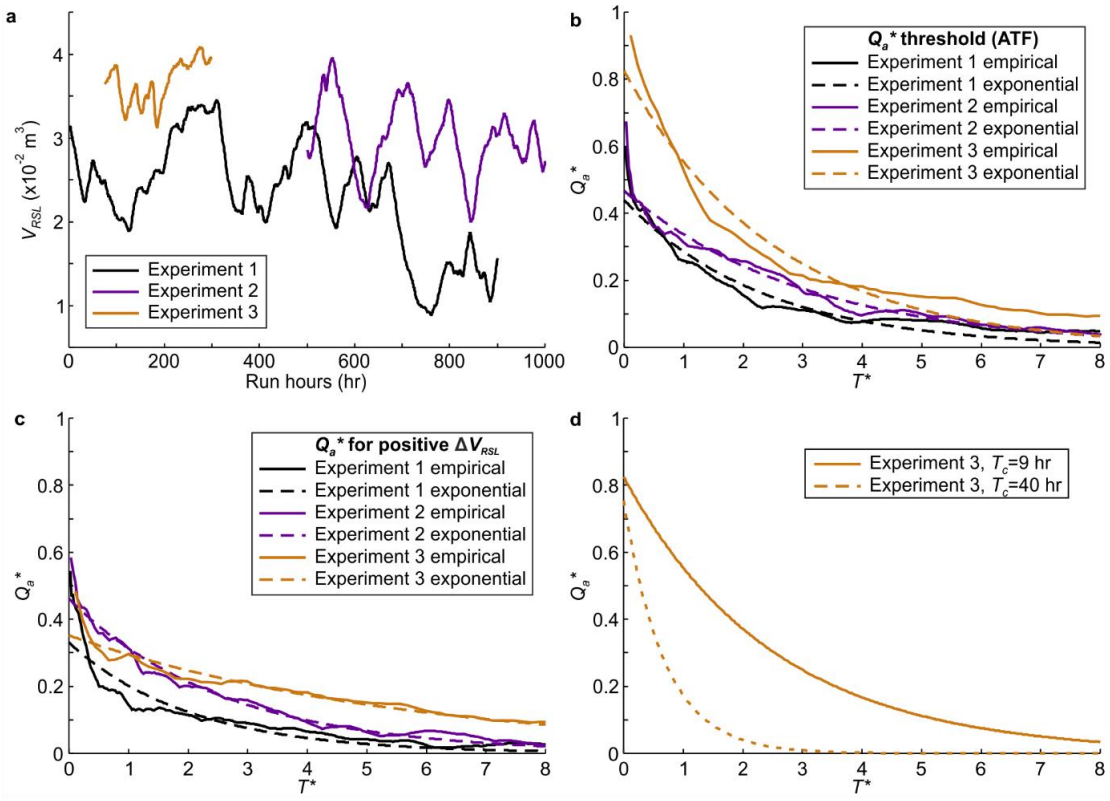

Figure 4.4. Calculation of Q_a* for each of the experiments.

(**a**) Terrestrial volume (V_{RSL}) defined as the volume of sediment stored above sea level. These time series are used to calculate Q_a* following methods outlined in (Toby et al., 2019a). (**b**) Maximum absolute rate of terrestrial volume change measured from a high-resolution dataset (solid line), and an exponential fit through the data for time windows up to $8T_c$ which gives the autogenic threshold function (ATF). Equations given in Table 4.2. Large-scale cycles in experiment 1 and 2 relate to lobe avulsions, but in experiment 3 these are generated by scouring channels. (**c**) Same as Figure b, but only using time windows of net positive terrestrial volume change. (**d**) Example of the Q_a* threshold in experiment 3 when a depth-estimate of the larger channels is used.

2. Autogenic threshold function (ATF) in the experiments

The autogenic threshold function (ATF) defined in Toby et al. (2019a) is calculated by measuring rates of autogenic volume changes for increasingly long time windows (Figure

4.4a). The maximum of these rates is Q_a*. The magnitude of Q_a* decreases with (T*) and is well described by an exponential function:

$$Q_a^* = Q_0^* e^{-bT^*} \quad \text{(Equation 1)},$$

where Q_0* is the intersect with the vertical axis (Figure 4.4b) and parameter b sets the decay rate of the exponential. We calculate this threshold function for each of the experiments (Table 4.2) and find that decay of Q_a* with T* is fairly similar for each of the experiments, except for experiment 3 (Figure 4.4b). At short timescales, experiment 3 shows much faster fluxes than the other two experiments. This may be caused by autogenic scours in experiment 3 that quickly erode large volumes of sediment (Figure 4.4a). Erosion is limited in experiment 1 and 2 because of the cohesive polymer. To test the possible effect of erosional events, we plot autogenic fluxes using time windows of net terrestrial volume (V_{RSL}) growth only. Figure 4.4c shows that this indeed takes away the large variation between experiments at short timescales. We note that shorter timescales are also more sensitive to measurement noise, which may explain relatively large deviations between the empirical data and the exponential regression (Figure 4.4c).

3. Field approximation of the ATF

For an approximation of the ATF for field systems, parameters Q_0* and b in equation 1 should be estimated from field data, which usually have low temporal and spatial resolution. For now, we focus on autogenic perturbations caused by excess sediment trapping. We approximate both parameters with a mass balance (Figure 4.5). Over long timescales, the allogenic sediment flux into the environment of interest (Q_{in}*) is split in two parts: a maintenance flux (Q_{acc}*) and bypass flux (Q_{bp}*). Maintenance flux is the sediment flux necessary to balance the rate of accommodation generated by subsidence or eustatic sea level rise. For simplicity we assume a constant rate of accommodation generation. This means that Q_{acc}* is constant and so the maintenance flux can be calculated from the plan-view area (A) and long-term aggradation rate: $Q_{acc}=A \cdot r$. The bypass flux, however, depends on the time window of measurement.

Over long time windows, the rate of accommodation generation is equal to the rate of sedimentation, as autogenic variations have leveled out at these long time windows. This means $Q_a^* \approx 0$ and $Q_{bp}^* = Q_{in}^* - Q_{acc}^*$. However, over short time windows $Q_a^* > 0$ because of autogenic variations in transport efficiency. The shape of the threshold tells us that the

maximum perturbation occurs for very short time windows, where T^* approaches 0. A theoretical maximum to Q_a^* occurs when all sediment is trapped within an environment, and thus $Q_{bp}^*=0$. This maximum value sets the intersect with the vertical axis, and thus gives us an estimate of Q_0^*. It follows that $Q_0^*=Q_{in}^*-Q_{acc}^*$.

Straub et al. (2015) analyzed each of the experiments used here and calculated long-term mean sediment capture rates of the deltas (Table 4.2), which we use as an estimate of Q_{acc}^*. Table 4.2 shows that our field approximation, given by $Q_0^*=Q_{in}^*-Q_{acc}^*$, gives a reasonable approximation to Q_0^* in the empirical exponential that uses positive volume changes only. The field approximation of experiment 1 is slightly lower than the empirical data, but this could be due to the general long-term negative trend in delta volume (Figure 4.4a) that reduces rates of positive volume change. Field estimates of Q_0^* for experiments 2 and 3 are slightly lower than the empirical functions suggest. The field estimates are based on average delta size, but higher rates of volume growth may occur at times where a delta is much smaller than the average size, leading to an underestimation of the threshold by our new field method. However, bearing in mind order of magnitude errors in sediment transport equations (e.g. Ma et al. (2017)), our field methodology approximates Q_0^* reasonably well.

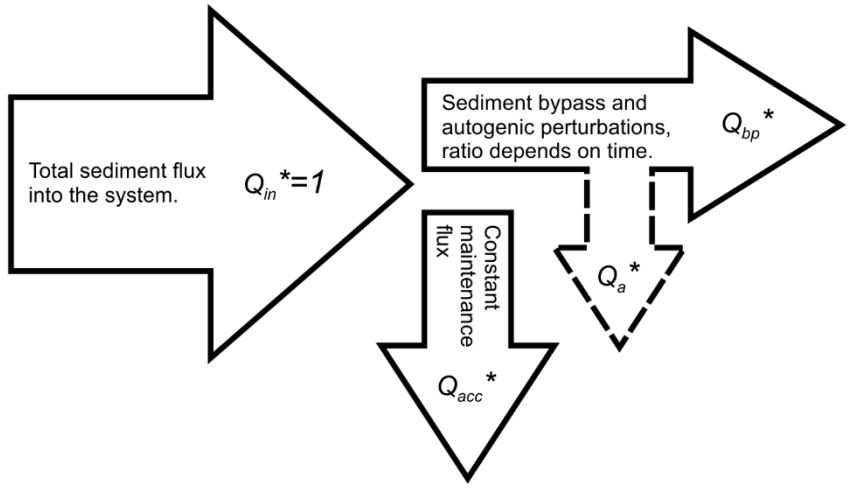

Figure 4.5. Schematic of sediment fluxes.

Part of the allogenic sediment flux into an environment is used to keep up with accommodation generation (Q_{acc}^*). The other portion may bypass (Q_{bp}^*) or generates perturbations on the long-term mean sedimentation rate (Q_a^*). The ratio between Q_{bp}^* and Q_a^* depends on the time window of measurement.

After estimating Q_0^*, parameter b is required to describe the exponential decay of the ATF. Any point on the ATF other than $T^*=0$ allows an estimation of b, and where field data allow this could be used to establish the ATF. In the absence of such data, we choose to approximate the timescale where the ATF approaches zero. Earlier we discussed that

autogenic perturbations average out over long timescales. In an exponential function this is given by an asymptote with $Q_a^*=0$. Inspired by the calculation of T_c as the 95th percentile channel depth to reduce the effects of rare extremes and measurement errors, we approximate a timescale (T_{95}) to reach the Q_a^*-asymptote to within 5% of the maximum threshold value, Q_0^*. In other words, T_{95} gives the point where the threshold value has reduced by 95% of the maximum value.

We use experiments 1 to 3 to investigate when Q_a^* moves towards asymptote. Even though the difference in cohesion generates very different morphodynamics, it appears that each of the experiments approaches the asymptote for timescales approximately 6-8 times longer than T_c (Figure 4.4b). Theoretically, T_c approximates the maximum time window of stochastic autogenic processes (Wang et al., 2011), but there may still be an autogenic flux resulting from the averaging over multiple autogenic cycles. For example, avulsion cycles in experiment 1 are of a timescale similar to T_c (Figure 4.4a), and so these cycles will only average out over timescales much longer than T_c. This is in agreement with other studies that conclude that autogenic processes completely level out at timescales required to build several channel depths worth of stratigraphy (Sheets et al., 2002), and the fact that it takes several avulsion cycles to approach a system as diffusive (Jerolmack and Sadler, 2007).

Most of the variability in terrestrial volume in experiment 1 and 2 relates to avulsion cycles, which are of a similar timescale as T_c. Avulsion cycles in field-scale delta systems are often at least an order of magnitude shorter than T_c. For example, Mississippi delta lobe avulsions occur roughly every 1.4 ky (Stouthamer and Berendsen, 2007), whereas T_c is approximately 200 ky (Li et al., 2016). The effect of avulsions may thus level out faster relative to T_c in field-scale systems than in laboratory experiments, and the most important autogenic process that changes delta volumes will be autogenic channel scouring.

Volume changes in experiment 3 are predominantly caused by autogenic oscillations between sheet flow and scouring channels. This suggests that even in systems where the largest autogenic processes are set by timescales of scouring, autogenic fluxes may exist at timescales several times longer than T_c. However, it should be noted that the volume changes in experiment 3 are mostly generated by channels with depths of 10 to 15 mm and occasionally even deeper, while H_c=2.3 mm was used to estimate T_c. This is because H_c is calculated as the 95th percentile channel depth, but it could be argued that the larger channels set the depth of reworking, and thus T_c (Wang et al., 2011). Using the deeper channels to estimate T_c would result in autogenic timescales that level out at timescales much closer to T_c. For example, a conservative H_c=10 mm for the larger channels in experiment 3 increases estimates of T_c to 40 hr. This effectively moves the dimensionless timescale at which autogenic processes level out much closer to T_c (Figure 4.4d). Therefore the timescales for

autogenic fluxes to level out may thus be much closer to T_c for field-scale systems where avulsion cycles are much smaller than T_c and the dominant autogenic scale is channel incision. Autogenic sediment fluxes occur by definition at timescales less than T_c, which means that T_c sets a minimum timescale for Q_a^* to approach 0.

To approximate the threshold, we could now state that the timescale at which the ATF approaches 0 is in the order of T_c or several times longer if significant autogenic processes (such as avulsions) generate cycles of volume change at timescales close to T_c. Using Equation 1, we estimate b by approximating the point where the ATF approaches the threshold to within 5%:

$$0.05\, Q_0^* = Q_0^*\, e^{-bT_{95}^*} \qquad \text{(Equation 2)}$$

$$b = -\frac{\ln(0.05)}{T_{95}^*} \qquad \text{(Equation 3),}$$

where T_{95}^* is T_{95} normalized by T_c. In a scenario where autogenic fluxes approach 0 in a time window of T_c, $b \approx 3$, while for the experiments, T_{95}^* is 6-8 times longer than T_c, and so this approximation suggests b is close to 0.4-0.5. We note that a better predictive understanding of the time windows at which long-term sedimentation rates persists will reduce uncertainty in approximating the ATF.

5. Delta morphodynamics and stratigraphy in the presence of sediment supply signals

Abstract

Sediment flux is an important control on morphodynamic processes in river deltas. Given constant rates of subsidence, an increase in sediment flux theoretically leads to increases in transport slope, system length, avulsion frequency, and channel mobility, whereas channel depth decreases and channel style may change. These processes in turn dictate stratigraphic architecture. In theory, this could be used to reconstruct Earth surface history, because sediment flux is influenced by climate, tectonics, and human activities. However, it may take up to 10^6 yr for sedimentary systems to equilibrate with changing forcing conditions. On shorter timescales, effects of changing sediment flux on geomorphology may be indistinguishable from stochastic internal dynamics of sedimentary systems (autogenics) that shape stratigraphy even in the absence of changing external (allogenic) forcing. Here we use laboratory experiments of aggrading deltas to test whether sediment supply cycles (SSCs) to the deltas generate a detectible signal in delta morphodynamics. Each of the four SSCs tested here has a different combination of signal duration and magnitude of change. We find that most landscape dynamics are dominated by irregular avulsions cycles, which obscure a geomorphic expression of the SSCs. However, signals with high rates of sediment supply change (signal acceleration) generate subtle cyclicity in landscape evolution. Long signals with low acceleration generate deep channels, but are ineffective in transmitting cyclicity to the landscape. The results of this work suggest that landscapes may record high-frequency environmental signals, although many characteristics of the stratigraphic record are predominantly the result of autogenic processes.

5.1. Introduction

The rate of sediment supplied from catchments to sedimentary basins imparts key information about environmental forcing conditions such as climate, tectonics, and human activities (Syvitski and Kettner, 2011; Allen et al., 2013b; Romans et al., 2016). Although numerous studies have shown that catchments and sediment transport systems buffer sediment flux signals (Castelltort and Van den Driessche, 2003; Armitage et al., 2013; Forzoni et al., 2014; Li et al., 2018), long-term changes in climatic and tectonic conditions can theoretically generate signals of varying sediment flux through sediment routing systems (Allen, 2008a; Romans et al., 2016). This is because catchment erosion and sediment transport relate to climatic forcing (Tucker and Slingerland, 1997; Braun et al., 2015; Mason and Romans, 2018) and the long-term balance between tectonic uplift and denudation of mountain catchments (Bonnet and Crave, 2003). Signals of varying sediment supply stored in the stratigraphic record may therefore inform us of past environmental change.

Stratigraphic architecture is often still interpreted in terms of external (allogenic) forcings without due consideration of the undoubted impact that autogenic processes can have on stratigraphic architecture. As a result, the interpretation of strata and sedimentary architecture is still debated (Hilgen et al., 2015; Muto et al., 2016; Paola, 2016). In part, this is because (1) sediment flux is notoriously difficult to measure or reconstruct (Allen et al., 2013b); (2) the interaction of autogenic dynamics with allogenic forcing, which leads to signal buffering of short-term sediment flux signals by processes of sediment transport, deposition, and erosion (Paola et al., 1992; Dade and Friend, 1998); and (3) complicated stratigraphic architecture is produced even under constant allogenic forcing conditions, over a wide range of temporal and spatial scales, including scales typically associated with external signals (Muto et al., 2007; Wang et al., 2011; Paola, 2016; Hajek and Straub, 2017; Burgess et al., 2019). This is because sediment transport and deposition in the landscape are self-organised as a consequence of local transport thresholds and flow dynamics (Beerbower, 1964; Van De Wiel and Coulthard, 2010; Jerolmack, 2011). These morphodynamic processes internal to sedimentary systems (autogenics) have limited our ability to unambiguously relate landscape morphology and stratigraphic architecture to environmental signals. In fact, when scales of allogenic signals and autogenic processes coincide, stochastic processes in landscape evolution may destroy or 'shred' allogenic signals, inhibiting their transfer to the stratigraphic record (Jerolmack and Paola, 2010; Li et al., 2016).

Nonetheless, field observations clearly support the existence of sediment flux signals over a range of scales, from floods and seasons (Wulf et al., 2010) to long-term climate change (Overeem et al., 2001; Foreman et al., 2012; Picot et al., 2019) and tectonics (Leeder, 2011).

It is well known that sediment flux sets the rates and scales of morphodynamic processes that in turn shape the stratigraphic record. In fluviodeltaic environments, for example, a positive correlation exists between sediment flux and river channel mobility, overbank flooding and avulsion frequency (Reitz and Jerolmack, 2012; Wickert et al., 2013; Shen et al., 2015). An increase in sediment flux will also prograde the shoreline location (Schlager, 1993) and grain size fronts (Marr et al., 2000), and increase the transport slope (Parker et al., 1998; Whipple et al., 1998). However, each of these theoretical relationships only effectively predicts long-timescale averages because autogenic processes create a range of scatter for any given sediment flux (Parker et al., 1998; Jerolmack and Mohrig, 2007). As a consequence, only long-term signals, in the order of 10^3-10^5 yrs, will equilibrate with supply conditions (Paola et al., 1992; Castelltort and Van den Driessche, 2003). Shorter signals will be distorted but may still influence landscape morphodynamics.

Several recent investigations demonstrate that in order for a periodic allogenic signal to be preserved in the stratigraphic record, the signal should exceed thresholds set by timescales and magnitudes of autogenic processes (Jerolmack and Paola, 2010; Li et al., 2016; Toby et al., 2019a). Below these thresholds, the signal frequency is spread out over other frequencies by autogenic sediment storage and release to such degree that it cannot be distinguished from autogenic dynamics (Jerolmack and Paola, 2010). The shredding thresholds predict a lower limit for allogenic signals to transfer to landscapes in terms of deposited volumes, but we currently do not know if and how periodic variations of a certain magnitude and duration produce a landscape morphology that is significantly different from purely autogenic morphology. This is critical for identifying signals in the stratigraphic record given the difficulties in reconstructing fluxes from stratigraphic data of limited spatial and temporal resolution (Allen et al., 2013b).

Periodic sediment supply signals of different durations and magnitudes may transfer to the landscape in different ways. Sediment supply signals of different magnitude may generate distinctly different morphology given that morphodynamic processes scale to the rate of sediment supply, and thus also to the magnitude of supply change (e.g. Bryant et al. (1995); Ashworth et al. (2004)). Signal duration may play a role because it takes time for a landscape to respond and equilibrate to changing forcing conditions, which increases the transfer potential for low-frequency signals (Paola et al., 1992; Castelltort and Van den Driessche, 2003; Allen, 2008b; Somme et al., 2009). However, high frequency signals may also modify landscape dynamics, because the rate of supply change (acceleration) seems to play an important role in landscapes dynamics (Sadler and Strauss, 1990a; Postma, 2014; Toby et al., 2019a). An acceleration threshold for the transfer of supply signals to landscapes may exist where sediment supply changes faster than the existing morphology can accommodate

that change (Toby et al., 2019a). Fast supply change would thus drive morphological change, but deposits produced by high frequency signals may not be thick enough to withstand erosion prior to permanent burial in the stratigraphic record.

Here, we test if and how periodic sediment supply signals that exceed the limits of autogenic scales, as defined in Toby et al. (2019a), also produce a recognisable morphological change in the landscape. To do so, we use physical models of aggrading deltas forced with different sediment supply histories. We analyse a range of different landscape processes and characteristics that theoretically relate to the rate of sediment supply, but may be obscured by stochastic autogenic dynamics. The results of this work demonstrate that a combination of signal magnitude, duration and acceleration determines how sedimentary systems accommodate sediment supply signals, and provides guidelines for the interpretation of ancient environmental signals from stratigraphy and predictions of future landscape change.

5.2. Methods

5.2.1. Experimental methods

We make use of the five stages of physical experiments presented in Toby et al. (2019a), which consisted of aggrading deltas formed under similar forcing conditions except for the rate of sediment supply. Experiments were conducted in the Tulane University Delta Basin (TDB), which is 4.2 m long, 2.8 m wide and 0.65 m deep. The basin floor initially consisted of a flat layer of coarse sand. Water level in the basin was controlled to submillimetre resolution through a computer-controlled weir that is in hydraulic communication with the basin. The computer also controlled the rate of water and sediment supplied to the basin. A mixture of water and sediment entered from a point source, which was fixed in horizontal directions but free to move up and down by erosion and deposition. Water was dyed blue to visualise flow paths on the delta. The sediment mixture mimicked earlier experimental work (Hoyal and Sheets, 2009). Grain sizes ranged from 1 to 1000 μm with a mean of 67 μm and a polymer was added to the mixture to enhance sediment cohesion. A quarter of the coarsest sand fraction was coloured red to highlight grain size variations.

Evolution of the delta was closely monitored with a FARO Focus3D-S 120 laser scanner that captured the topography of the terrestrial and shallow marine delta once per hour. These data were gridded on a horizontal grid with 5x5 mm cells with a vertical resolution of less than 1 mm. The topographic scans were stacked and clipped for erosion to create a 'synthetic stratigraphy' of preserved timelines (Martin et al., 2009a). RGB colour data

were co-registered with the scans. Every 15 minutes an overhead photograph was taken, which was used to create time-lapse videos of the experiments. After each experiment, stratigraphic cross-sections were made at locations 0.7 and 1.1 m from the apex by freezing sediment onto a 1.2 m wide panel.

In this manuscript we compare morphodynamic processes of four experimental stages of variable sediment flux with an experimental stage of constant sediment flux. We refer to the final 900 h in experiment TDB-12-1 (Li and Straub, 2017a) as the control stage, during which water level in the basin was rising at a constant rate of 0.25 mm/hr to generate accommodation space, analogous to relative sea level (RSL) rise. Water discharge (Q_w) was kept constant at 1.7 x 10^{-4} m^3/s and sediment feed rate (Q_s) at 3.9 x 10^{-4} kg/s. The balance between sediment supply and RSL rise generated an aggrading delta of consistent size (~1.1 m from the feeding point) with only autogenic variations in shoreline position. The other four stages are based on the control stage, with the same forcing conditions except for sediment flux into the basin (Q_{in}), which followed a sine-wave pattern. The amplitude and period of supply cycles was scaled to time and space scales of autogenic dynamics in the control stage (Table 5.1). Theory detailing the scaling of the sediment supply cycles (SSCs) was outlined in Toby et al. (2019a).

Table 5.1. Key parameters for each stage, modified from Toby et al. (2019a).

	Control	LMSP	LMLP	HMSP	MMLP
Experiment	TDB-12-1	TDB-16-1	TDB-16-2	TDB-16-3	TDB-16-3
Data	(Li and Straub, 2017a)	(Toby and Straub, 2019a)	(Toby and Straub, 2019b)	(Toby et al., 2019b)	(Toby et al., 2019b)
Run time (hr)	385-1285	140-630	140-630	140-385	385-875
Q_w (l/h)	618	618	618	618	618
$\bar{r}$ (mm/h)	0.25	0.25	0.25	0.25	0.25
Mean Q_s (kg/h)	1.41	1.41	1.41	1.41	1.41
T_s (hr)	-	24.5	98	24.5	98
Q_s (kg/hr)	-	0.22	0.22	0.87	0.43
Q_s*	-	0.5	0.5	2	1
T_s*	-	0.5	2	0.5	2
S*	-	1	0.25	4	0.5

5.2.2. Scaling of the sediment supply signals

The duration and magnitude of sediment supply cycles is scaled to characteristic autogenic parameters, both to ease comparison with field-scale systems and to systematically test the stratigraphic transfer threshold presented by Toby et al. (2019a). The scaling of signal magnitude is based on autogenic variations in the amount of sediment stored above sea level.

This terrestrial volume (V_{RSL}) varies by autogenic variations in sediment capture versus bypass on the delta. Sediment flux is scaled to M, defined as the fastest rate of V_{RSL} change measured over a consistent phase of terrestrial volume increase or decrease in the control stage. M is 31% of the mean sediment supply rate. Peak-to-peak signal amplitude (Q_s) of the SSC is scaled relative to M to create a dimensionless sediment flux: $Q_s^*=Q_s/M$ (Table 5.1).

Time (t) is made dimensionless (T^*) using the compensation timescale (T_c; Wang et al. (2011)): $T^*=t/T_c$. T_c approximates the time window over which autogenic processes average out and marks the transition from stratigraphy dominated by autogenic processes to stratigraphy controlled by changing allogenic forcing conditions (Straub and Wang, 2013). This timescale is set by the time it takes for deposition to fill in accommodation evenly, which is quantified by the standard deviation of sedimentation/subsidence (σ_{ss}; Straub et al. (2009)):

$$\sigma_{ss}(T_w)=\left(\int_0^W \frac{r(T_w,x)}{r(x)}-1\right)^{\frac{1}{2}},$$

where $r(T_w,x)$ is the local sedimentation rate measured over a time window T_w at distance x into the basin, $r(x)$ is the long-term average sedimentation rate at this point in the basin and W is the width of the cross-section. The decay of σ_{ss} follows a power-law as a function of T_w (Straub et al., 2009):

$$\sigma_{ss}=aT_w^{-\kappa},$$

where a and κ are coefficients. The value of κ describes to what degree deposition fills in topographic lows. Over short timescales, deposition tends to stay in one location, for example by a fixed channel belt. For a long timescale of observation, lateral migration of the sediment transport network over the basin fills in accommodation more evenly over the basin width. Over increasingly long timescales, this means that κ will shift from $\kappa<1$ to $\kappa\approx1$. The cross-over between $\kappa<1$ and $\kappa=1$ marks T_c (Straub et al., 2009). This is the maximum time window over which stochastic autogenic processes spread sediment non-uniformly over the basin. T_c can be approximated by $H_c/\bar{r}$, where H_c is the maximum topographic roughness, approximated by the depth of larger channels, and $\bar{r}$ the long-term aggradation rate, which equals the RSL rise rate in the experiments (Wang et al., 2011). Using the 95th percentile channel depth to estimate H_c=12.2 mm in the control stage, (Li et al., 2016) approximate T_c=49 hr, which we also use in our study. The equivalent timescale in field-scale river systems is in the order of 1 ky to several 100 ky (Li et al., 2016).

The values of T_c and M in the control experiment are used to scale four experimental stages with SSCs, each with a different combination of amplitude and periodicity (Table 5.1). Dimensionless signal acceleration follows from the ratio of signal magnitude and period: $S^*=Q_s^*/T^*$. The naming scheme of the experiments is an acronym for the sediment supply signals present during that stage: LMSP (Low Magnitude Short Period), LMLP (Low Magnitude Long Period), HMSP (High Magnitude Short Period), and MMLP (Medium Magnitude Long Period).

5.3. Results

5.3.1. General description of the experiments

The experimental deltas formed by a wide range of autogenic processes as described in other studies on experimental deltas and natural systems (Hoyal and Sheets, 2009). Typical avulsion cycles for the cohesive sediment mixture used in our experiments start with a new channel that follows a steep path into the basin, resulting in a straight channel prograding far into the basin. The maximum distance these lobes reach is similar for all lobes as it is limited by the development of mouth bars that force flow to bifurcate. The channels fill backwards as bifurcations progressively move upstream, while at the same time crevasse splays deposit around the main channel. This process continues until the lobe is backfilled sufficiently for flow to be routed through one of the crevasses to a new topographic low, causing a compensational stacking pattern of delta lobes.

In the next sections, we analyse rates of morphodynamic processes (avulsion, mobility of the transport system, deposition rate) and geomorphology (shoreline position, transport slope, channel depth, number of channels) for each of the experiments. In each section, we describe and test a theoretical relationship between sediment supply and some aspect of delta evolution. However, our analyses will show that stochastic autogenic processes may complicate these theoretical relationships.

5.3.2. Avulsion time scales

Avulsions are a key process that drives the large-scale architecture of fluvial stratigraphic successions (Slingerland and Smith, 2004; Stouthamer and Berendsen, 2007). Although stochastic variations in the timing and location of avulsions may conceal the effects of varying

sediment flux (Mackey and Bridge, 1995; Jerolmack and Paola, 2010), previous work predicts that the avulsion frequency is a function of sediment supply (Bryant et al., 1995; Ashworth et al., 2004; Ashworth et al., 2007; Reitz et al., 2010). Theoretically, transport slopes increase when sediment supply increases relative to water supply (Parker et al., 1998; Whipple et al., 1998) and channel beds may aggrade by an increase in sediment flux (Exner, 1925; Paola and Voller, 2005; East et al., 2018). Aggradation and super-elevation of channels trigger avulsions (Mohrig et al., 2000) and so it could be expected that avulsions preferentially occur during high supply. Decreasing sediment supply leads to incision, which stabilises channels and causes a potential drop in avulsion frequency. In addition, Toby et al. (2019a) suggested that fast change in supply conditions can push the transport system out of equilibrium, which means avulsions may occur more frequently around mean supply conditions, when the rate of supply change is fast.

In the supplementary material we describe a method for defining the timing of channel avulsions. This method allows us to approximate the duration of inter-avulsion phases (T_a, Figure 5.1). T_a in all of the stages used in this study ranged between 7 and 124 hr, with a mean duration ($\overline{T}_a$) of 44 hr (0.9 T_c; Table 5.2) and a median ($\widehat{T}_a$) of 40 hr (0.8 T_c). The variation between each of the experimental stages is large, with $\overline{T}_a$ ranging from 36 to 58 hr. We use a t-test to demonstrate that, given the wide range of inter-avulsion durations, $\overline{T}_a$ of the cyclic stages is statistically not different from the control stage (a=0.05; Table 5.2).

Next, we test our hypothesis that avulsions occur preferentially during high supply. To do so, we mark the timing of avulsions on the sediment supply curves in Figure 5.1a. In all experimental stages, avulsions occur during all stages of sediment supply. We count the number of avulsions during high supply (Q_{high}) and low supply (Q_{low}). Stage LMSP suggests that avulsions preferentially occur during low supply (Table 5.2). In contrast, in stage LMLP more avulsions occur during high supply, although many of the avulsions occur close to mean supply conditions. Stage HMSP has the highest amplitude signal, yet just 4 out of 7 avulsions occur during higher than average supply. Stage MMLP is also spread quite evenly again. For all experiments combined, 19 out of 37 avulsions are during high supply and so we conclude that there is no evidence for avulsions primarily occurring during phases of high supply in these experiments.

We investigate a potential link between the timing of avulsions and the rate of supply change by splitting the supply curve into two regimes of equal total duration. The first regime comprises that part of the sediment flux signal that is within plus or minus 50% from peak amplitude, characterised by fast supply acceleration. The second regime covers the slowly changing sediment flux regime, where flux conditions are closer to peak or trough conditions than mean supply. Table 5.2 shows the number of avulsions during high supply acceleration

(S_{high}) and during low supply acceleration (S_{low}). Avulsions are spread quite evenly over high and low acceleration phases for each experiment. Again, we conclude that there is no link between the timing of avulsion and the supply curve.

Finally, we count the number of avulsion occurring when supply increases (Q_{inc}) versus when supply decreases (Q_{dec}). Both LP stages have a similar number of avulsions during phases of supply increase and decrease (Table 5.2). Most avulsions in stage LMSP occur during decreasing sediment supply, and during increasing supply in stage HMSP. Combined, 19 avulsion occur during increasing supply, 18 during decreasing supply. Given that the SP experiments have opposite trends and the LP experiments are relatively evenly distributed, there is no deterministic relation between the supply curve and the ratio of Q_{inc} and Q_{dec}. We conclude that there is no link between the rate of supply change and avulsion timing in our experiments.

Now we have ruled out a direct link between avulsions and the sediment supply signals, we check for temporal trends in T_a. Figure 5.1b suggests a general increase in avulsion frequency in the longer experiments: TDB-16-3 (HMSP and MMLP) and in particular TDB-12-1 (control stage). This may be caused by an autogenic process known as auto-retreat (Muto and Steel, 1992; Muto, 2001), which is a long-term transgression on the delta as a consequence of increasing foreset height due to continuous RSL rise. The volume of sediment required to build foresets increases, which causes a decrease in propagation rates. As avulsions occur where a more efficient transport slope is found, decreasing propagation rates means a slower decrease of the transport slope and thus an increase of the inter-avulsion timescale (Edmonds et al., 2009; Bijkerk et al., 2016). Note that the control stage covers the final 900 hr of a 1285 hr long experiment, whereas other experiments do not exceed 875 total run hours (Table 5.1), and so the auto-retreat effect is strongest in the control stage.

Table 5.2 Avulsion statistics.

	Control	LMSP	LMLP	HMSP	MMLP	All
$\overline{T_a}$ (hr)	46.6	53.3	36.7	36.2	57.7	44.4
$\widehat{T_a}$ (hr)	38.0	54.5	37.0	29.5	53.0	40
σ_a	29.5	18.8	11.1	19.2	23.5	22.8
P (t-test)	-	0.52	0.24	0.37	0.37	-
Q_{high}	-	3	8	4	4	19
Q_{low}	-	6	4	3	5	37
S_{high}	-	4	6	4	5	19
S_{low}	-	5	6	3	4	18
Q_{inc}	-	2	7	5	5	19
Q_{dec}	-	7	5	2	4	18

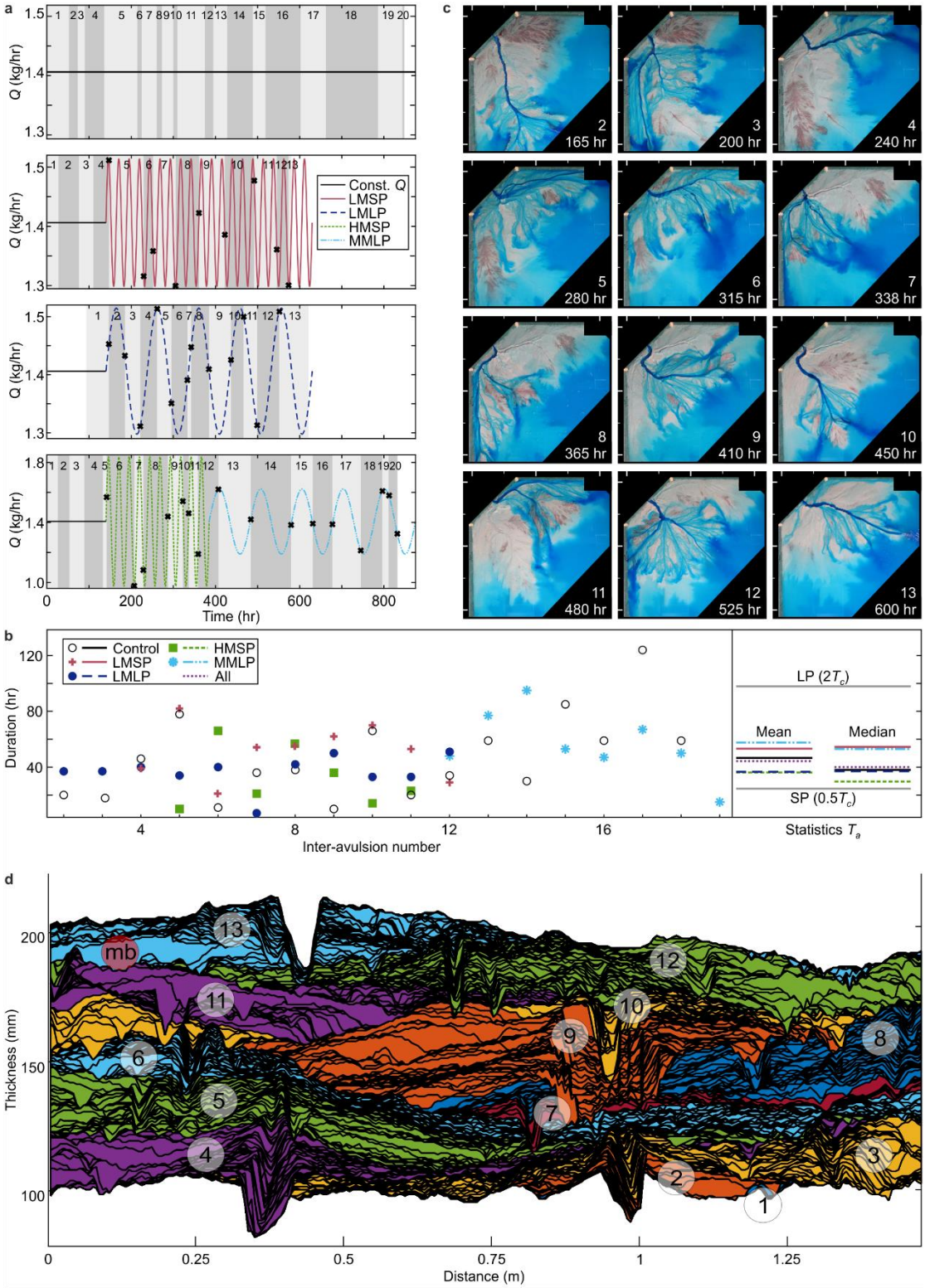

Figure 5.1. Avulsion timescales.

(**a**) Duration of inter-avulsion phases in each of the experimental stages. The background shading of these figures changes at the moment an avulsion occurs, as determined by methods detailed in the supplement. The timing of avulsions is indicated with a black marker on the sediment supply curve (Q) to visualise the timing of an avulsion relative to the sediment supply curve. (**b**) Duration of inter-avulsion phases (T_a). Each of the phase numbers is indicated in Figure a. Mean and median T_a are shown on the right. Only complete

inter-avulsion phases are used in the calculation of mean and median T_a. The duration of the short period (SP) and long period (LP) supply signals are given for reference. (**c**) Overhead images for each of the inter-avulsion phases of the LMLP stage. Numbers correspond to Figure a. (**d**) Synthetic stratigraphic section through experimental stage LMLP at 0.5 m from the delta apex, as if looking down the transport direction. Black lines represent preserved timelines at a 1 hr interval. Various colours represent each of the inter-avulsion phases shown and numbered in Figure a. mb=mouth bar deposit (top left).

5.3.3. Avulsion stratigraphy

Avulsions play an important role in stratigraphic architecture. Compensational stacking, the tendency for deposits to fill topographic lows, distributes channel belts over a landscape. As a consequence, the stacking density of channel belts relates to avulsion frequency and aggradation rate, with a higher density expected for low aggradation rates and high avulsion rates (Allen, 1978; Leeder, 1978; Bridge and Leeder, 1979; Hajek et al., 2010). However, autogenic variations in the location and timing of avulsions may cause a hierarchy of avulsions, leading to an autogenic clustering of channel belts in stratigraphy (Mackey and Bridge, 1995; Hajek et al., 2010). Our analysis showed that autogenic processes generate a wide range of inter-avulsion durations (Figure 5.1a-b), and those avulsions have a range of different lateral shifts (Figure 5.1c). To visualise how this behaviour translates into stratigraphic architecture, we link our observations of avulsions on the surface to a cross-section of synthetic stratigraphy at 0.5 m from the delta apex (Figure 5.1d). This location is at the downstream end of the area analysed for our avulsion timescale analysis and should thus demonstrate variation that correlates directly to the inter-avulsion frequency.

The images in Figure 5.1c and synthetic stratigraphy in Figure 5.1d show that lateral shift by avulsions varies widely. For example, phases 4-5-6 have a very limited shift in channel location. Together, these form a lobe that remained on one side of the basin for 114 hr. This demonstrates that channel avulsions stack compensationally at a local scale, while compensational stacking of lobes occurs at a larger basin-wide scale. This creates a hierarchy in stacking patterns. Stacking of phase 4-5-6 is compensational at a local level, but anti-compensational at a basin-wide scale. Delta lobes stack compensationally at the basin-wide level and may involve several channel avulsions. As a consequence, lobe-scale inter-avulsion timescales may be longer than channel-scale avulsions. However, many channel avulsions in the experiments have a larger lateral shift (Figure 5.1c-d), and these channel avulsions form individual lobes. For example, each of the channel avulsions of phases 10-11-12 is also a lobe-scale avulsion, which formed over timescales of 33, 33, and 52 hr respectively. It takes approximately 2 to 3 lobe avulsions to cover the entire cross-sectional width.

5.3.4. Mobility of the transport system

We discussed how channel aggradation during high sediment supply may cause an increase in avulsion rate, but found no link between the timing of avulsions and sediment supply conditions. Although timescales of large avulsions on the deltas may not change systematically in response to the sediment flux signal, smaller scale autogenic processes may reveal the sediment supply curve. For example, overbank flow and crevasses may also be more common during high sediment supply because of in-channel aggradation. In addition, the rate of lateral channel migration increases with an increase in sediment supply (Wickert et al., 2013).

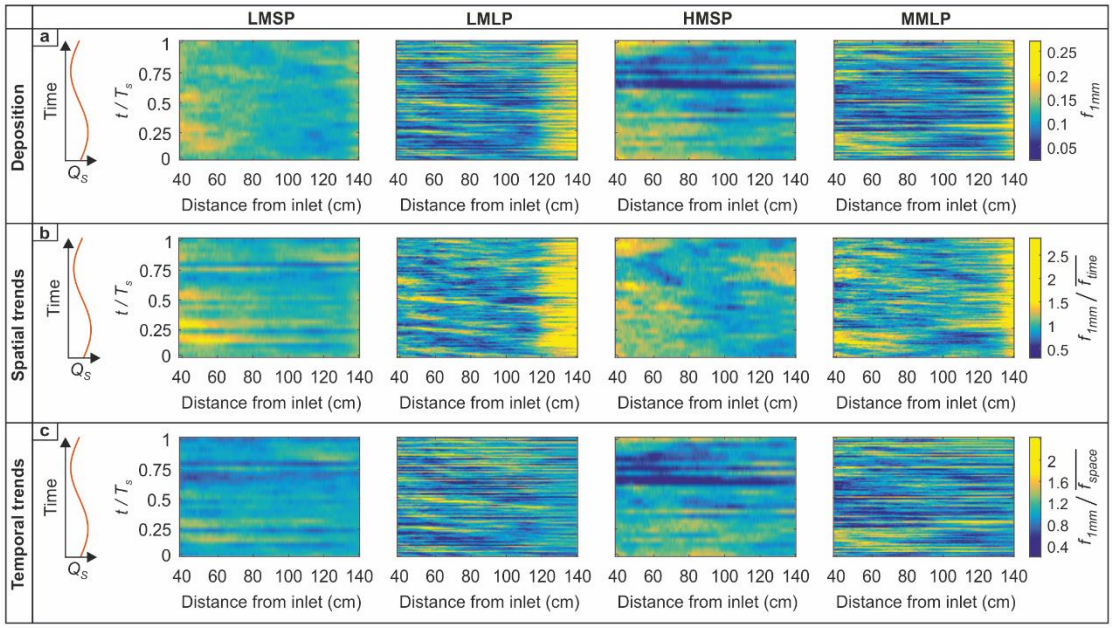

Figure 5.2. Sediment transport system mobility.

(**a**) The fraction of a transect that deposited more than 1 mm in 1 hr. Details in text. Time in the diagrams is presented as fraction of a complete supply cycle (t/T_s) and lines up with the schematic supply cycle on the left. (**b**) Data of Figure 5.2a where each pixel value is normalised by the mean of the row. This highlights spatial trends. (**c**) Data of Figure 5.2a where each pixel value is normalised by the mean of the column. This highlights temporal trends.

Inspired by Yu et al. (2017), we construct diagrams that visualise spatial and temporal variations in the mobility of the sediment transport system (Figure 5.2). To make these diagrams, we create a semi-circular cross-section where all points of the section are at the same distance from the inlet. We then measure the proportion of that section that was actively depositing sediment by calculating the fraction of the grid points in a section where more

than 1 mm of deposition occurred in one run hour (f_{1mm}). The 1 mm threshold excludes noise in the topographic scans. We repeat this for sections at increasing distance from the inlet, with steps of 5 mm each time, and for all run hours of the experimental stage. Next, we create a mean cycle by averaging the results of every point on the supply cycle. The result is a mean f_{1mm} for every stage of a supply cycle ($\overline{f_{1mm}}$, Figure 5.2a). To highlight spatial trends, we normalise $\overline{f_{1mm}}$ by the mean value of each row in Figure 5.2a: ($\overline{f_{time}}$). Temporal trends are emphasised by normalising $\overline{f_{1mm}}$ by the mean of each column in Figure 5.2a: ($\overline{f_{space}}$). Results of the normalisations are shown in Figure 5.2b and c.

Deposition was more widespread during high supply than during low supply in stage LMSP (Figure 5.2c). This may occur by increases in overbank flow, channel mobility and number of channels. High supply mainly affects proximal regions (Figure 5.2b). This may be because the absolute change in sediment supply is largest proximally, before flow splits and spreads out over the delta. Additionally, a supply increase also increases the equilibrium slope of the transport system (Parker et al., 1998) and thus available accommodation, which allows proximal deposition. Low supply has the opposite effect: a decrease in equilibrium slope could be achieved by bypass or erosion proximally and progradation of the shoreline. Supply cycles will thus not necessarily lead to a shoreline response by progradation during high supply, or retrogradation during low supply, as may be expected from a simple mass-balance. Instead, the transport slope will adjust first, and shoreline progradation and retrogradation may follow after the slope has reached a new equilibrium. A shoreline response in line with supply signals is thus more likely for signals with a long duration; that is signal durations that exceed the equilibrium timescale of the system (Paola et al., 1992).

The pattern in stage HMSP is similar to LMSP. Deposition is least extensive during low supply. The effect of proximal deposition during high supply and bypass during low supply is much more pronounced here, with widespread distal deposition during lowest supply (Figure 5.2b). Interestingly, Figure 5.2c shows most deposition occurs when the supply rate accelerates quickly, i.e. at the start and end of the sine wave. At this time, accommodation space according to the equilibrium profile may have been underfilled during lower supply, which facilitates rapid proximal infill during supply increase.

Stage MMLP shows a clear phase shift ($0.25t/T_s$) between the supply cycle and the response of $\overline{f_{1mm}}$. Supply decrease correlates with low $\overline{f_{1mm}}$ values, whereas deposition is more widespread when supply increases (Figure 5.2c). Like stage HMSP, accommodation seems to control to what degree supply can modify f_{1mm}. However, the change in supply in MMLP is much slower (S^*=0.5, Table 5.1), which means that while supply is increasing, deposition can more closely keep up with the change in potential accommodation set by the equilibrium

profile. When supply rates decrease again, proximal accommodation potential is limited. Right after peak supply, equilibrium slope decreases, and the sediment flux will mainly be accommodated distally (Figure 5.2, MMLP).

Most of the LMLP supply cycle (0 – 0.75 t/T_s) shows variations in $\overline{f_{1mm}}$ that are seemingly uncorrelated to patterns of supply and accommodation. Higher values during the last part of the supply cycle may be consistent with widespread deposition filling in accommodation created during low supply (Figure 5.2c). Inaccuracies in the measurements of submerged topography in the distal section cause high values in the distal section.

To conclude, this data analysis reveals systematic trends in the mobility of the sediment transport network in response to all supply cycles, except for LMLP. The exact effect of supply cycles is a consequence of the magnitude and duration of supply cycles in relation to potential accommodation. As the equilibrium slope shifts in response to sediment supply signals, a gradient in potential accommodation is generated by the signal itself. The signal as preserved in the landscape may have a phase shift compared to the sediment supply signal, because the transfer of the SSC depends not only on temporal variations in sediment supply, but also on accommodation potential.

5.3.5. Shoreline position

Reorganizations of the channel network and lobe-scale avulsions clearly have a significant influence on the location of the shoreline (Figure 5.1b). Whereas the shoreline may be prograding where active channels feed sediment to the shoreline, areas of the delta that do not receive sediment, or not sufficient sediment, transgress because of ongoing RSL rise (Martin et al., 2009b; Yu et al., 2017). We investigate whether the frequency of the SSCs can be distinguished from autogenic frequencies in shoreline movement. First, we calculate the distance between the delta apex and the shoreline from dip-sections of delta topography. We then calculate a mean shoreline position at a 1 hr interval by averaging over all dip-sections the coordinate system allows (Figure 5.3a). Supply cycles could only influence the shoreline of the active delta lobe, and may therefore influence shoreline rugosity (Kim and Jerolmack, 2008). To quantify the rugosity of the shoreline, Figure 5.3b shows the standard deviation of shoreline location in the dip sections. Shoreline rugosity may also obscure measurements of shoreline position from dip sections, because each section may contain several shorelines. Only the furthest shoreline is included in Figure 5.3a. To overcome this problem, we calculate a more accurate time series of shoreline extent by quantifying the terrestrial area of the delta (Figure 5.3c).

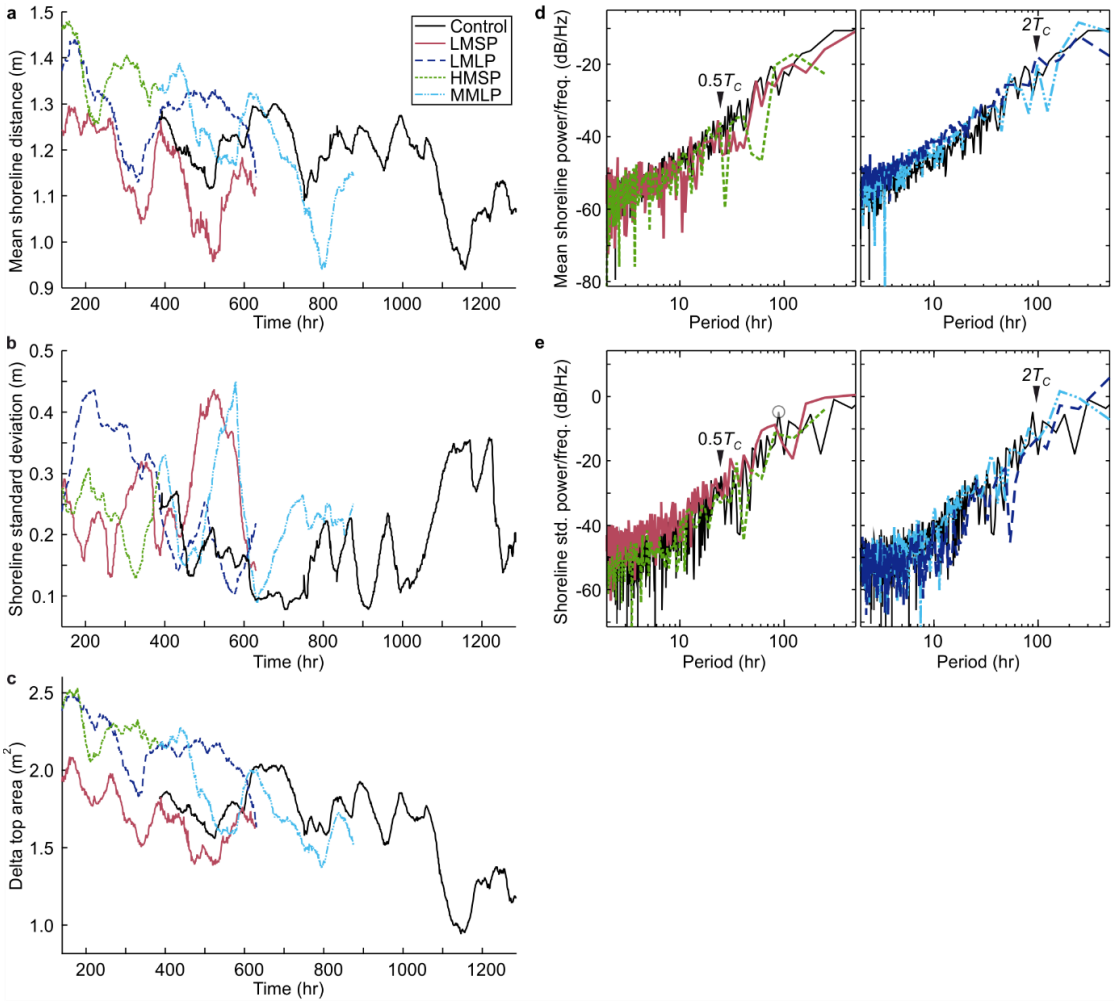

Figure 5.3. Shoreline position.

(**a**) Time series of mean shoreline distance calculated by averaging the distance from delta apex to the shoreline in down-dip sections. (**b**) Time series of standard deviation of shoreline distance in the down-dip sections. (**c**) Time series of delta top area. (**d**) Power spectra of delta top area for short periodicity ($0.5T_c$) and long periodicity ($2T_c$) experimental stages, and the control stage. (**e**) Power spectra of shoreline distance standard deviation for short and long periodicity experimental stages, and the control stage. A circle highlights a periodicity of 90 hr in the control stage.

We observe a long-term retreat in shoreline location (Figure 5.3a and c), which may relate to autoretreat (Muto, 2001). Shoreline location and rugosity are clearly related. Episodes where a stable channel progrades far into the basin (e.g. Control, ~1100 hr), are characterised by a low mean shoreline position (Figure 5.3a) and a high standard deviation. This is because the active lobe is narrow relative to the sediment-starved shoreline, which causes a major transgression during constant RSL rise. After a major lobe avulsion, a new lobe quickly progrades into the basin, causing a decrease in shoreline rugosity. This continues until the prograded lobe starts backstepping (Hoyal and Sheets, 2009) and the rate of progradation

relative to inactive lobe flooding drops again in favour of the transgression. As SSCs may feed sediment to the shoreline at different rates, they could influence progradation rates accordingly. High supply would consequently lead to a larger delta and a more rugose shoreline than low supply.

Both mean shoreline position and shoreline rugosity develop a cyclicity, which has previously been observed in other studies (Kim and Jerolmack, 2008). The clearest example of this is in the three cycles between approximately 750 and 1000 run hours in the control stage (Figure 5.3b). In fact, cyclicity of that approximate duration seems dominant in the control stage, as shown by a spectral peak for periodicities of 90 hr (Figure 5.3e). This supports earlier findings that autogenics can cause remarkably periodic trends, even in the absence of allogenic forcing (Kim and Jerolmack, 2008; Burgess et al., 2019). However, cycles exist over a range of other frequencies. To test whether the frequencies of the supply signals cause a distinct pattern in shoreline characteristics we construct periodograms of the time series of terrestrial area (Figure 5.3d) and shoreline standard deviation (Figure 5.3e). Both periodograms show no dominant periodicity. The movement of the shoreline is thus dominated by autogenic processes, whereas SSCs of the scale tested here do not contribute to significant changes in shoreline position.

5.3.6. Transfer of signal magnitude

The degree to which an SSC influences local deposition rates depends on both signal magnitude and available accommodation. We develop a metric that quantifies whether a certain change in sediment supply leads to a similar change in deposition rate (T_{cycle}):

$$T_{cycle} = \left\langle \frac{\dot{\bar{\eta}}}{\langle \dot{\bar{\eta}} \rangle} \frac{Q_t - Q_{mean}}{0.5(Q_{max} - Q_{min})} \right\rangle ,$$

where $\dot{\bar{\eta}}$ is the mean deposition rate along a strike oriented transect at time t, $\langle \dot{\bar{\eta}} \rangle$ is the mean deposition rate along a cross-section for an entire stage, Q_t is the sediment flux to a basin at time t, Q_{mean} is the mean sediment flux over an entire cycle, and Q_{max} and Q_{min} are respectively the maximum and minimum sediment fluxes in a cycle. T_{cycle} essentially defines whether deposition rates correlate with supply conditions. $T_{cycle}>0$ means deposition primarily occurs during higher than average supply, whereas $T_{cycle}<0$ indicates deposition rate is inversely correlated with supply rate as deposition increases when supply drops below average supply. A perfect correlation, $T_{cycleEQ}$, follows from:

$$T_{cycleEQ} = \left\langle \frac{Q_t}{\langle Q_{mean} \rangle} \frac{Q_t - Q_{mean}}{0.5(Q_{max} - Q_{min})} \right\rangle.$$

$T_{cycle}=T_{cycleEQ}$ means that a certain increase in sediment supply immediately leads to exactly the same change in deposition rate. It follows that $T_{cycle}>T_{cyclEQ}$ means a change in sediment supply leads to a larger change in deposition rate (amplification), while $T_{cycle}<T_{cyclEQ}$ indicates that a change in sediment supply leads to a weak change in deposition rate (attenuation).

To investigate whether the response of different parts of the delta amplify or attenuate supply signals, we define $T_{amp}=T_{cycle}/T_{cyclEQ}$. We calculate T_{amp} for cross-sections of synthetic stratigraphy at different distances from the delta apex for each of the experimental stages (Figure 5.4). Deposition rates are calculated over a 1 h window. Generally, sediment supply signals are attenuated in medial sections (~0.6-0.8 m), but proximal and distal sections show evidence of signal amplification and, in some instances, reversal. An explanation for these trends can be found in the same accommodation versus supply effects we discussed for the transport mobility diagrams (Figure 5.2). Variations in Q_s:Q_w lead to changing equilibrium slope, which drives proximal deposition during high supply and distal deposition during low supply. This effect is most pronounced at either end of the system (Figure 5.4b). The medial zone appears to act as a hinge point. The LMSP stage is a clear example of this with high T_{amp} values proximally indicating high supply leads to proximal sediment storage and sediment starvation at the shoreline. In contrast, after a small drop in T_{amp} from the proximal to medial section, stage HMSP shows signal amplification in the distal section. Maybe the high amplitude signal in stage HMSP overwhelms proximal storage rates and so the distal section still receives a surplus of sediment.

The effect of LP signals is different from the SP signals. The MMLP signal is strongly attenuated in the proximal and medial sections, but correlates well in the distal section (Figure 5.4). An explanation for this may be found in signal acceleration. Slowly changing signals will not push existing channels out of equilibrium, and so the MMLP signal could largely bypass the delta without significantly influencing overbank sedimentation. However, at the shoreline the signal could drive changes in progradation. Figure 5.4a shows that the LMLP signal is absent proximally, then slightly buffered in the medial section and strongly anti-correlated with deposition rates distally. This pattern is different from the other stages, and could not be explained with similar mechanisms. We test whether the T_{amp} metric can be driven by stochastic changes by correlating the LMLP supply signal with synthetic stratigraphy from run hours 140-630 of the control stage. T_{amp} shows a similar trend to the LMLP stage even though there is no supply signal. Supported by the absence of a characteristic response to the LMLP signal in other analyses, we conclude that trends in the LMLP stage are the result of

stochastic changes in deposition rate rather than an expression of the sediment supply signal. Although trends for LMSP, HMSP and MMLP could be related to other analyses, the results of this metric should thus be treated with care.

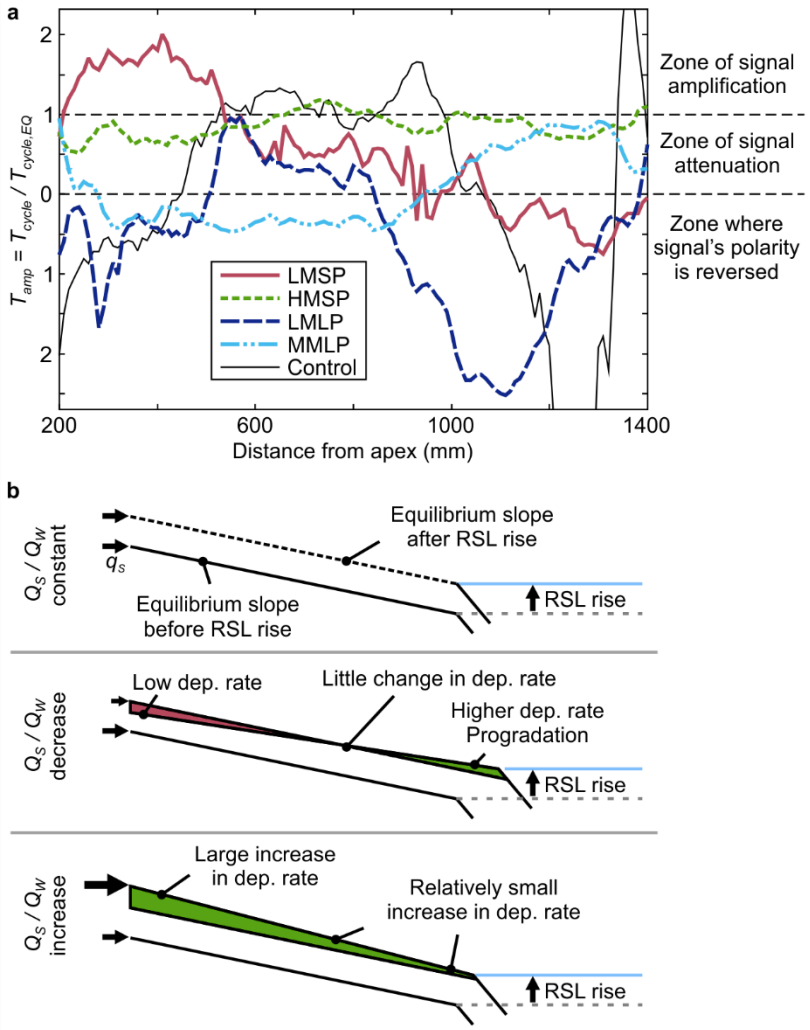

Figure 5.4. Signal amplification and attenuation.

(**a**) Spatial trends in the magnitude of signal transfer. T_{amp} describes to what degree a change in sediment supply leads to proportional change in deposition rates. We calculated T_{amp} for distances between 200 and 1400 mm with a 10 mm interval following methods detailed in text. (**b**) Schematic of changes in equilibrium slope and their effect on the spatial distribution of supply signals.

5.3.7. Slope

We previously found evidence that SSCs influence the mobility of the transport system and linked this to the system slope. Fan slope is linearly related to the ratio of water supply and sediment supply (Parker et al., 1998; Whipple et al., 1998). Given that water discharge remained constant throughout the experiment, the slope of the deltas should go up and down

in response to the SSCs. However, experimental studies previously found that fan slope also varies around a mean slope as a result of autogenic morphodynamics (Jerolmack, 2011; Paola, 2016), which may obscure slope effects caused by SSCs (Reitz and Jerolmack, 2012).

We estimate the surface slope for each of the five experimental stages by plotting elevation above sea level versus distance to the delta apex for each point on the topographic grid (Figure 5.5a). As we focus on the delta top, we limit our analysis to points within 1 m from the apex and less than 15 mm below sea level so that river channels cutting down below water level are included. A linear trend line through the data then gives an estimate of the delta-wide mean slope. Time series of these slope estimates show how slope varies in each of the experimental stages, including the control stage (Figure 5.5b). The original transport slope of a system may be estimated from empirical relations based on grain size and channel or bar dimensions (Duller et al., 2012; Castelltort, 2018). We therefore use topographic surfaces and not synthetic stratigraphy to estimate slope.

We previously found that the impact and timing of SSCs on delta morphodynamics depends on proximity to the delta apex. We therefore create separate time series for the proximal and distal slope (Figure 5.5c). Our estimates of the proximal slope are derived from a linear trend line through grid points within a 100-400 mm radius from the apex, and distal slope is calculated for points at 600-900 mm from the apex (Figure 5.5a). The range of distal slopes is consistent throughout each experimental stage and between the stages. The proximal slope shows two phases of unusual steep slopes in stages LMSP and LMLP, which are also present in estimates for the entire delta top slope (Figure 5.5b). These phases are significantly longer than T_c or the SSCs.

To assess whether slope changes occur at characteristic frequencies, we convert the slope time series to periodograms (Figure 5.5d). All the periodograms show a trend of increasing spectral power with cycle duration, typical for correlated noise. Interestingly, the spectra show no evidence of cyclicity at the frequency of the SSCs, nor any other dominant frequencies that stand out from the noise trend. Previously we explained patterns in transport system mobility and the ability of the system to accommodate supply signals as the result of changing equilibrium slope set by sediment and water discharge. The absence of slope cycles related to the allogenic supply signal means that slope cycles are overshadowed by autogenic dynamics. As slope changes only affect the active area on the delta, local slope variations may be insufficient to cause a signal in our delta-wide averaged slope estimates. Creating time series of slope for the active delta only is practically not meaningful because of high-frequency changes in the sediment transport configuration. In addition, Parker et al. (1998) note that equations relating slope to supply predict mean conditions, averaged over many avulsion

cycles. Given that $\overline{T}_a \approx 0.9T_c$ and the longest SSCs have a duration of $2T_c$, it may require a much longer signal than tested here to create a deterministic change in delta slope.

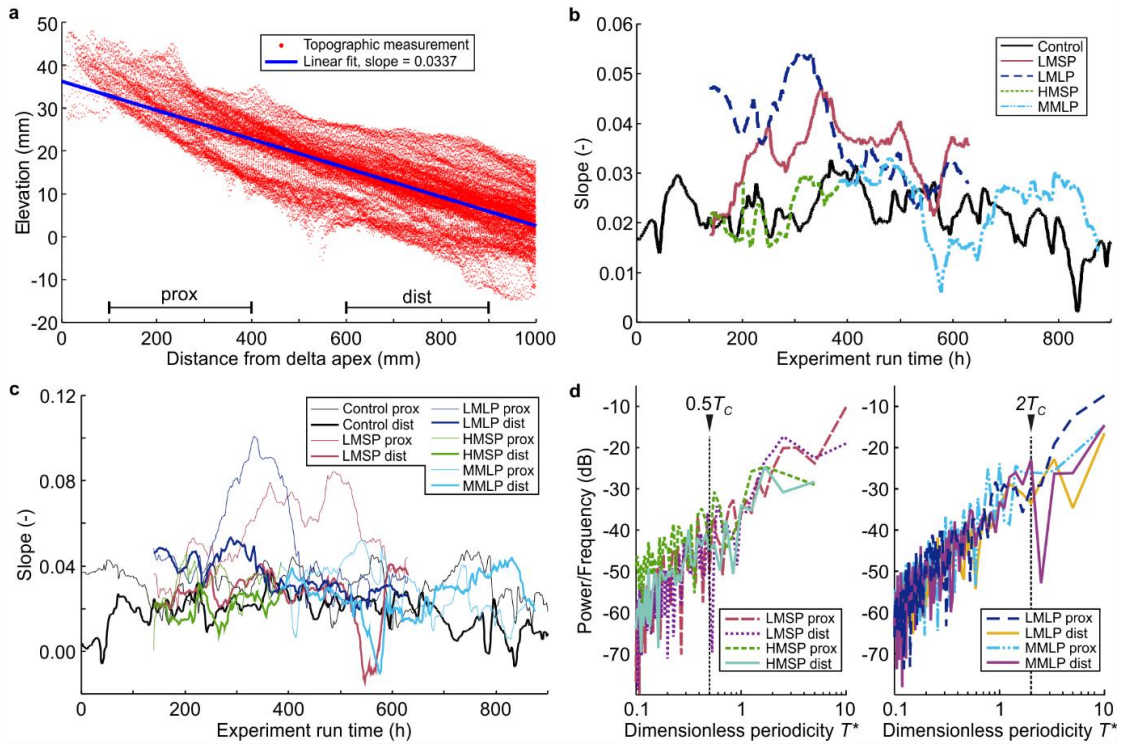

Figure 5.5. Slope.

(**a**) Elevation above water level versus distance from delta apex for run hour 70 into the LMSP stage. The slope of the linear fit to these data gives a delta-wide average of delta top slope. (**b**) Evolution of delta-top slope in each of the experimental stages. The graphs are smoothed with a 3-point moving average filter to reduce high-frequency noise. (**c**) Time series of delta top slope for proximal and distal transects separately. (**d**) Periodograms of delta top slope for proximal and distal transects. A vertical line show the SSC periodicity.

5.3.8. Channel depth

Channel depth is an important control in the scaling of the experiments, as the depth of the larger channels sets T_c. Li et al. (2016) approximated H_c=12.2 mm in the control stage given by the 95th percentile channel depth from a distribution of channel depths at 0.5 m from the delta apex (Li (2019), personal communication). To calculate H_c for the cyclic stages, we measure channel depths in every 10th timeline of surface topography at 0.5 m from the apex. We only include channels with active flow and, given the resolution of the laser scanner, only channels >1 mm.

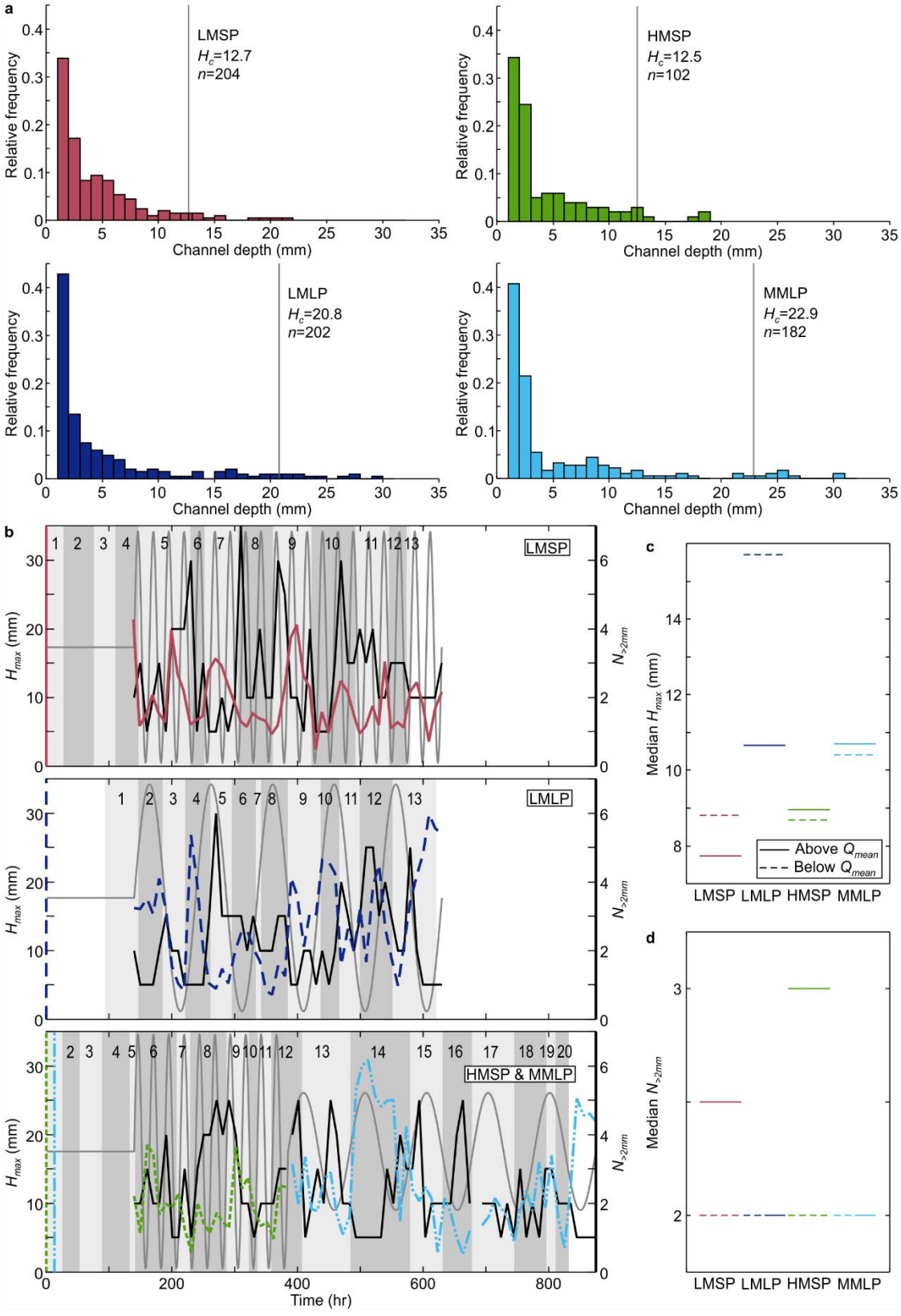

Figure 5.6. Channel depth.

(**a**) Distribution of active channel depths measured in every 10th timeline of surface topography. A vertical line indicates the 95th percentile channel depth (H_c). n=number of measurements. (**b**) Maximum channel depth (H_{max}, coloured lines) and number of channels deeper than 2mm ($N_{>2mm}$, black lines) for each of the

cyclic experimental stages. Background shading and numbers refer to inter-avulsion cycles (Figure 5.1a) and grey lines illustrate supply cycles. (**c**) Median of H_{max} measurements during phases of above average sediment supply (solid line) and below average sediment supply (dashed line). (**d**) Median of $N_{>2mm}$ measurements during phases of above average sediment supply (solid line) and below average sediment supply (dashed line).

We observe several types of channels on the delta. In general, one or two main trunk channels connect the apex to the shoreline, which are generally >5 mm deep. Many smaller channels in the form of bifurcations or distributary channels and crevasses split off from this main channel, which are generally <5 mm deep, but often in the order of 1-2 mm deep. Figure 5.6 shows the distribution of channel depths for each stage. Using the 95th percentile channel depth, measurements of H_c in stages LMSP (12.7 mm) and HMSP (12.5 mm) are very close to estimates for the control stage, whereas channel-based estimates of H_c are significantly deeper for LMLP (20.8 mm) and MMLP (22.9 mm). Figure 5.6a shows that even though we measured many small (<2 mm) channels in the LP stages, H_c is higher than in SP stages because of a higher trunk channel depth. The largest channels in LP stages are approximately 30 mm, compared to ~20 mm in LMSP and HMSP.

We previously discussed that theoretically sediment supply is negatively correlated with channel depth. To test whether SSCs cause cyclicity in channel depth, we plot the depth of the deepest channel (H_{max}) for each run hour (Figure 5.6b). In addition, we plot the number of channels that exceed 2 mm depth ($N_{>2mm}$). This excludes the smallest channel because their number is less accurate given the resolution of the laser scanner. The figure includes the sediment supply curves and the avulsion cycles given in Figure 5.1a. The number of channels shows a reverse trend from the maximum channel depth because a constant flow volume is distributed over the active channels. For this reason, H_{max} often is high just after an avulsion, when a single channel progrades into the basin. Once this channel starts backfilling, more channels develop, which leads to a decrease H_{max} and an increase of $N_{>2mm}$ as distributary channels initiate at more upstream locations.

At first sight, channel depth and number seem to be primarily related to the avulsion cycle. To test whether there is a link with the supply cycle, we compare the median channel depth and number during phases of higher-than-average sediment supply and lower-than-average sediment supply. Figure 5.6c shows that median H_{max} is higher while sediment supply is below average in stages LMSP and LMLP, and vice versa in HMSP and MMLP. Changes in channel depth could thus not be used to unambiguously reconstruct supply cycles, although LP stages overall have higher channel depth. Figure 5.6d suggests no difference in the number of active channels between high supply phases and low supply in both LP stages.

However, we observe more active channels during high supply than low supply in SP stages. This result of Figure 5.6d is consistent with our observations of increased mobility of the transport network in proximal areas during high supply (Figure 5.2).

5.3.9. Deposition rates in cross-sections

Our analyses show that the mobility of the transport system is influenced by SSCs, which can create cyclic patterns on the delta. However, we also observed a complicated pattern of signal amplification, attenuation, and phase shifts depending on signal magnitude and duration shifts, which may relate to the equilibrium slope set by the Q_s:Q_w ratio. Inspired by Li et al. (2016), we test whether the SSCs influence time series of mean deposition rate per hour by averaging deposition rates over the width of semi-circular cross-sections of synthetic stratigraphy. We make three sections at proximal (300 mm), medial (600 mm) and distal (900 mm) locations on the delta for each of the experimental stages (Figure 5.7). This allows us to study spatial trends in deposition rates rather than the delta-wide volumetrics presented in Toby et al. (2019a). Following Li et al. (2016), we use a multi-taper method to construct power spectra of the time series (Figure 5.7). The confidence bands in this figure are based on the assumption that stochastic autogenics generate a red noise pattern. The validity of this assumption could be debated as not all parts of the spectra are equally well approximated by the red noise trend. Strict application of the confidence bands leads to many positives that could be mistaken for allogenic signals (Hajek and Straub, 2017).

Generally, the power spectra of Figure 5.7 show no clear cyclicity at the periodicity of the SSCs, which give a rather pessimistic outlook on identifying SSCs from deposition rates in cross-sections. Although there are some presumably significant peaks in the LMLP stage power spectra, the supply signal frequency has not transferred. Spectral power at the LMSP frequency is particularly low, supporting earlier claims that this signal is shredded. At the most proximal cross-section, power at the HMSP periodicity seems to fall within the general trend of increasing power with increasing periodicity. The medial and distal section show peaks in spectral power that could indicate signal transfer. A remarkable feature in the HMSP power spectra are the high noise levels for short periodicities. This could be a real signal, a consequence of the shorter time series for this stage, or increased noise in the topographic measurements. Although there are spectral peaks close to the MMLP periodicity, these are not evidently different from the general trend of increasing of spectral power with periodicity up to timescales of T_c that could be expected in these plots (Hajek and Straub, 2017).

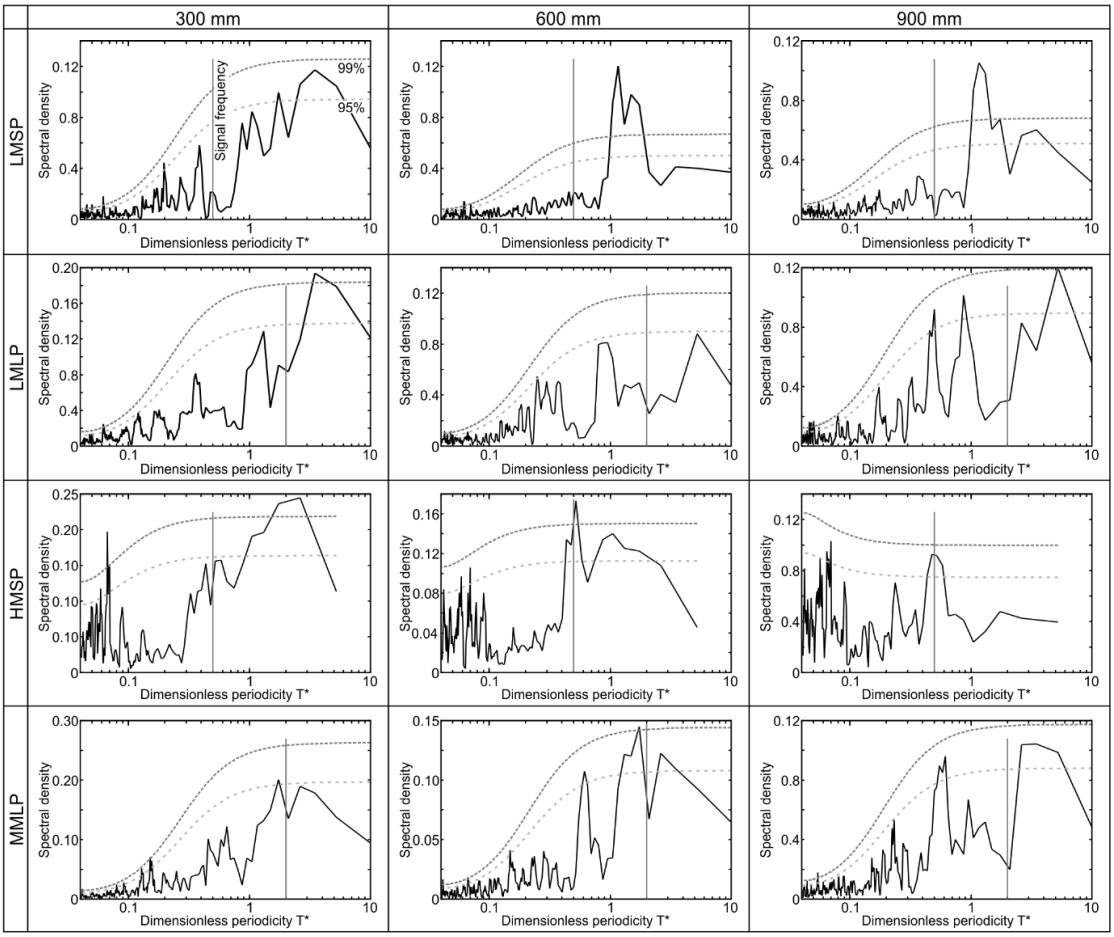

Figure 5.7. Deposition rates in cross-sections.

Power spectra of mean deposition rate per hour in semi-circular cross-sections of synthetic stratigraphy at proximal, medial and distal locations from the feeder. A vertical line shows the frequency of sediment supply signals. Dotted lines show 95% and 99% confidence bands calculated using an AR-1 method.

Even in the most convincing case, the HMSP signal in the medial and distal sections, it is difficult to distinguish those signals from the general noise trend without a priori knowledge of the supply frequency. However, there are clear differences between the LP and SP stages. Theory behind T_c predicts that at timescales longer than T_c autogenic noise has levelled out and only allogenic processes can drive changes in stratigraphy (Straub and Wang, 2013). For timescales shorter than T_c, a general increase in the magnitude of autogenic processes with increasing timescale is expected. Hence without allogenic signals, the power spectra in Figure 5.7 should increase towards T_c, after which power spectra should diminish (Hajek and Straub, 2017). This trend holds for the medial and distal sections of LMSP and HMSP, which have no allogenic signal at a timescale longer than T_c. Proximal sections increase in spectral power at time scales $>>T_c$. Given that the most proximal avulsions are the least frequent as even delta lobe-scale avulsions may start slightly downstream, autogenic noise over long timescales

could be expected. In addition, we observe occasional scours in the most proximal regions at the transition from feeder channel to open basin, which would increase T_c.

Although neither of the LP signals is unambiguously identified in Figure 5.7, both LMLP and MMLP show relatively high noise levels for timescales longer than T_c of the control stage. This could be expected given a higher value for H_c, and thus T_c, in both stages. In addition, allogenic signals may contribute to noise at long timescales because the signal duration is much longer than T_c. Here we note that the LMLP signal presumably has been shredded, which effectively means that autogenic processes have distributed the energy of the signal over a range of different frequencies. The conversion of this signal to noise over a range of long periodicities may explain high spectral power for timescales longer than T_c, which could thus be indicative of the presence of LP supply signals.

5.3.10. Variations in T_c

Our analysis of channel depths shows a significantly higher H_c for LP experimental stages, suggesting a higher T_c compared to the SP and control stages. We test variations in T_c with channel depth and down-dip distance by estimating T_c from measurements of σ_{ss} ($T_{c,\sigma ss}$). This also allows us to test spatial trends in T_c. So far we discussed the compensation timescale as a spatially uniform timescale, with one value that sets the limits of stochastic autogenics on the entire delta top. However, as flow splits up and the channel network changes with proximity to the shoreline, the compensational stacking trend and the value of T_c may change. Figure 5.8a shows estimates of T_c based on measurements of H_c and estimates based on the decay of σ_{ss} with T_w ($T_{c,\sigma ss}$). Measurements of $T_{c,\sigma ss}$ for sections between 400 and 900 mm from the delta apex are quite consistent for each experimental stage, but the variation between stages is large. The channel-based estimate of T_c=49 hr is a close match to $T_{c,\sigma ss}$. Estimates for stage HMSP are slightly lower than channel-based estimates ($T_{c,\sigma ss}$≈ 35 to 38 hr), but not far off from the control experiment. $T_{c,\sigma ss}$ in the LMLP stage (60 to 70 hr) and the MMLP stage (66 to 79 hr) are a bit higher than the control stage but are also slightly lower than our estimates of H_c would suggest. $T_{c,\sigma ss}$ between 103 and 122 hr in stage LMSP is distinctly higher than $T_{c,\sigma ss}$ in the control stage, or estimates based on H_c would suggest. This stage shows a general decrease with distance from the apex.

In many cases the topographic roughness scale is set by the larger channels on the delta, but from the synthetic stratigraphic cross-sections it appears that delta lobes and levees form significant topography (Figure 5.1d). To test whether lobe topography sets an important roughness scale, we calculate the maximum elevation change along a timeline of a semi-circular section of synthetic stratigraphy. This method gives the height between the highest

levee and the lowest inter-lobe depression. From this, we estimate a lobe-scale equivalent of T_c: $T_{c,L}=H_L/r$, where H_L is the maximum elevation change on a cross-section. Given that intra-lobe areas may include the sea floor, $T_{c,L}$ could far exceed a channel-based T_c. We calculate $T_{c,L}$ for sections at increasing distances from the delta apex to investigate spatial trends.

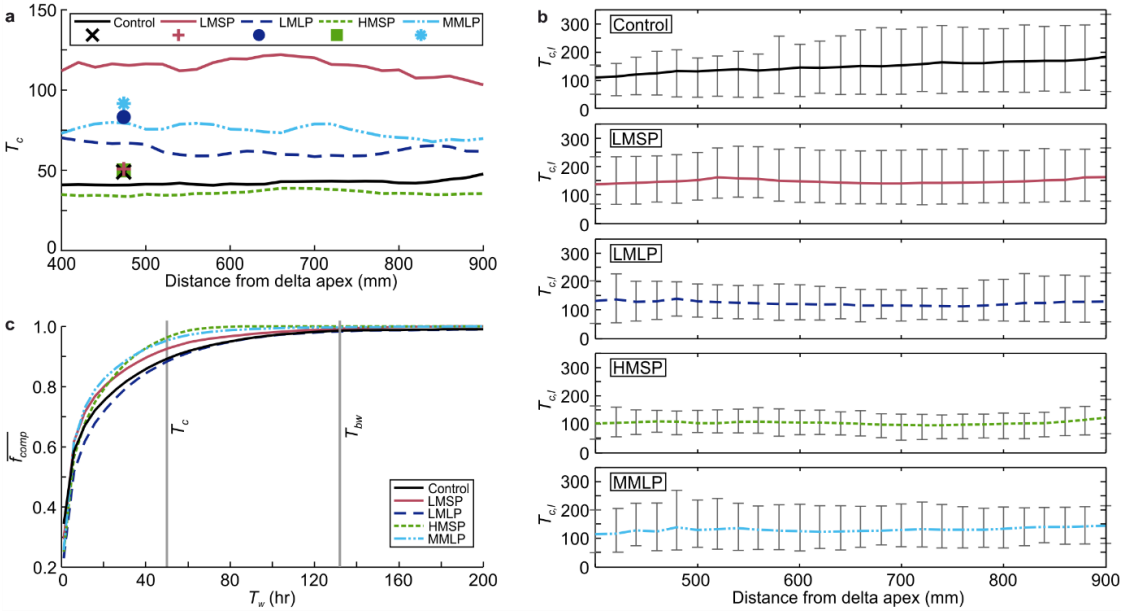

Figure 5.8. T_c and time windows of stratigraphic completeness.

(**a**) Estimates of T_c from measurements of σ_{ss} (Straub et al., 2009)) in semi-circular cross-sections at distances of 400-900 mm from the delta apex (lines) and estimates of T_c based on channel depth at 500 mm from the apex (markers). (**b**) Estimate of lobe-scale T_c ($T_{c,L}$), calculated as the maximum elevation change in a cross-section divided by the long-term aggradation rate. Bars show the range of $T_{c,L}$ measurements for all timelines in a section and a line connects the mean. (**c**) Mean stratigraphic completeness ($\overline{f_{comp}}$) as a function of time window of measurement (T_w). See text for details on the calculation method. Vertical lines show T_c for the control experiment, and an approximation of the time required for lobes to cover the entire basin (T_{bw}).

As there are many timelines for each section location, Figure 5.8b shows the maximum, minimum and mean $T_{c,L}$ of all timelines in a section location. Generally, the mean $T_{c,L}$ for all stages falls within the range 100-150 hr and the maximum is in the order of 130-280. Again, stage HMSP gives the lowest estimates, followed by LMLP, MMLP and LMSP. Measurements of $T_{c,L}$ vary little with distance from the apex in all cyclic stages, but the control stage shows a steady increase in both mean and maximum $T_{c,L}$. This could relate to the autoretreat effect we previously observed in this experiment. Basin depth is deeper than in the other stages, and the average size of the delta top slightly smaller, creating potentially deeper inter-lobe topographic depressions between prograded lobes and the basin floor. The

range of $T_{c,L}$ measurements is smallest in stage HMSP, followed by LMLP, MMLP and LMSP. In the control stage the range of $T_{c,L}$ increases with distance.

Measurements of σ_{ss} directly quantify compensational stacking statistics, and our calculations of $T_{c,\sigma ss}$ thus give the best estimates of T_c. Using the roughness of larger channels on the delta gives a reasonable approximation of T_c for the control stage and both LP stages. T_c in the LP stages is longer than the control stage, but this is in line with measurements of H_c. Estimates of T_c based on lobe roughness are markedly longer than $T_{c,\sigma ss}$ except for the LMSP stage. In fact, $T_{c,\sigma ss}$ for the LMSP stage is more than two times longer than an estimate of T_c from H_c would suggest, and seems better approximated by $T_{c,L}$ instead.

5.3.11. Stratigraphic completeness

Completeness of the stratigraphic record relates to the efficiency of the transport network to spread sediment over the delta and the potential to store some thickness of this sediment in the stratigraphic record (Straub and Esposito, 2013). We previously found that SP supply signals lead to more coeval channels during high supply (Figure 5.6d). In addition, LMSP, HMSP and MMLP signals lead to increased transport system mobility in the proximal delta during high supply, and distal delta during low supply (Figure 5.2). As these signals cause a wider spread of sediment over the delta, we hypothesize that they increase completeness of the stratigraphic record.

We quantify stratigraphic completeness (f_{comp}) in 1D vertical successions of synthetic stratigraphy as the number of time steps with some preserved thickness out of the total number of time steps and average f_{comp} for all locations on the fan ($\overline{f_{comp}}$) (Straub and Esposito (2013) and Yu et al. (2017)). To focus on the delta top, we limit our analysis to vertical successions within 1.1 m from the delta apex.

Figure 5.8c shows $\overline{f_{comp}}$ for T_w between 1 and 200 hr. Stratigraphic completeness initially increases quickly with increasing T_w, but slows down and approaches 100% completeness at timescales >>T_c. Except for LMLP, the cyclic stages approach completeness quicker than the control experiment, confirming our hypothesis that increased channel mobility reduces stratigraphic incompleteness. Stage HMSP reaches completeness fastest, which is a logical consequence of having the highest signal magnitude and the strongest response in mobility of the transport system and number of coeval channels. MMLP follows closely, ahead of LMSP.

Our definition of stratigraphic completeness relies on sediment being fed and preserved on all locations on the delta, and so completeness also relates to timescales of

sediment distribution over the delta, in addition to timescales of reworking given by T_c (Straub and Esposito, 2013). Given that avulsions occur on average every 44 hr ($\overline{T}_a \approx 0.9T_c$), and the width of the active lobe is approximately 1/3 of the delta top (Figure 5.1b), we estimate the timescale for deposition to cover the entire basin width (T_{bw}) is approximately $T_{bw} \approx 3\overline{T}_a \approx 132$ hr. Given this, it is not surprising that stratigraphy approaches 100% completeness for values in the order of T_{bw}, which is much longer than T_c in this experiment (Figure 5.8c).

5.3.12. Threshold in cyclic stages

Toby et al. (2019a) constructed the Q_a threshold using data from the control stage, characterised by constant boundary conditions, and tested this threshold with four cyclic stages. Allogenic forcing conditions are generally unknown in outcrop studies, and so the threshold would ideally be constructed without prior knowledge of the presence or absence of sediment flux signals. Although SSCs cause no significant change in many of our analyses, some differences between the control stage and the cyclic stages appear. To test whether cyclic stratigraphy itself can be used to establish the threshold, we follow the methods outlined in Toby et al. (2019a) to calculate Q_a from each of the cyclic stages (Figure 5.9a). Figure 5.9b shows an exponential fit through the data of Figure 5.9a. These figures show a trend of decreasing magnitude of Q_a with increasing time window that is similar for each of the experimental stages. Stage LMSP, HMSP, and MMLP group closely together, generally below the values of the control stage, whereas stage LMLP closely approximates the control stage. Time series of V_{RSL} show a long-term trend of decreasing V_{RSL} (Figure 5.9c), which, in addition to cyclic changes, contributes to high values of Q_a. Taking the long-term trend of V_{RSL} decrease out would inevitably lead to lower estimates of Q_a, which would be more in line with the other cyclic stages. At short timescales (<0.25 T_c), residuals between the measured value of Q_a and the exponential fit are largest. Although this may indicate a break from the exponential decay of Q_a, at least some of this misfit is caused by noise in the topography measurements, the effects of which diminish for measurements of longer timescales.

The Q_a thresholds are calculated from the terrestrial volume time series shown in Figure 5.9c. High magnitudes of Q_a occur where terrestrial volume is consistently increasing or decreasing. The largest autogenic cycles are set by avulsions. Our analysis on avulsion frequency shows that there is no significant difference between the stages. However, the maximum inter-avulsion timescale is longest in the control stage (Figure 5.1b). Long stages of consistent volume change lead to higher estimates of Q_a, and so this explains some of the

difference. From Figure 5.9c, it appears that V_{RSL} change in the control stage is smoother than in the cyclic stages, and the total magnitude difference of intermediate (~0.5 T_c-2T_c, or 25-100 hr) cycles is visibly larger in the control stage than the other stages. V_{RSL} trends of this scale in the stages of cyclic sediment supply seem to be interrupted by higher frequency cycles. These will not influence long-term estimates of Q_a, measured over timescales longer than avulsion cycles, and may even boost Q_a at very short timescales (<0.25T_c). However, the lack of consistent V_{RSL} change at intermediate timescales decreases the magnitude of Q_a, as shown in Figure 5.9a.

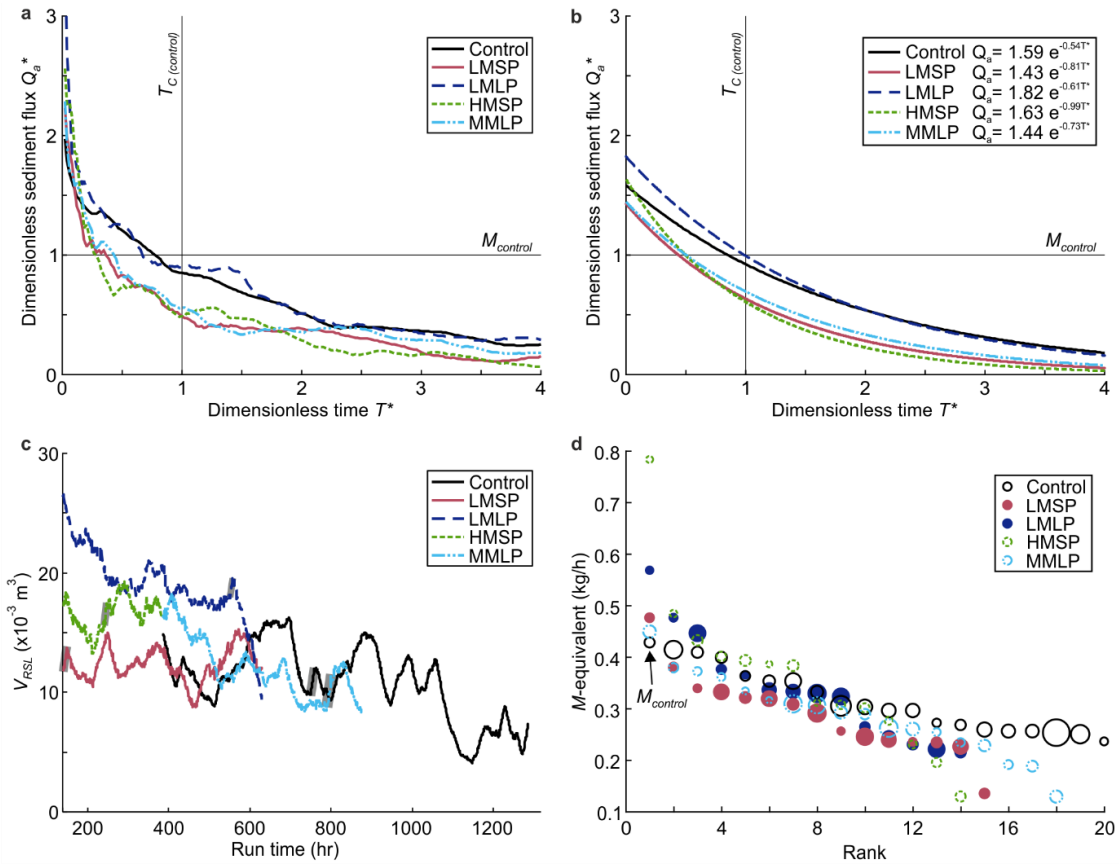

Figure 5.9. Calculation of *Qa thresholds.**

(**a**) Dimensionless maximum rate of terrestrial volume change (Q_a^*) versus time window of measurement for each of the experimental stages for time windows up to 4T_c. In order to store a sediment supply signal, the combination of signal magnitude and duration should exceed Q_a^* (Toby et al., 2019a). (**b**) Exponential fit through the measurements of Q_a^* shown in Figure 5.9a. (**c**) Time series of terrestrial volume (V_{RSL}) for each of the experimental stages. High frequency noise in the measurements is reduced with a 3-point moving average filter. We calculated rates of volume change for time intervals of consistent V_{RSL} change, i.e. between a peak and a trough in V_{RSL}. M is defined as the maximum of these fluxes in the control stage, and is used for normalising sediment fluxes (e.g. Figure 5.9a). Grey bars show time intervals where these maximum fluxes occur in each of the experimental stages. (**d**) Rates of consistent V_{RSL} change (M-equivalent), ranked in order of flux magnitude and converted to sediment mass (porosity=53%,

density=2650 kg/m^3). These are measured following the same method used to calculate M (Figure 5.9c), and the maximum flux in the control stage actually is M. The size of the circle is proportional to duration of the time window the flux is measured over, which ranges from 5 hr to 90 hr. Stages <5h are left out to exclude high-frequency noise.

An interesting observation in the threshold diagram of the control stage is that Q_a, when calculated over a time window of T_c, closely approximates M (Figure 5.9a). Given that T_c marks a temporal cross-over from stratigraphy partly constructed by stochastic autogenic processes to stratigraphy completely constructed by allogenic forcing (Straub et al., 2009; Wang et al., 2011), it is perhaps not surprising that the magnitude of autogenic variations is limited to a time window of T_c. We calculate the equivalent of M for each of the cyclic stages to test the consistency of this rate between different stages. The time interval over which flux M is calculated is bounded by a peak and a trough in the V_{RSL} plots, as indicated in Figure 5.9c. In addition to the maximum M, we show measurements of consistent V_{RSL} change in Figure 5.9d from other phases of the experimental stages, in decreasing order of magnitude. Generally, these measurements are quite consistent, except for the maximum rate. HMSP gives the largest deviation from $M_{control}$, as M_{HMSP} is 83% higher. Experimental stages LMSP (+11%), MMLP (+5%) and LMLP (+33%) are much closer to $M_{control}$ and the range is much smaller for lower ranked measurements. This, and the threshold diagrams in Figure 5.9a-b, tells us that the rate of sediment capture and release is quite consistent between the experiments, even though supply conditions are very different.

5.4. Discussion

Our analyses show a complex transfer of allogenic sediment supply signals to deltas. Autogenic morphodynamics processes occur over a range of spatial and temporal scales, but generally not at set frequencies. Power spectra demonstrate that the magnitude of autogenic variations increases with periodicity. Consequently, we observe the dominance of long-term autogenic processes in our analyses, the most important being delta-lobe avulsions. The avulsion cycle is the dominant control on the morphology and dynamics on the delta, and appears to override any potential slope or shoreline effects caused by the SSCs.

The exact timing of avulsions is stochastic, but a general increase because of autoretreat can be expected as the basin depth increases. Our analyses show no relation between SSCs and the timing of avulsions. For both SP signals, this could be because signal periodicity is much shorter than the mean inter-avulsion timescale and T_c. Previous studies

suggest that avulsions are triggered when a channel becomes superelevated by about one channel depth (Mohrig et al., 2000; Jerolmack and Mohrig, 2007). In addition, the size of individual lobes in fan systems is roughly consistent, and lobes avulse when the maximum size is reached (Prelat et al., 2010; Reitz and Jerolmack, 2012). Given that this volume required for super-elevation cannot be reached in the duration of a single SP supply signal, these signals are unlikely to trigger avulsions. The duration of LP signals, however, far exceeds the mean avulsion timescale. The magnitudes of LP signals are within close reach of the shredding thresholds, and so this signal may not be of sufficient amplitude or duration to make a significant change to avulsion frequency. Avulsion frequency in the experiments is highly variable, so a supply signal should make a large change in avulsion frequency before it is significantly different from the control stage. For a sediment supply signal to influence highly variable, large scale processes such as avulsions, the supply signal should thus far exceed autogenic limits as defined in Toby et al. (2019a).

Avulsion cycles are the dominant control on large-scale delta morphology, but on a smaller scale the SSCs produce subtle differences, the characteristics of which depend on signal magnitude, duration and supply acceleration. Although there is no correlation between trunk-channel avulsions and their timing relative to avulsions, we observed a small increase in the number of co-existing channels during high supply conditions in stages with high supply acceleration (Figure 5.6c). A rapid increase in supply seems to clog up channels, which leads to an increase in the number of secondary channels (Figure 5.6d). This means that less flow is routed through the main channel and channel depth is relatively low. Signals with a gentler change in supply have a different feedback loop between supply signal and channel depth and number. Slow, long-term decrease in supply may lead to scouring of the trunk channel, creating a deeper channel (Figure 5.6a and c). As a single deep channel is more efficient at transporting sediment than several shallow channels, a subsequent increase in supply will mostly bypass. Hereby channels can remain deep and no new channels are generated as a consequence of increased supply. Channel depth in the LP stages is thus controlled by low supply phases, whereas high supply phases are buffered and have little effect on channel width or the number of channels. Given the same mean sediment supply and constant water discharge, unusually deep channels could thus be an indicator for gradual changes in sediment supply, and fast supply change is characterized by a higher number of co-existing channels.

The efficiency of sediment supply signal transfer to landscape morphology depends not only on the magnitude of the sediment supply signal, but also on the generation of accommodation. Delta top accommodation is given by the equilibrium profile. Given constant water discharge, the equilibrium slope increases during high supply. The increased

accommodation potential facilitates proximal deposition during high supply, and distal deposition during low supply. Distal locations on the delta may thus show cyclicity that is out of phase or even anti-correlated with the original catchment signal and proximal deposits. This may lead to correlation errors when cyclicity in stratigraphy is used to connect vertical successions (Figure 5.10). However, as accommodation is limited, high magnitude sediment supply signals are more likely to exceed storage potential. Given that signals with low acceleration create deep trunk channels and few distributary channels, these signals bypass the delta top and are thus more likely to be found in shoreline position or marine environments. However, we observe no allogenic cyclicity in shoreline position, which may be because the tested signals are of insufficient amplitude or duration.

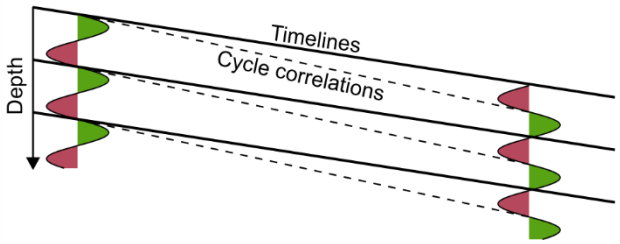

Figure 5.10. Correlation of cycles.

Schematic of two vertical successions with cyclicity of the same periodicity. These cycles may be due to the same forcing mechanism, but if a phase lag exists, here half a cycle, correlation of the cycles is not a correlation of deposits of the same age.

Diffusion equations predict that it takes time for landscapes to re-equilibrate after changing supply. As a consequence, longer signals are more likely to equilibrate with landscapes and systematically influence geomorphology. The time to reach this equilibrium (T_{eq}) is in the order of $T_{eq}=L^2/\nu$, where L is system length and ν is the diffusivity (Paola et al., 1992). We calculate T_{eq} to test whether the signals applied here exceed the equilibrium timescale of the delta. We approximate the diffusivity as $\nu=\frac{Q_{out}}{W_{fp}\,\bar{s}}$, where Q_{out} is the sediment flux out of the system, W_{fp} is the width of the floodplain and $\bar{s}$ is the mean slope. Straub et al. (2015) calculated a long-term mean sediment capture rate of 53% for the control stage and so we approximate $Q_{out}=0.47Q_{mean}$. Using L=1.1 m, a mean basin width of 1.5 m and a slope of $2\text{x}10^{-2}$, we approximate $T_{eq}\approx$61 hr. Although T_{eq} is only a rough estimate for systems to reach equilibrium, this result suggests that our LP signals should have transferred to the landscape, because their periodicity (98 hr) exceeds T_{eq}. However, these diffusion equations do not explicitly model autogenic morphodynamics. Given that autogenic processes in the experiments occur on timescales that may exceed the estimated T_{eq}, or the LP periodicity (for

example, see the analyses on avulsion frequencies, shorelines, deposition rates), it is not surprising that autogenics disturb the transfer of LP allogenic signals. Whether significant autogenic processes occur on timescales longer than T_{eq} depends on system characteristics. For example, autogenic scales are smaller in less cohesive systems (Straub et al., 2015) where they may thus not exceed T_{eq}.

Overall, our analysis, and the results of Toby et al. (2019a), show that signals most likely influence landscape morphology when sediment supply acceleration is high relative to autogenic processes, although T_c-theory predicts that long-term preservation of these signals is easier for long duration signals (Chapter 3). Other studies show that long signals transfer by changing the mean state of a system (Yu et al., 2017). The state of a delta in terms of, for example, shoreline position, avulsion frequency, and slope, is variable because of autogenic processes. Sediment supply can only predict these delta characteristics when averaged over many avulsion cycles. It would therefore require very long signals before SSC can be recognised from the mean state. It may thus be much easier to recognise physical changes in the stratigraphic record resulting from high-frequency signals than from low-frequency signals.

Completeness of 1D vertical successions, defined as the number of time windows with preserved deposits, increases when the time window of discretisation increases (Straub and Esposito, 2013). We showed that this occurs for time windows of approximately 2 to 3 times longer than T_c, which is a consequence of lobe-scale avulsions occurring on average every $0.9T_c$ hr, and covering roughly a third to half of the delta. The completeness of the stratigraphic record relates to the dimensions of the data being analysed (Jerolmack and Sadler, 2007). Completeness increases when instead of a 1D section, a 2D cross-section is analysed and approaches 100% when $T_w \geq T_c$ in basin-wide cross-sections (Straub and Foreman, 2018). Proxy-signals (chemistry, isotopes) can be reconstructed if the signal is at least $2T_c$ long (Foreman and Straub, 2017). Analysis of mean deposition rates in basin-wide cross-sections shows that this rule does not apply to sediment supply signals. Signals of 2Tc duration could not be identified in the power spectra of Figure 5.7. Only the highest amplitude signal shows some evidence of periodic sediment supply signals in this dataset. Limiting the analysis to a cross-section reduces the strength of the signal by excluding allogenically forced changes in sedimentation rate at other locations than the section. All SSCs tested in this manuscript are close to the stratigraphic transfer threshold proposed by Toby et al. (2019a), which is based on a 3D volumetric dataset, and so their signal-to-noise ratio is low even in volumetrically complete datasets. As the magnitude of signals exceeds Q_a by a larger margin, the likelihood of detecting signals in incomplete dataset increases. We found that sediment supply cycles are not transmitted to all parts of the delta equally strong. The

best location to store high frequency (rapidly changing) sediment supply signals is in the proximal delta. Gradual long-period signals likely travel to the shoreline and beyond, although signals should be very long to influence metrics such as shoreline location. In addition, sediment transport on the delta will distribute the energy of these signals over a range of frequencies (Jerolmack and Paola, 2010). This effect increases with transport distance, making distal sections the least likely place to detect the frequency of an allogenic signal.

Wang et al. (2011) suggested that T_c in deltaic stratigraphy is well approximated by the depth of larger channels on the delta, but other authors speculated on lobe-scale topography as the roughness scale that sets T_c (Hajek and Straub, 2017; Trampush et al., 2017). We found that T_c is much better approximated from estimates of channel depth than lobe height in most of our experimental stages (control stage, HMSP, MMLP and LMLP stages), even though lobe roughness is generally several times higher than channel roughness. The reason behind this could be that long-term aggradation on the delta top is set by the rate of RSL rise, whereas submarine deposition can occur at much higher rates in prograding mouth bars, as shown by extremely high deposition rates in synthetic stratigraphy (Figure 5.1d). Timescales of compensation on the floodplain are thus set by the rate of accommodation generation, whereas compensation at the lobe scale is set by local sediment delivery. However, if lobe-scale topography is not filled in by rapid sedimentation, it does set a significant roughness scale, which may explain the unusually high $T_{c,\sigma ss}$ in stage LMSP.

5.5. Conclusions

Existing theory predicts and quantifies how constant allogenic forcing sets average scales in landscape morphology and rates of morphodynamic processes. On top of those predictable mean conditions, stochastic processes generate significant autogenic variations in landscape evolution, which may be difficult to distinguish from temporary change in allogenic forcing. We used physical experiments to test whether delta morphodynamic processes reveal the presence of periodic changes in sediment supply rate. This is essential for the preservation of allogenic signals in the stratigraphic record, because these morphodynamic processes determine landscape morphology, and thereby stratigraphic architecture.

The tested sediment supply signals have different combinations of signal amplitude and duration, which together set supply acceleration. We find that large-scale morphology formed in these experiments is controlled by avulsions. Avulsion frequency is not significantly different from an experiment with the same, but constant mean long-term sediment supply. We find no correlation between the timing of avulsions and the sediment supply curve. On a

smaller scale, each of the four tested signals has a different influence on morphodynamic processes, set by the signal's characteristics.

Large scale morphology was controlled by the avulsion cycle, which generates autogenic variations in slope, shoreline and channel network configuration. This autogenic control on landscape evolution obscures the presence of allogenic sediment supply signals. However, fast sediment supply change in particular can drive change in the landscape. Quick changes in sediment flux leads to more wide-spread activity of the sediment transport system. Slowly changing signals have limited influence on the delta top environment, but increase channel depth. This creates a conduit for the supply signals to be bypassed to marine environments. Long signals may theoretically influence slope and shoreline position, but this was not observed in response to signals of the scales tested here. However, sediment supply influences the equilibrium slope and thereby the potential to store sediment in different parts of the delta. High supply leads to increased activity in the proximal delta in order to increase slope, whereas low supply leads to increased activity in distal areas to decrease slope. This leads to phase shifts of the signal as preserved in stratigraphy, compared to the catchment-derived signal, the details of which depend on the location in the system.

Our results demonstrate that the transfer of periodic sediment supply cycles is complicated by: (1) the variability in landscape structure by autogenic processes that is difficult and sometimes impossible to distinguish from allogenic forcing; (2) variations in the location of signal transfer, and phase shifts between catchment-signal and stratigraphic signal; and (3) limited spatial and temporal data. However, the effects of these complications could be roughly predicted by comparing signals to rates and scales of autogenic processes. This allows stratigraphers to make informed decisions on where to look for allogenic sediment supply signals, and how these signals may have shaped the stratigraphic record.

Acknowledgments

This study was supported by the National Science Foundation (grant EAR-1424312), the Natural Environment Research Council (NERC) EAO Doctoral Training Partnership (grant NE/L002469/1) and the University of Liverpool. We thank members of the Tulane Sediment Dynamics and Stratigraphy Lab for help with the experiments and providing access to data from the control experiment. The data used are listed in the references.

Supplementary information to Chapter 5

1. Calculation of avulsion timescales

We aim to test whether sediment supply cycles systematically influence the timing and frequency of avulsions. However, quantification of avulsion frequencies is complicated by a wide range of spatial and temporal scales of avulsion frequencies channel and network reorganisations. Small changes such as bifurcations and crevasse splays occur frequently. Less frequent, but at a larger scale, are avulsions of the trunk channel. Defining the exact timing of an avulsion is also complicated by the fact that it takes time to fully switch from one channel to the other, if the original channel even is fully abandoned. In an effort to objectively identify large changes in the transport configuration of the experimental deltas, we quantify changes in the area on the delta receiving active flow. To do so, we identify the blue-dyed water from RGB colour information registered with the laser scanner. For each point on the grid we calculate a blueness-index ($BI_{x,y}$) as:

$$BI_{x,y}=\frac{B_{x,y}-G_{x,y}}{B_{x,y}+G_{x,y}},$$

where $B_{x,y}$ is the blue colour index at a grid location and $G_{x,y}$ the green colour index at the same location. To focus on large avulsions on the delta top, we limit this analysis to pixels above sea level and within 0.5 m from the delta apex. We classify all locations on the grid as either a wet pixel (P_w, high *BI*) or dry pixel (P_d, low *BI*) using Otsu's method (Otsu, 1979). We repeat this for all topographic scans at a 1 hr interval. The mobility of the transport system can now be quantified by comparing the wetted pixels of two topographic scans.

We calculate the number of wet pixels on the delta for one time step. Next, define f_P as the number of pixels that have remained wet in a later time step, as a fraction of the number of wet pixels in the initial time step. In other words, f_P=0.3 means that 70% of wet pixels in the original photo are no longer receiving water. Next, we calculate $T_{f=0.3}$, which is the time it takes to reach f_P=0.3. We calculate this duration for each of the scans in the experiments to generate a time series of $T_{f=0.3}$. This metric can be used to identify avulsions, because consistent and slow changes in $T_{f=0.3}$ mark gradual change in the transport system, whereas rapid jumps in $T_{f=0.3}$ indicate large changes in the transport configuration such as an avulsion. We visually inspected time-lapse videos of the experiments to verify whether the jumps in $T_{f=0.3}$ indicate large changes in the channel network. Figure 5.11 shows $T_{f=0.3}$ for each time

step in the experimental stages. Some noise in these plots can be expected as dry sediment may be dyed blue by the dye, but most of the high-frequency noise in these plots relates to short-lived splays and unconfined floods. Where we could correlate jumps in $T_{f=0.3}$ to avulsions, we changed the background shading of the plots in Figure 5.11, and recorded the last time step before the jump as the timing of avulsion. One clear avulsion in stage LMSP (phase 7-8) was not picked up by our metric but is based on observations from the time-lapse video.

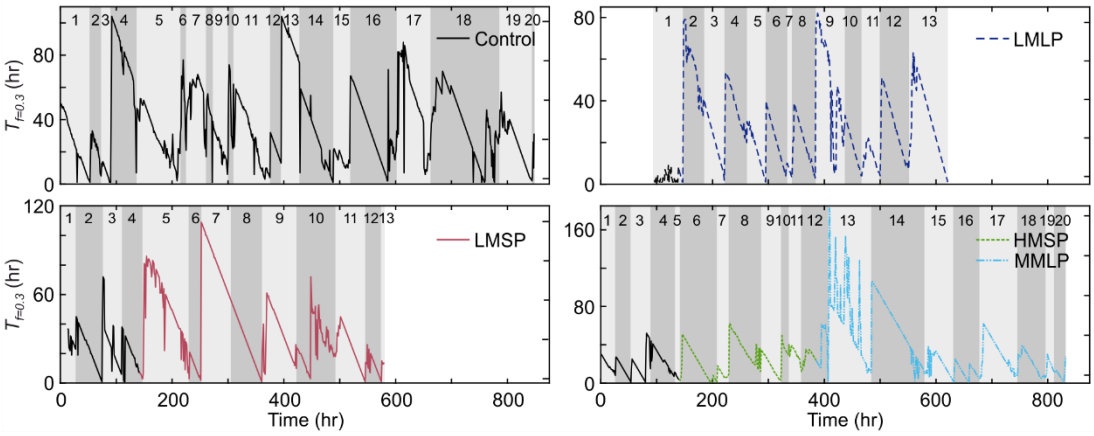

Figure 5.11 Timing of channel avulsions.

The timing of channel avulsions was approximated with a metric ($T_{f=0.3}$) based on automatic image classification. We split photographs of the terrestrial delta into wet and dry pixels and calculate the time necessary to convert 70% of the wet pixels into dry pixels ($T_{f=0.3}$), starting at every run hour in the experiments. Detailed methods to calculate $T_{f=0.3}$ are described in text. Upward jumps in $T_{f=0.3}$ suggest large shifts in the sediment transport network, while steady decrease of $T_{f=0.3}$ indicates no or little change in the transport network. The automatic image classification generates noise, so we visually inspected time-lapse videos of the experiments to verify whether jumps in $T_{f=0.3}$ could be correlated to an avulsion. Each of the inter-avulsion stages identified with this method were visualised by changing the background shading of the figure. The inter-avulsion stages are numbered and referred to in Figure 5.1.

6. Synthesis

6.1. Summary of results

Chapter 1 summarized the current state of science on environmental signal propagation through the landscape and preservation in the stratigraphic record. The aim of this thesis was to develop a quantitative theoretical basis that can be used to assess the stratigraphic record as an archive for allogenic signals of varying sediment flux. To achieve this aim, three objectives were defined and addressed in Chapters 3, 4, and 5. Each of these chapters were presented as stand-alone research papers on one of the objectives. In Chapter 3 we developed a theoretical framework that quantifies which sediment supply signals survive signal shredding and are transferred to the stratigraphic record. Chapter 4 builds on this with a new workflow to construct the signal shredding framework from field-scale stratigraphy. Chapter 5 discussed how sediment supply signals influence landscape dynamics, the results of which may guide the identification of sediment supply signals. Below, the main findings of these chapters are summarized and related back to the original thesis aim.

Previous work suggests that the transfer of environmental signals to stratigraphy depends on two independent thresholds: a minimum signal magnitude and a minimum signal duration (Jerolmack and Paola, 2010; Li et al., 2016). In Chapter 3 we built on this concept and came up with a novel theoretical framework that links signal duration and threshold magnitude into a threshold function. We hypothesised that a minimum magnitude for the transfer of sediment supply signals to the stratigraphic record is set by the maximum rate of autogenic sediment storage or release within the environment of interest. This autogenic rate, and thus the threshold magnitude, decreases with time window of measurement, which is a consequence of stochastic autogenic variations averaging out over long time scales. We made use of this concept to create a theoretical approximation of the threshold function in Chapter 4.

In Chapter 3, we tested the threshold function using high-resolution datasets of delta experiments. First, we quantified the threshold using an autogenic control experiment, characterised by constant allogenic forcing conditions. Next, we used four experimental stages with similar allogenic forcing conditions other than sediment supply. Sediment supply rate in these four stages followed a sine wave pattern, each with different combinations of signal magnitude and duration. The two signals that fall below threshold conditions could not be traced in stratigraphy, while the two signals that exceed our threshold were successfully transferred to the stratigraphic record, supporting the threshold function. Chapter 3 includes

a limited analysis of the experiments, presenting power spectra of terrestrial delta volume and mean elevation above sea level. We analysed both metrics as geomorphic datasets, i.e. volumes and elevations as they occur in the landscape, and as stratigraphic datasets, i.e. buried in the stratigraphic record. The two are not necessarily the same because sediment, and thus environmental signals, that is stored close to the surface can be reworked prior to permanent burial. This is important because the results of Chapter 3 show that one of the tested signals influenced the geomorphic dataset, but disappeared in the stratigraphic dataset. This signal had a particularly low duration and magnitude relative to autogenics. Interestingly, a signal of similar magnitude but with a much longer duration did not leave a trace in either dataset. In Chapter 3, we suggest that the quicker change in supply conditions (acceleration) for the shorter signal pushes a landscape out of equilibrium, and we support this with a more detailed analysis of the same experiments in Chapter 5. The preservation potential of such quickly accelerating, but short-term signals is limited because short signals produce thin deposits, making them prone to significant reworking.

The results of Chapter 5 support the importance of sediment supply acceleration. This chapter presents an in-depth analysis of the same experiments conducted for Chapter 3. The focus here are morphodynamic processes on the delta, and their relation with the sediment supply cycles. We found that stochastic autogenic processes control large-scale geomorphology such as slope and shoreline location. The most important autogenic process is avulsion. The timing of avulsions and inter-avulsion duration are not related to sediment flux signals of the scale tested in the experiments. This is because stochastic autogenic processes produce a wide range of avulsion frequencies for any sediment supply rate, even a constant one. It should be noted that each of the tested signals were close to threshold conditions (Chapter 3), and their influence on delta morphology was limited (Chapter 5). A future study could explore stronger signals that exceed the autogenic threshold function by a larger margin (e.g.: Qs^*=2, T^*=2, see Figure 3.2b). Signals with a much higher amplitude or duration than tested here could potentially influence large-scale morphodynamics in a systematic way, but these limits are yet to be determined. In some cases this limit may be estimated by the equilibrium timescale (T_{eq}) of a system based on diffusion equations (Paola et al., 1992), but in the case of our experiments autogenic 'noise' occurred at timescales similar to T_{eq}. This obscured a relation between sediment supply cycles, and geomorphic characteristics such as shoreline position and slope.

On a smaller scale though, periodic sediment flux signals are preserved in the stratigraphic record, as shown in Chapters 3 and 5. The mobility of the transport network is the main indicator of sediment flux signals. However, signals of different duration and amplitude transfer in different ways as the sediment supply signals themselves influence the

spatial and temporal distribution of accommodation on the delta. Given a constant water flux, a changing ratio of water flux versus sediment flux changes the equilibrium slope on the delta and thereby the accommodation potential (Parker et al., 1998; Whipple et al., 1998). High sediment supply leads to a steeper equilibrium slope, and so the delta top becomes more active in proximal areas. Low supply has the reverse effect, where a lower transport slope increases sediment bypass in the proximal delta and boosts deposition on the distal delta top. Phases of low sediment supply also leave space available for phases of higher supply. However, when supply changes rapidly, this space is filled in quickly, after which the transfer of high supply phases to delta top stratigraphy is limited by available accommodation. Sediment supply signals are thus not transmitted uniformly to all locations in a basin, but as a function of local accommodation space and sediment supply, the balance of which is a function of signal magnitude, duration and acceleration. This is in addition to autogenic dynamics spreading sediment unevenly over the basin by migrations in the transport network.

We find more coeval channels during high supply than during low supply for signals with a high acceleration. High acceleration supply signals tend to clog up channels, creating more distributary channels in addition to the trunk channel. Long periodicity signals are dominated by low supply conditions instead. This is because low sediment supply deepens the trunk channel, enhancing the transport capacity. Subsequent higher supply conditions are largely bypassed because of the transport efficiency of the deep channel. As a consequence, gentle changes in supply are less efficient in generating cyclicity on the delta top, but are probably more likely to transfer to distal environments, for example by shifting the shoreline or enhancing sediment transport to marine environments.

Delta morphodynamics change in response to signals that (1) are above a magnitude threshold for stratigraphic transfer, as defined in Chapter 3, or (2) exceed some acceleration threshold, the magnitude of which is yet to be defined. However, the potential to detect signals close to these thresholds is limited. The thresholds are based on time series of volumetric data. Most field data are of a much lower spatial and temporal resolution. The results of Chapter 5 inform stratigraphers which geomorphic elements could be used to detect the presence of supply signals, although this would still require a high spatial resolution dataset. Field data are typically limited to 1D vertical successions and 2D stratigraphic panels, and thus volumetrically incomplete. Sediment flux signals should thus be well above the shredding threshold to be detectable in field datasets.

Even when field data cannot be used to accurately identify environmental signals of a certain periodicity, changes in sediment flux may still influence stratigraphic architecture. Chapter 4 describes a method to approximate the stratigraphic transfer threshold function from field data, based on long-term average sediment fluxes. The threshold function

presented in Chapter 3 requires measurements of sediment fluxes at a high temporal resolution. The strength of the field approximation is that the threshold function can be established using a long-term estimation of sediment fluxes. This approximation is based on a few assumptions: (1) at very short timescales, all sediment can be trapped within one environment; (2) sediment trapping decays following an exponential function, as found in the experiments of Chapter 3; and (3) autogenic processes average out over long timescales. There is some uncertainty in predicting the exact timescale at which autogenic fluxes level out. Experiments suggest this may be as long as $8T_c$ and should at least include several avulsion cycles. However, field-scale system autogenic fluxes, and thus the threshold function, likely approach zero at timescales much closer to $1T_c$. Based on these assumptions, the threshold function can be approximated from limited field data of channel depths and long-term accumulation rate, which set the compensation timescale, and the long-term ratio of sediment deposition versus bypass as this sets the maximum threshold magnitude.

In Chapter 4, we apply this field approximation to field-scale systems using published literature data from the Pleistocene Kerinitis Delta in Lake Corinth, Greece. The Kerinitis delta is a roughly 2 km long aggradational Gilbert-type delta on the hanging wall of a normal fault (Barrett et al., 2019). Our threshold suggests that Milankovitch-scale sediment supply signals would likely influence stratigraphic architecture. Next, we apply this method to five different segments of the Eocene Escanilla sediment routing system (Michael et al., 2014). The most proximal segments are alluvial fans of the Sis and Montsor members. These converge into the fluvial Escanilla-Graus segment, which transfers into the fluvial Escanilla-Ainsa segment. The last segment includes shallow to deep marine environments in the Jaca basin. Using published data of channel depths and sedimentation rates in each of these sections, we test whether each of these sections could store hypothetical sediment supply signals of 20 ky, 40 ky and 100 ky duration and a 30% change in supply rate. The 20 ky signal is unlikely to transfer to the stratigraphic record in any of the segments. The alluvial fans are most likely to record the 40 ky and 100 ky signals. Given that T_c is much higher in the fluvial segments than in the proximal fans, our method predicts that the 40 ky and potentially the 100 ky singals are unlikely to be preserved in the stratigraphic record of the fluvial segments.

Chapter 4 also discussed the propagation of environmental signals through a sediment routing system using the Escanilla system as an example. Chapter 3 concluded that allogenic processes are transferred to the landscape when they exceed the stratigraphic transfer threshold, or when supply acceleration is particularly high. These signals are not shredded by sediment transport and can thus propagate through to downstream segments, even if the signal is not permanently stored by later-on reworking. However, signals of slowly

changing sediment supply, below the stratigraphic transfer threshold, cannot transfer to more distal environments once shredded by transport dynamics.

Chapters 3, 4, and 5 together provide a complete workflow for the interpretation of sediment supply signals from the stratigraphic record. First, we developed a theoretical framework that quantifies transfer and shredding conditions in the stratigraphic record. Next, this framework was translated into a field workflow that allows application of these quantitative concepts to the stratigraphic record. Finally, we explore how different classes of signals modify the landscape and thereby show which metrics may be used to identify environmental signals in the stratigraphic record.

6.2. Implications

6.2.1. Implications for our understanding of landscape dynamics and the stratigraphic record

This thesis provides new insights into the preservation of environmental signals in the stratigraphic record. It is well known that sediment supply is an important control on landscape dynamics and stratigraphy (Schlager, 1993; Bryant et al., 1995). We knew from model results that not all sediment supply signals are stored in the stratigraphic record (Paola et al., 1992; Paola, 2000), and that the transfer of supply signals to the landscape depends on the duration or magnitude of supply signals relative to autogenic scales (Jerolmack and Paola, 2010). Chapter 3 showed that the transfer of supply signals to stratigraphy depends on a combination of signal duration and magnitude. One implication of the field estimation presented in Chapter 4 is that the stratigraphic shredding threshold depends on mass extraction, whereas 1D models depended on system length (Paola et al., 1992; Marr et al., 2000; Jerolmack and Paola, 2010).

Contrary to most previous studies on the transfer of supply signals to the stratigraphic record, the results of this thesis (Chapter 3 and 5) reveal an important role for the rate of supply change that may enable the transfer of high-frequency environmental signals. However, these signals should be sought after in the structure of the stratigraphic record rather than deposition rates as reworking will erase volumetric signals. This suggests that the shape of a signal may also be important for signal transfer. Signals tested in this thesis followed a perfect sine wave. Although often illustrated as sine waves, signals in nature are unlikely to be perfectly sinuous. For example, rates of RSL fluctuations are generally

asymmetric (Hillgartner and Strasser, 2003; Ritchie et al., 2004). Sediment supply curves generated by glacial-interglacial cycles may also be asymmetric. Large volumes of sediment are generated during glacials, but this sediment is mainly transported to basins during interglacials (Malatesta et al., 2018; Watkins et al., 2018). As a consequence, sediment flux through a sediment routing system is low during a glacial, but rapidly increases at the start of an interglacial until it slowly drops when proximal sediment reservoirs are exhausted. The highly accelerating part of an asymmetric environmental signal may influence landscapes easily, whereas the more slowly accelerating part of that same signal has a relatively long duration, and thus a higher stratigraphic storage potential.

The importance of signal acceleration has interesting consequences for human influences on landscapes. Chapter 3 discussed the influence of humans in modifying the sediment yield of river systems. Given the almost instantaneous drop in sediment yield after constructing dams, theories of Chapter 3 and 4 could give a first glance at whether river engineering may have had such a significant impact that it could be preserved in the stratigraphic record. The same applies to current fast rates of anthropogenic climate change, although models predict that climate signals of short duration are buffered by the catchment (see review in Chapter 1) and so the short-term effects of current climate change on sediment flux will be more limited than those of river engineering works.

Although the general concepts of signal preservation, propagation and shredding are well-known among field stratigraphers, direct application of these concepts to field stratigraphy is difficult. The field approximation presented in Chapter 4 provides stratigraphers with a new predictive method that can be estimated from stratigraphy. One example where this tool could be used is in studies that found potential evidence for sediment supply signals. This interpretation could be quantitatively underpinned by constructing the threshold function and testing it for realistic supply scenarios. Field studies that did not find evidence of supply signals may test whether this is likely due to the absence of sediment supply signals, or limits to their dataset. In the latter case, sediment supply may still be an important control on morphodynamics and thereby stratigraphic architecture, but the signal could not be identified. This is the case in many of our analyses of delta morphodynamics in Chapter 5. The theory of Chapter 3 may also be used to predict whether experimental results, conceptual models, and existing interpretations of field data would change if sediment supply signals are included. However, it is important to keep in mind that stochastic autogenic processes are an important control on stratigraphic architecture that cannot be ignored, even when sediment supply signals exceed the threshold (Chapter 5).

The theories presented in Chapter 3 and 4 may also be used to inform study site selection. Where Earth scientists have reason to believe that sediment supply signals of a

certain duration and magnitude were generated by a catchment, the framework presented here can help predict which segment of a sediment routing system is most likely to record these signals using limited data such as a subsidence profile and channel depths. Chapter 5 could then serve as a guideline in a more detailed study looking for potential evidence of sediment supply cycles.

6.2.2. Implications for theories of environmental signal shredding

The results of Chapter 3 and 5 show clear similarities with results of Burgess et al. (2019) on submarine fans. For this work, which is not included as a separate chapter in this thesis, we set up a new reduced-complexity model called Lobyte3D. Deposition in this model was proportional to flow volume and basin slope. We compared two model runs that simulated 1000 gravity flows each. Flow volume was constant in the first model run. In the second run, the total supplied volume was the same as run 1, but flow volume followed a sinusoidal pattern with a period of 25 flows and an amplitude equal to 80% of mean flow volume. In order to analyse bed thickness patterns, vertical successions of bed thickness were extracted from the model, analogous to bed thickness measurements from sedimentary logs or wireline logs. Small lateral movements of each successive flow, and larger lobe avulsions caused hiatus in the vertical successions and moved the depocenter around the basin. The organisation of beds into compensationally stacked lobes also created an ordered pattern of bed thicknesses over long timescales, longer than the periodicity of the allogenic signal. The patterns caused by basin topography were dominant over those caused by varying flow volume. Autogenic controls on deposition thus modified or even destroyed the signal of supply variations in single vertical successions. However, combining bed thickness patterns from multiple vertical successions increased the chance of recovering the sediment supply signal. The routing of sediment gravity flows in Lobyte3D clearly showed how autogenic processes can form stratigraphic architecture that may resemble allogenic control. This result of Lobyte3D is similar to Chapter 5, where an analysis on shoreline rugosity showed periodic trends that may also be mistaken for external forcing. Lobyte3D also shows that even strong external signals often generate stratigraphic patterns indistinguishable from patterns purely driven by autogenic controls.

A comparison between the results of this study with Lobyte3D and the delta experiments shows interesting insights on the destruction of allogenic signals, because the process that destroys allogenic signals in Lobyte3D is different from the experiments. Lobyte3D does not model erosion and so the total volume in each flow follows the exact same sine-wave pattern as the supplied volume. In the delta experiments, sediment can be

stored temporarily, and reworked later-on. This happens on a range of scales: from the transport of individual grains through a channel to the scouring of old floodplain deposits by new channels. These stochastic processes generate noise in landscape evolution (Jerolmack, 2011). The preserved volume on the delta in each time step does not necessarily correspond to the supplied volume in each time step. In fact, preserved sediment volume between two stratigraphic timelines can be smaller than supplied volume because of net sediment erosion during later time steps, or larger than supplied volume following remobilisation of old sediment in the basin. These stochastic differences in sediment deposition and erosion on the delta dissipate the sediment flux variations at the frequency of the signal over a range of other frequencies, which shreds the signal (Jerolmack and Paola, 2010).

This difference between the Lobyte3D fan and the delta experiments illustrates the difference between signal shredding and signal loss due to completeness. Signal loss due to incompleteness, from here on referred to as signal fragmentation, is much like shredding a paper document. The content of the document cannot be reconstructed from an individual paper strip, but the message is not permanently destroyed and can be recovered by combining enough strips (Figure 6.1a). This occurs in landscapes where sediment is spread out over space by the dynamics of the transport network. A signals may not be identified in a single vertical succession, but in a complete three-dimensional dataset the signal is still present. This is the reason allogenic signals could not be identified in individual vertical succession of the Lobyte3D model runs in Burgess et al. (2019). This signal fragmentation is a consequence of our limited ability to create complete datasets from field data, but technically signals are not permanently destroyed.

The term signal shredding has become popular in scientific literature since Jerolmack and Paola (2010) introduced it in their paper titled 'Shredding of environmental signals by sediment transport'. However, the analogy with shredding may cause some confusion over the exact meaning. To bring back the analogy of a paper document: the effect of signal shredding is much like burning the document, because the message is permanently deleted no matter how much of the burned material is collected. Signal shredding as described in Jerolmack and Paola (2010) is the destruction of environmental signals by stochastic autogenic processes, where the frequency of allogenic signals is distributed over a range of other frequencies. I described earlier how stochastic changes in bypass and reworking distribute the supply signal's frequency over a range of other frequencies. For a shredded signal, collecting more data will not help in reconstructing the allogenic signal (Figure 6.1b). Chapter 3 showed examples of signals that are stratigraphically shredded. Volumetric datasets of the entire delta top did not contain the frequency of the supply signal. In fact, one of the

experiments showed that a supply signal travelling through the landscape was reworked and therefore not present in stratigraphy.

In a stratigraphic sense, signal shredding means that a signal's frequency has not transferred to the stratigraphic record. This shredding is different from fragmentation in the sense that a timeline of sediment volume is not a definitive and may change until sediment is permanently buried. As a consequence, preserved deposition rates at a high temporal resolution do not necessarily match the input signal. In contrast to preserved deposition rates, a timeline of the total sediment volume in an enclosed basin faithfully records the amount of supplied sediment, with or without reworking. By focusing analysis on a fraction of the entire basin, i.e. the delta top, a dataset becomes incomplete and both signal fragmentation and shredding contribute to destroying environmental signals.

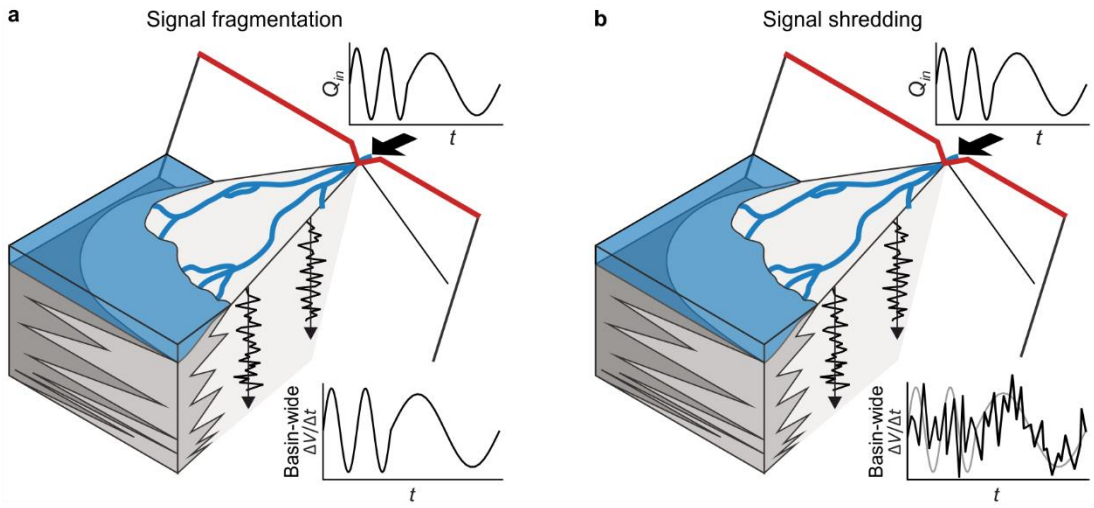

Figure 6.1. Signal fragmentation versus signal shredding.

(**a**) Schematic delta to illustrate signal fragmentation. Examples of deposition rates in 1D vertical successions may or may not contain the input signal frequency because of autogenic variations in the distribution of sediment over the basin. However, when the total deposited volume in a time step (basin-wide $\Delta V/\Delta t$) follows supplied terrigenous sediment perfectly, the signal is technically not destroyed. Instead, identification of this signal is limited by our limitations of collecting complete and accurate stratigraphic datasets. (**b**) Schematic delta to illustrate signal shredding. Preserved deposition rates between two timelines may not match the sediment supply rate because of autogenic sediment storage and release. No matter how much data are collected, only signals that exceed autogenic thresholds can be distinguished from autogenic signals.

6.3. Suggestions for future work

This work provides a framework for the transfer potential of periodic sediment flux signals to landscapes and into the stratigraphic record. Numerous studies have investigated the effect of changing boundary conditions on landscape dynamics (see Chapter 5), and few have linked this to stratigraphy. This thesis clearly demonstrates that transfer of environmental signals to landscapes and stratigraphy are not necessarily the same, because signals that influence landscape morphology may be erased before burial below the active surface (Chapter 3). Timescales for surface processes to equilibrate with environmental conditions have often been approached with diffusion equations (Paola et al., 1992; Castelltort and Van den Driessche, 2003), whereas timescales of stratigraphic preservation relate to the maximum depth of reworking (Wang et al., 2011). Estimations of equilibrium timescales (T_{eq}) and reworking timescales (T_c) for the experiments suggests that the two are very similar (Chapter 5). Future work could investigate whether this is a coincidence or a predictable theoretical relation between T_c and T_{eq}.

The relation between timescales of surface processes and T_c is also important for approximations of the autogenic threshold function, and the completeness of the stratigraphic record. Avulsion timescales may be much shorter relative to T_c in field-scale systems than on laboratory scale, which influences the timescales over which autogenic processes may obscure sediment flux signals (Chapter 4). In addition, Straub and Esposito (2013) found that the time window of completeness of the stratigraphic record is a function of T_c and the mobility of the sediment transport system. Theoretical relations between horizontal timescales that describe surface mobility and vertical timescales that describe preservation (i.e. T_c) could be improved, which would enable better predictions on the information preserved in the stratigraphic record.

The transfer of allogenic signals to sedimentary systems relates to the timescale of forcing, the magnitude of change, and the rate of change. Studies that vary only the magnitude of forcing between experiments may elucidate landscape dynamics in a state of dynamic equilibrium (e.g. Bryant et al. (1995)), but care should be taken when extrapolating these results to systems forced by temporally varying climatic and tectonic conditions. Model results have demonstrated the transient response of landscapes and stratigraphy to different types of signals, but more work could be done to identify when, where and how these signals influence sediment routing systems. A particular topic to focus on is the effect of acceleration on allogenic signal transfer. Future studies may find new relations between signal acceleration and morphodynamic processes. Contrary to many earlier studies that identify landscapes as

low-pass filters for environmental signals, signal acceleration could be a mechanism to transfer higher-resolution signals to sedimentary systems than previously predicted.

This thesis isolated the problem of sediment supply by setting all other allogenic forcing conditions as a constant, but signal transfer thresholds may change by interaction with other allogenic forcings (e.g. Simpson and Castelltort (2012)). As a first step, the community could build a thorough understanding of signal transfer and shredding for all types of allogenic forcing, one at the time. A new threshold framework may be explored for allogenic water flux signals. As climates change, differences in precipitation and meltwater could lead to significant discharge variations. This should have a profound influence on the landscape, because water flux sets the transport capacity of sediment and shapes landscape morphology such as channel dimensions (Phillips and Jerolmack, 2016) and slope (Parker et al., 1998). The transfer of periodic changes in grain size to landscape dynamics may also be complex, given that the threshold for grain motion depends on supplied sediment characteristics, but also varies with autogenic processes (Van De Wiel and Coulthard, 2010).

Once we have a solid understanding of the transfer and shredding of individual forcing signals, a next step could be to develop quantitative theory that accounts for the interaction of different types of signals. Other allogenic forcings coeval to sediment flux signals may influence the sediment supply signal threshold by changing the conditions for accommodation generation and sediment transport (Simpson and Castelltort, 2012; Bijkerk et al., 2014). The relative timing and absolute magnitudes and durations of different allogenic signals in a sediment routing system are still poorly constrained because of feedbacks between different forcing mechanisms, signal buffering and response timescales in landscapes.

Maybe the largest challenge in this field is still relating our theoretical knowledge to field systems (Paola, 2000). We now have datasets with a reasonably high spatial resolution, such as 3D seismic data (Klausen et al., 2019), GPR (Bristow and Pucillo, 2006), and virtual outcrop models made with UAVs (Chesley et al., 2017) and LiDAR (Eide et al., 2016). However, old stratigraphic successions in particular cannot be dated at a meaningful resolution for many autogenic processes. Our understanding of signal propagation, preservation and shredding is therefore largely based on numerical and physical model predictions. A lot of work remains to be done in integrating model results with field data to guide more accurate qualitative and quantitative reconstructions of Earth's surface history from the stratigraphic record.

Appendices

1. Experimental datasets

1.1. Tulane Delta Basin Experiments

A large part of this thesis is based on physical experiments in the Tulane University Delta Basin (TDB). A description of these experiments is outlined in Chapter 2. A total of seven experimental stages have been used in this thesis. The control stage refers to the final 900 h of experiment TDB-12-1, which is characterised by constant boundary conditions. Three new experiments with cyclic sediment supply have been conducted for this thesis: TDB-16-1 (incl. LMSP), TDB-16-2 (incl. LMLP), and TDB-16-3 (incl. HMSP and MMLP). Experiment TDB-13-1 includes stages referred to as experiment 2 (moderately cohesive) and experiment 3 (non-cohesive) in Chapter 4.

All experimental data and metadata are available online through the SEAD (Sustainable Environment through Actionable Data) data repository. The next section provides references to experiments TDB-12-1 and TDB-13-1. Metadata of these experiments can be accessed on SEAD. Metadata for the newly conducted experiments (TDB-16) is provided in the next section and is also available on SEAD.

1.2. Experiment TDB-12-1 general metadata

Reference:

Li, Q., Straub, K. M., 2017, TDB_12_1, SEAD, doi:10.5967/M03N21GX.

Experiment name:

TDB-12-1

Link:

http://doi.org/10.5967/M03N21GX.

See the dataset on SEAD for metadata of this experiment.

1.3. Experiment TDB-13-1 general metadata

Reference:

Li, Q., Straub, K. M., 2017, TDB_13_1, SEAD, doi:10.5967/M07D2S7Q.

Experiment name:

TDB-13-1

Link:

http://doi.org/10.5967/M07D2S7Q.

See the dataset on SEAD for metadata of this experiment.

1.4. Experiment TDB-16-1 general metadata

Reference:

Toby, S. C., Straub, K. M., 2019. TDB_16_1, SEAD, doi:10.26009/s0iorjdx

Experiment Name:

TDB-16-1

Link:

http://doi.org/10.26009/s0iorjdx

Experimental Facility:

Tulane Delta Basin – This basin has approximate dimensions of 0.65 m deep, 4.2 m long and 2.8 m wide. Base level is controlled to millimeter precision via a motorized weir in hydraulic communication with the basin. Base level, sediment feed, and water feed to the basin are controlled through a computer interface. Topography is collected with a FARO Focus3D-S 120 laser scanner system and gridded on a 5x5 mm grid. Digital images were taken every 15 min.

Dates Run:

05 March 2016 – 25 April 2016

Primary individual responsible for experiment:

Stephan Toby, Kyle Straub.

Secondary support for experiment:

Qi Li, Christopher Esposito, Tushar Bishnoi, Lizhu Yu, Meg Harlan.

Purpose of experiment:

To define the storage conditions of sediment supply signals in stratigraphy. Sediment supply in this experiment followed a sine wave pattern with a low magnitude and short period relative to the system's autogenic processes.

General description:

This experiment started with sea level 25 mm above a flat basin floor consisting of coarse 'play sand'. Water level was kept constant for 57 h to allow progradation of a delta by constant sediment supply and water discharge ('PreSubs'). After this stage, the clock is reset to zero and a 630 h long stage of constant sea level rise starts ('Subside'). Water discharge and mean sediment supply during the subside stage remain unchanged. Starting at run hour 140, sediment supply rate follows a sine wave pattern for a total of 490 h.

Boundary Conditions:

Total Run Hours: 57 h (PreSubs) + 630 h (Subside).

Water Supply: 1.72 x 10^{-4} m^3/s.

Mean sediment Supply: 1.41 kg/h.

Sediment Supply Change: During run hour 140-630 of the subside stage, sine wave with mean supply 1.41 kg/h, periodicity 24.5 h, peak-to-peak amplitude 0.22 kg/h (scaled to autogenic dynamics: T_s*=0.5, Q_s*=0.5).

Initial Ocean Level: 25 mm.

Ocean Level Change: constant sea level rise of 0.25 mm/h during subside stage.

Dye (Including Frequency): Introduced to the basin for 1 min every 15 minutes.

Sediment Description: Each batch of sediment had 50 lbs of 120 Mesh Silica Sand, 25lbs of WF-1 fine sieved sand, 18.5 lbs of Kosse Industrial 18/100 Dry, 2366 ml of Aquagel Bentonite, 2366 ml of Better way flushable Kitty Litter, 10 lbs of Spheriglass A Glass 2429, 80 gram of NewDrill plus polymer, 6.5lbs of Sandtastic Dark Red (Floral) sand.

Sediment Supplier(s): Mesh Silica Sand, WF-1 fine sieved sand, Kosse Industrial 18/100 Dry from U.S. Silica, Aquagel Bentonite from Haliburton, Better way flushable Kitty Litter from Better way, Spheriglass A Glass 2429 from Potter Industries, NewDrill plus polymer from Baker Hughes, Sandtastic Dark Red (Floral) Sand from Santastik.

Photograph Metadata:

Photo angle of raw image: Overhead images taken with Cannon G10 camera.

Frequency of Capture: 1 image every 15 minutes.

Timing: 1 every 15 minutes.

Topographic Metadata:

Method of Collection: 3D laser scanner

Spatial Coverage: 2.5 m from the proximal river-right corner in both the cross-basin and down-basin directions.

Resolution: Vertical resolution of 1 mm, point cloud gridded to a resolution of 5 mm in the cross-stream and down-stream directions.

Frequency of collection: One dry scan is taken at the end of each hour when the whole system is paused. One wet scan is taken at 55 minutes into each hour of the run when river flow is active.

Other: Run hour 6 – 10 and 12 are missing because of a problem with the scanner.

Stratigraphic Cuts Metadata:

Location of Sections: See basin coordinates in Original Data/Subside/Cuts.

Method of sectioning: Freezing wedge cutting method.

1.5. Experiment TDB-16-2 general metadata

Reference:

Toby, S. C., Straub, K. M., 2019. TDB_16_2, SEAD, doi:10.26009/s0xtyi86

Experiment Name:

TDB-16-2

Link:

http://doi.org/10.26009/s0xtyi86

Experimental Facility:

Tulane Delta Basin – This basin has approximate dimensions of 0.65 m deep, 4.2 m long and 2.8 m wide. Base level is controlled to millimeter precision via a motorized weir in hydraulic communication with the basin. Base level, sediment feed, and water feed to the basin are controlled through a computer interface. Topography is collected with a FARO Focus3D-S 120 laser scanner system and gridded on a 5x5 mm grid. Digital images were taken every 15 min.

Dates Run:

06 May 2016 – 09 August 2016

Primary individual responsible for experiment:

Stephan Toby, Kyle Straub.

Secondary support for experiment:

Qi Li, Christopher Esposito, Tushar Bishnoi, Lizhu Yu, Meg Harlan.

Purpose of experiment:

To define the storage conditions of sediment supply signals in stratigraphy. Sediment supply in this experiment followed a sine wave pattern with a low magnitude and long period relative to the system's autogenic processes.

General description:

This experiment started with sea level 25 mm above a flat basin floor consisting of coarse 'play sand'. Water level was kept constant for 57 h to allow progradation of a delta by constant sediment supply and water discharge ('PreSubs'). After this stage, the clock is reset to zero and a 630 h long stage of constant sea level rise starts ('Subside'). Water discharge and mean sediment supply during the subside stage remain unchanged. Starting at run hour 140, sediment supply rate follows a sine wave pattern for a total of 490 h.

Boundary Conditions:

Total Run Hours: 57 h (PreSubs) + 630 h (Subside).

Water Supply: 1.72 x 10^{-4} m^3/s.

Mean sediment Supply: 1.41 kg/h.

Sediment Supply Change: During run hour 140-630 of the subside stage, sine wave with mean supply 1.41 kg/h, periodicity 90 h, peak-to-peak amplitude 0.22 kg/h (scaled to autogenic dynamics: T_s*=2, Q_s*=0.5).

Initial Ocean Level: 25 mm.

Ocean Level Change: constant sea level rise of 0.25 mm/h during subside stage.

Dye (Including Frequency): Introduced to the basin for 1 min every 15 minutes.

Sediment Description: Each batch of sediment had 50 lbs of 120 Mesh Silica Sand, 25lbs of WF-1 fine sieved sand, 18.5 lbs of Kosse Industrial 18/100 Dry, 2366 ml of Aquagel Bentonite, 2366 ml of Better way flushable Kitty Litter, 10 lbs of Spheriglass A Glass 2429, 80 gram of NewDrill plus polymer, 6.5lbs of Sandtastic Dark Red (Floral) sand.

Sediment Supplier(s): Mesh Silica Sand, WF-1 fine sieved sand, Kosse Industrial 18/100 Dry from U.S. Silica, Aquagel Bentonite from Haliburton, Better way flushable Kitty Litter from Better way, Spheriglass A Glass 2429 from Potter Industries, NewDrill plus polymer from Baker Hughes, Sandtastic Dark Red (Floral) Sand from Santastik.

Photograph MetaData:

Photo angle of raw image: Overhead images taken with Cannon G10 camera.

Frequency of Capture: 1 image every 15 minutes.

Timing: 1 every 15 minutes.

Topographic Metadata:

Method of Collection: 3D laser scanner.

Spatial Coverage: 2.5 m from the proximal river-right corner in both the cross-basin and down-basin directions.

Resolution: Vertical resolution of 1 mm, point cloud gridded to a resolution of 5 mm in the cross-stream and down-stream directions

Frequency of collection: One dry scan is taken at the end of each hour when the whole system is paused. One wet scan is taken at 55 minutes into each hour of the run when river flow is active.

Other: Run hour 1-95 are missing because of a problem with the scanner.

Stratigraphic Cuts Metadata:

Location of Sections: See basin coordinates in Original Data/Subside/Cuts.

Method of sectioning: Freezing wedge cutting method.

1.6. Experiment TDB-16-3 general metadata

Reference:

Toby, S. C., Straub, K. M., Dutt, R., Akintomide, A., 2019. TDB_16_3, SEAD, doi:10.26009/s0c20606

Experiment Name:

TDB-16-3

Link:

http://doi.org/10.26009/s0c20606

Experimental Facility:

Tulane Delta Basin – This basin has approximate dimensions of 0.65 m deep, 4.2 m long and 2.8 m wide. Base level is controlled to millimeter precision via a motorized weir in hydraulic communication with the basin. Base level, sediment feed, and water feed to the basin are controlled through a computer interface. Topography is collected with a FARO Focus3D-S 120 laser scanner system and gridded on a 5x5 mm grid. Digital images were taken every 15 min.

Dates Run:

10 October 2016 – 14 December 2016

Primary individual responsible for experiment:

Stephan Toby, Kyle Straub, Ripul Dutt, Akinbobola Akintonmide.

Secondary support for experiment:

Tushar Bishnoi, Qi Li.

Purpose of experiment:

To define the storage conditions of sediment supply signals in stratigraphy. There are two different stages in this experiment where sediment supply followed a sine wave pattern. The first sine wave had a high magnitude and short period relative to the system's autogenic processes. The second had a medium magnitude and long duration.

General description:

This experiment started with sea level 25 mm above a flat basin floor consisting of coarse 'play sand'. Water level was kept constant for 57 h to allow progradation of a delta by constant sediment supply and water discharge ('PreSubs'). After this stage, the clock is reset to zero and an 875 h long stage of constant sea level rise starts ('Subside'). Water discharge and mean sediment supply during the subside stage remain unchanged. Starting at run hour 140, sediment supply rate follows a sine wave pattern for a total of 245 h, after which sediment supply follows a sine wave with a different combination of amplitude and frequency for another 490 h.

Boundary Conditions:

Total Run Hours: 57 h (PreSubs) + 875 h (Subside).

Water Supply: 1.72 x 10^{-4} m^3/s.

Mean sediment Supply: 1.41 kg/h.

Sediment Supply Change: During run hour 140-385 of the subside stage, sine wave with mean supply 1.41 kg/h, periodicity 24.5 h, peak-to-peak amplitude 0.87 kg/h (scaled to autogenic dynamics: T_s*=0.5, Q_s*=2).During run hour 385-875 of the subside stage, sine wave with mean supply 1.41 kg/h, periodicity 90 h, peak-to-peak amplitude 0.43 kg/h (scaled to autogenic dynamics: T_s*=2, Q_s*=1).

Initial Ocean Level: 25 mm.

Ocean Level Change: constant sea level rise of 0.25 mm/h during subside stage.

Dye (Including Frequency): Introduced to the basin for 1 min every 15 minutes.

Sediment Description: Each batch of sediment had 50 lbs of 120 Mesh Silica Sand, 25lbs of WF-1 fine sieved sand, 18.5 lbs of Kosse Industrial 18/100 Dry, 2366 ml of Aquagel Bentonite, 2366 ml of Better way flushable Kitty Litter, 10 lbs of Spheriglass A Glass 2429, 80 gram of NewDrill plus polymer, 6.5lbs of Sandtastic Dark Red (Floral) sand.

Sediment Supplier(s): Mesh Silica Sand, WF-1 fine sieved sand, Kosse Industrial 18/100 Dry from U.S. Silica, Aquagel Bentonite from Haliburton, Better way flushable Kitty Litter from Better way, Spheriglass A Glass 2429 from Potter Industries, NewDrill plus polymer from Baker Hughes, Sandtastic Dark Red (Floral) Sand from Santastik.

Photograph Meta Data:

Photo angle of raw image: Overhead images taken with Cannon G10 camera.

Frequency of Capture: 1 image every 15 minutes.

Timing: 1 every 15 minutes.

Topographic Meta Data:

Method of Collection: 3D laser scanner.

Spatial Coverage: 2.5 m from the proximal river-right corner in both the cross-basin and down-basin directions.

Resolution: Vertical resolution of 1 mm, point cloud gridded to a resolution of 5 mm in the cross-stream and down-stream directions.

Frequency of collection: One dry scan is taken at the end of each hour when the whole system is paused. One wet scan is taken at 55 minutes into each hour of the run when river flow is active.

Other: Run hour 204-208 (wet) and 203-207 (dry) are missing because of a problem with the scanner.

Stratigraphic Cuts Meta Data:

Location of Sections: See basin coordinates in Original Data/Subside/Cuts.

Method of sectioning: Freezing wedge cutting method.

2. List of symbols and acronyms

a	Parameter in the ATF that sets the threshold magnitude at t=0.
A	Plan-view area.
ATF	Autogenic threshold function, also referred to as the Qa*-threshold.
BI	Blueness index, metric to quantify blue colour in an image.
B	Blue colour channel in an image (range 0-255).
BQART	Empirical equation to predict sediment flux from catchment conditions (Syvitski and Milliman, 2007).
$\dot{\bar{\eta}}$	Mean deposition rate along a strike-oriented transect at time t.
$\langle\dot{\bar{\eta}}\rangle$	Mean deposition rate along a strike-oriented transect for an entire experimental stage.
f_{1mm}	Number of grid cells depositing >1mm in 1 run hour divided by the total number of cells in a section.
$\overline{f_{1mm}}$	Mean f_{1mm} for the same point in all supply cycles
f_{comp}	Number of time steps, discretised at a window of T_w, with some preserved deposits as a fraction of the total number of time steps.
$\overline{f_{comp}}$	Mean of f_{comp} for all locations on a section within a 1.1 m radius from the apex.
f_p	Number of matching blue pixels in an image and a reference image.
Fr	Froude number.
f_{space}	Mean $\overline{f_{1mm}}$ of all time steps for one location on a section.
f_{time}	Mean $\overline{f_{1mm}}$ of all section locations for one time step.
G	Green colour channel in an image (range 0-255).
GPR	Ground-penetrating radar.
h	River depth.
H_c	Depth of larger channels, defined as the 95th percentile channel depth from a distribution of channel depths.
H_L	Maximum elevation change in a section at time t.
H_{max}	Maximum channel depth at time t.
HMSP	High Magnitude ($2M$) Short Period ($0.5T_c$). Describes the sediment supply signal of run hour 140-385 in TDB experiment TDB-16-3.
HMSP	Medium Magnitude ($1M$) Long Period ($2T_c$). Describes the sediment supply signal of run hour 385-875 in TDB experiment TDB-16-3.
L	Down-dip system length.

LMLP	Low Magnitude (0.5M) Long Period (2T_c). Describes the sediment supply signal of run hour 140-630 in TDB experiment TDB-16-2.
LMSP	Low Magnitude (0.5M) Short Period (0.5T_c). Describes the sediment supply signal of run hour 140-630 in TDB experiment TDB-16-1.
M	Maximum rate of consistent terrestrial volume change, bounded between a peak and through in terrestrial volume. M=0.43 kg/hr in the control stage of TDB-12-1.
M_{max}	Magnitude threshold (Jerolmack and Paola, 2010).
MTM	Multi-taper method.
n	Sample size.
$N_{>2mm}$	Number of co-existing active channels deeper than 2 mm at time t.
P-value	Probability of the null-hypothesis being true (reject null-hypothesis if P<α).
Q	Sediment flux. Subscript specifies what sediment flux.
Q^*	Dimensionless sediment flux (either Q_a/Q_{in} or Q_a/M, see chapter for definition). Subscripts specify type of sediment flux.
Q_0	Parameter in the ATF that sets the threshold magnitude at t=0. Estimated as Q_{in}-Q_{acc}.
Q_0^*	Dimensionless version of Q_0 (Q_0/Q_{in}).
q_0	Input sediment flux in m²/s
Q_a	Maximum rate of autogenic volume change.
Q_A^*	Dimensionless version of Q_a (Q_a/M).
Q_a^*	Dimensionless version of Q_a (Q_a/Q_{in}).
Q_{acc}	Long-term rate sediment accumulation rate in a particular environment.
Q_{acc}^*	Dimensionless version of Q_{acc} (Q_{acc}/Q_{in})
Q_{dec}	Number of avulsions while supply is decreasing.
Q_{high}	Number of avulsions during above average sediment supply conditions.
Q_{in}	Mean sediment supply rate.
Q_{inc}	Number of avulsions while supply is increasing.
Q_{low}	Number of avulsions during below average sediment supply conditions.
Q_s	Signal magnitude, defined as peak-to-peak amplitude.
r	Long-term vertical aggradation rate, set by the rate of RSL rise in the experiments.
R	Red colour channel in an image (range 0-255).
Re	Reynolds number.
RSL	Relative Sea Level, the combined effect of subsidence and eustatic sea level.

S	Supply signal acceleration, simplified to Q_s/T_s.
S^*	Dimensionless version of S, defined as Q_s^*/T_s^*.
S_c	Threshold failure slope.
S_{high}	Number of avulsions during high supply acceleration.
S_{low}	Number of avulsions during low supply acceleration.
SOC	Self-organised criticality.
SRS	Sediment routing system.
SSC	Sediment supply cycle.
t	Time.
T^*	Dimensionless time defined as t/T_c.
T_a	Time between two avulsions.
$\overline{T}_a$	Mean time between two successive avulsions.
$\widehat{T}_a$	Median time between two successive avulsions.
T_{amp}	Measure for degree to which deposition rate follows sediment supply cycles ($T_{cycle}/T_{cycleEQ}$).
T_{bw}	Time to cover all locations on the delta with new sediment.
T_c	Compensation time scale.
$T_{c,L}$	H_L/r.
$T_{c,\sigma ss}$	T_c estimated by calculating σ_{ss}.
T_{cycle}	Metric to correlate deposition rate and supply rate.
$T_{cycleEQ}$	Expected value for T_{cycle} when a change in deposition is directly proportional to a change in supply.
T_{eq}	Equilibrium timescale: $T_{eq}=L^2/v$ (Paola et al., 1992).
$T_{f=0.3}$	Time required to reach f_p=0.3.
t_R	Landscape response time (e.g. Li et al., 2018).
T_s	Signal periodicity.
T_w	Time window of measurement.
T_x	Saturation timescale (Jerolmack and Paola, 2010).
u	Flow velocity.
UAV	Unmanned Aerial Vehicle (drone).
V_{RSL}	Terrestrial volume, the volume of sediment stored above RSL at time t.
W	Width of a cross-section.
x	Horizontal distance.

a	Significance level. In order to reject a null-hypothesis, P should be smaller than α.
κ	Coefficient in the decay of σ_{ss} with T_w.
ν	Diffusivity.
σ_{ss}	Standard deviation of sedimentation/subsidence (Straub et al., 2009).
τ	Bed shear stress.

References

Abels, H. A., Kraus, M. J., and Gingerich, P. D., 2013, Precession-scale cyclicity in the fluvial lower Eocene Willwood Formation of the Bighorn Basin, Wyoming (USA): Sedimentology, v. 60, no. 6, p. 1467-1483.

Ager, D. V., 1973, The nature of the stratigraphical record, New York,, Wiley.

Allen, J. P., Fielding, C. R., Gibling, M. R., and Rygel, M. C., 2014, Recognizing products of palaeoclimate fluctuation in the fluvial stratigraphic record: An example from the Pennsylvanian to Lower Permian of Cape Breton Island, Nova Scotia: Sedimentology, v. 61, no. 5, p. 1332-1381.

Allen, J. P., Fielding, C. R., Rygel, M. C., and Gibling, M. R., 2013a, Deconvolving Signals of Tectonic and Climatic Controls from Continental Basins: An Example from the Late Paleozoic Cumberland Basin, Atlantic Canada: Journal of Sedimentary Research, v. 83, no. 9-10, p. 847-872.

Allen, J. R. L., 1978, Studies in Fluviatile Sedimentation - Exploratory Quantitative Model for Architecture of Avulsion-Controlled Alluvial Suites: Sedimentary Geology, v. 21, no. 2, p. 129-147.

Allen, P. A., 2008a, From landscapes into geological history: Nature, v. 451, p. 274-276.

-, 2008b, Time scales of tectonic landscapes and their sediment routing systems: Geological Society, London, Special Publications, v. 296, no. 1, p. 7-28.

-, 2017, Sediment routing systems : the fate of sediment from source to sink, Cambridge, United Kingdom ; New York, NY, Cambridge University Press.

Allen, P. A., Armitage, J. J., Carter, A., Duller, R. A., Michael, N. A., Sinclair, H. D., Whitchurch, A. L., and Whittaker, A. C., 2013b, The Qs problem: Sediment volumetric balance of proximal foreland basin systems: Sedimentology, v. 60, no. 1, p. 102-130.

Allen, P. A., and Densmore, A. L., 2000, Sediment flux from an uplifting fault block: Basin Research, v. 12, no. 3-4, p. 367-380.

Anderson, R. C., Dohm, J. M., Williams, J. P., Robbins, S. J., Siwabessy, A., Golombek, M. P., and Schroeder, J. F., 2019, Unraveling the geologic and tectonic history of the Memnonia-Sirenum region of Mars: Implications on the early formation of the Tharsis rise: Icarus, v. In press.

Armitage, J. J., Duller, R. A., Whittaker, A. C., and Allen, P. A., 2011, Transformation of tectonic and climatic signals from source to sedimentary archive: Nature Geoscience, v. 4, no. 4, p. 231-235.

Armitage, J. J., Dunkley Jones, T., Duller, R. A., Whittaker, A. C., and Allen, P. A., 2013, Temporal buffering of climate-driven sediment flux cycles by transient catchment response: Earth and Planetary Science Letters, v. 369, p. 200-210.

Armitage, J. J., Whittaker, A. C., Zakari, M., and Campforts, B., 2018, Numerical modelling of landscape and sediment flux response to precipitation rate change: Earth Surface Dynamics, v. 6, no. 1, p. 77-99.

Ashworth, P. J., Best, J. L., and Jones, M., 2004, Relationship between sediment supply and avulsion frequency in braided rivers: Geology, v. 32, no. 1, p. 21-24.

Ashworth, P. J., Best, J. L., and Jones, M. A., 2007, The relationship between channel avulsion, flow occupancy and aggradation in braided rivers: insights from an experimental model: Sedimentology, v. 54, no. 3, p. 497-513.

Ashworth, P. J., Best, J. L., Leddy, J. O., and Geehan, G. W., 1994, The Physical Modelling of Braided Rivers and Deposition of Fine-grained Sediment, *in* Kirkby, M. J., ed., Process Models and Theoretical Geomorphology: Chichester, John Wiley & Sons, p. 115-139.

Backert, N., Ford, M., and Malartre, F., 2010, Architecture and sedimentology of the Kerinitis Gilbert-type fan delta, Corinth Rift, Greece: Sedimentology, v. 57, no. 2, p. 543-586.

Barrett, B. J., Collier, R. E. L., Hodgson, D. M., Gawthorpe, R. L., Dorrell, R. M., and Cullen, T. M., 2019, Quantifying faulting and base level controls on syn-rift sedimentation using stratigraphic architectures of coeval, adjacent Early-Middle Pleistocene fan deltas in Lake Corinth, Greece: Basin Research, p. 1-26.

Bayliss, N. J., and Pickering, K. T., 2015, Deep-marine structurally confined channelised sandy fans: Middle Eocene Morillo System, Ainsa Basin, Spanish Pyrenees: Earth-Science Reviews, v. 144, p. 82-106.

Beerbower, J. R., 1964, Cyclothems and Cyclic Depositional Mechanisms in Alluvial Plain Sedimentation: Symposium on cyclic sedimentation: Kansas Geological Survey, Bulletin, v. 169, p. 31-42.

Bijkerk, J. F., Eggenhuisen, J. T., Kane, I. A., Meijer, N., Waters, C. N., Wignall, P. B., and McCaffrey, W. D., 2016, Fluvio-Marine Sediment Partitioning as a Function of Basin Water Depth: Journal of Sedimentary Research, v. 86, no. 3, p. 217-235.

Bijkerk, J. F., ten Veen, J., Postma, G., Mikes, D., van Strien, W., and de Vries, J., 2014, The role of climate variation in delta architecture: lessons from analogue modelling: Basin Research, v. 26, no. 3, p. 351-368.

Blum, M., Rogers, K., Gleason, J., Najman, Y., Cruz, J., and Fox, L., 2018, Allogenic and Autogenic Signals in the Stratigraphic Record of the Deep-Sea Bengal Fan: Scientific Reports, v. 8, no. 1.

Blum, M. D., and Hattier-Womack, J., 2009, Climate Change, Sea-Level Change, and Fluvial Sediment Supply to Deepwater Depositional Systems: External Controls on Deep-Water Depositional Systems, SEPM Special Publication, no. 92, p. 15-39.

Blum, M. D., and Roberts, H. H., 2009, Drowning of the Mississippi Delta due to insufficient sediment supply and global sea-level rise: Nature Geoscience, v. 2, no. 7, p. 488-491.

Blum, M. D., and Tornqvist, T. E., 2000, Fluvial responses to climate and sea-level change: a review and look forward: Sedimentology, v. 47, p. 2-48.

Bonnet, S., and Crave, A., 2003, Landscape response to climate change: Insights from experimental modeling and implications for tectonic versus climatic uplift of topography: Geology, v. 31, no. 2, p. 123-126.

Braun, J., Voisin, C., Gourlan, A. T., and Chauvel, C., 2015, Erosional response of an actively uplifting mountain belt to cyclic rainfall variations: Earth Surface Dynamics, v. 3, no. 1, p. 1-14.

Bridge, J. S., and Leeder, M. R., 1979, A simulation model of alluvial stratigraphy: Sedimentology, v. 26, p. 617-644.

Bristow, C. S., and Pucillo, K., 2006, Quantifying rates of coastal progradation from sediment volume using GPR and OSL: the Holocene fill of Guichen Bay, south-east South Australia: Sedimentology, v. 53, no. 4, p. 769-788.

Brooke, S. A. S., Whittaker, A. C., Armitage, J. J., D'Arcy, M., and Watkins, S. E., 2018, Quantifying Sediment Transport Dynamics on Alluvial Fans From Spatial and Temporal Changes in Grain Size, Death Valley, California: Journal of Geophysical Research-Earth Surface, v. 123, no. 8, p. 2039-2067.

Bryant, M., Falk, P., and Paola, C., 1995, Experimental-Study of Avulsion Frequency and Rate of Deposition: Geology, v. 23, no. 4, p. 365-368.

Burgess, P. M., Masiero, I., Toby, S. C., and Duller, R. A., 2019, A Big Fan of Signals? Exploring Autogenic and Allogenic Process and Product in a Numerical Stratigraphic Forward Model of Submarine-Fan Development: Journal of Sedimentary Research, v. 89, no. 1, p. 1-12.

Burpee, A. P., Slingerland, R. L., Edmonds, D. A., Parsons, D., Best, J., Cederberg, J., McGuffin, A., Caldwell, R., Nijhuis, A., and Royce, J., 2015, Grain-Size Controls on the Morphology and Internal Geometry of River-Dominated Deltas: Journal of Sedimentary Research, v. 85, no. 6, p. 699-714.

Caldwell, R. L., and Edmonds, D. A., 2014, The effects of sediment properties on deltaic processes and morphologies: A numerical modeling study: Journal of Geophysical Research-Earth Surface, v. 119, no. 5, p. 961-982.

Carson, R., 1951, The Sea around us, Oxford University Press.

Carvajal, C., Steel, R., and Petter, A., 2009, Sediment supply: The main driver of shelf-margin growth: Earth-Science Reviews, v. 96, no. 4, p. 221-248.

Castelltort, S., 2018, Empirical relationship between river slope and the elongation of bars in braided rivers: A potential tool for paleoslope analysis from subsurface data: Marine and Petroleum Geology, v. 96, p. 544-550.

Castelltort, S., and Van den Driessche, J., 2003, How plausible are high-frequency sediment supply-driven cycles in the stratigraphic record?: Sedimentary Geology, v. 157, no. 1-2, p. 3-13.

Castelltort, S., Whittaker, A., and Verges, J., 2015, Tectonics, sedimentation and surface processes: from the erosional engine to basin deposition: Earth Surface Processes and Landforms, v. 40, no. 13, p. 1839-1846.

Catuneanu, O., Abreub, V., Bhattacharya, J. P., Blum, M. D., Dalrymple, R. W., Eriksson, P. G., Fielding, C. R., Fisher, W. L., Galloway, W. E., Gibling, M. R., Giles, K. A., Holbrook, J. M., Jordan, R., Kendall, C. G. S. C., Macurda, B., Martinsen, O. J., Miall, A. D., Neal, J. E., Nummedal, D., Pomar, L., Posamentier, H. W., Pratt, B. R., Sarg, J. F., Shanley, K. W., Steel, R. J., Strasser, A., Tucker, M. E., and Winker, C., 2009, Towards the standardization of sequence stratigraphy: Earth-Science Reviews, v. 92, no. 1-2, p. 1-33.

Cazanacli, D., Paola, C., and Parker, G., 2002, Experimental steep, braided flow: Application to flooding risk on fans: Journal of Hydraulic Engineering, v. 128, no. 3, p. 322-330.

Chesley, J. T., Leier, A. L., White, S., and Torres, R., 2017, Using unmanned aerial vehicles and structure-from-motion photogrammetry to characterize sedimentary outcrops: An example from the Morrison Formation, Utah, USA: Sedimentary Geology, v. 354, p. 1-8.

Clark, P. U., Archer, D., Pollard, D., Blum, J. D., Rial, J. A., Brovkin, V., Mix, A. C., Pisias, N. G., and Roy, M., 2006, The middle Pleistocene transition: characteristics. mechanisms, and implications for long-term changes in atmospheric PCO2: Quaternary Science Reviews, v. 25, no. 23-24, p. 3150-3184.

Clarke, L., Quine, T. A., and Nicholas, A., 2010, An experimental investigation of autogenic behaviour during alluvial fan evolution: Geomorphology, v. 115, no. 3-4, p. 278-285.

Clarke, L. E., 2015, Experimental alluvial fans: Advances in understanding of fan dynamics and processes: Geomorphology, v. 244, p. 135-145.

Clift, P. D., Giosan, L., BIusztajn, J., Campbell, I. H., Allen, C., Pringle, M., Tabrez, A. R., Danish, M., Rabbani, M. M., Alizai, A., Carter, A., and Lueckge, A., 2008, Holocene erosion of the Lesser Himalaya triggered by intensified summer monsoon: Geology, v. 36, no. 1, p. 79-82.

Coulthard, T. J., and Van de Wiel, M. J., 2013, Climate, tectonics or morphology: what signals can we see in drainage basin sediment yields?: Earth Surface Dynamics, v. 1, no. 1, p. 13-27.

Dade, W. B., and Friend, P. F., 1998, Grain-size, sediment-transport regime, and channel slope in alluvial rivers: Journal of Geology, v. 106, no. 6, p. 661-675.

Duller, R. A., Warner, N. H., De Angelis, S., Armitage, J. J., and Poyatos-More, M., 2015, Reconstructing the timescale of a catastrophic fan-forming event on Earth using a Mars model: Geophysical Research Letters, v. 42, no. 23, p. 10324-10332.

Duller, R. A., Whittaker, A. C., Fedele, J. J., Whitchurch, A. L., Springett, J., Smithells, R., Fordyce, S., and Allen, P. A., 2010, From grain size to tectonics: Journal of Geophysical Research-Earth Surface, v. 115, p. F03022.

Duller, R. A., Whittaker, A. C., Swinehart, J. B., Armitage, J. J., Sinclair, H. D., Bair, A., and Allen, P. A., 2012, Abrupt landscape change post-6 Ma on the central Great Plains, USA: Geology, v. 40, no. 10, p. 871-874.

East, A. E., Logan, J. B., Mastin, M. C., Ritchie, A. C., Bountry, J. A., Magirl, C. S., and Sankey, J. B., 2018, Geomorphic Evolution of a Gravel-Bed River Under Sediment-Starved Versus Sediment-Rich Conditions: River Response to the World's Largest Dam Removal: Journal of Geophysical Research-Earth Surface, v. 123, no. 12, p. 3338-3369.

Edmonds, D., Slingerland, R., Best, J., Parsons, D., and Smith, N., 2010, Response of river-dominated delta channel networks to permanent changes in river discharge: Geophysical Research Letters, v. 37.

Edmonds, D. A., Hoyal, D. C. J. D., Sheets, B. A., and Slingerland, R. L., 2009, Predicting delta avulsions: Implications for coastal wetland restoration: Geology, v. 37, no. 8, p. 759-762.

Edmonds, D. A., and Slingerland, R. L., 2010, Significant effect of sediment cohesion on delta morphology: Nature Geoscience, v. 3, no. 2, p. 105-109.

Eide, C. H., Howell, J. A., Buckley, S. J., Martinius, A. W., Oftedal, B. T., and Henstra, G. A., 2016, Facies model for a coarse-grained, tide-influenced delta: Gule Horn Formation (Early Jurassic), Jameson Land, Greenland: Sedimentology, v. 63, no. 6, p. 1474-1506.

Einsele, G., 2000, Sedimentary basins : evolution, facies, and sediment budget.

Esposito, C. R., Di Leonardo, D., Harlan, M., and Straub, K. M., 2018, Sediment Storage Partitioning in Alluvial Stratigraphy: The Influence of Discharge Variability: Journal of Sedimentary Research, v. 88, no. 6, p. 717-726.

Esposito, C. R., Shen, Z. X., Tornqvist, T. E., Marshak, J., and White, C., 2017, Efficient retention of mud drives land building on the Mississippi Delta plain: Earth Surface Dynamics, v. 5, no. 3, p. 387-397.

Exner, F. M., 1925, Über die Wechselwirkung zwischen Wasser und Geschiebe in Flüssen: Akad. Wiss. Wien Math. Naturwiss. Klasse, v. 134(2a), p. 165-204.

Fedele, J. J., and Paola, C., 2007, Similarity solutions for fluvial sediment fining by selective deposition: Journal of Geophysical Research-Earth Surface, v. 112, no. F2.

Fielding, C. R., Alexander, J., and Allen, J. P., 2018, The role of discharge variability in the formation and preservation of alluvial sediment bodies: Sedimentary Geology, v. 365, p. 1-20.

Flint, S. S., and Bryant, I. D., 1993, The Geological modelling of hydrocarbon reservoirs and outcrop analogues, Special publication number 15 of the International Association of Sedimentologists.

Foreman, B. Z., Heller, P. L., and Clementz, M. T., 2012, Fluvial response to abrupt global warming at the Palaeocene/Eocene boundary: Nature, v. 491, no. 7422, p. 92-95.

Foreman, B. Z., and Straub, K. M., 2017, Autogenic geomorphic processes determine the resolution and fidelity of terrestrial paleoclimate records: Science Advances, v. 3, no. 9.

Forzoni, A., Storms, J. E. A., Whittaker, A. C., and de Jager, G., 2014, Delayed delivery from the sediment factory: modeling the impact of catchment response time to tectonics on sediment flux and fluvio-deltaic stratigraphy: Earth Surface Processes and Landforms, v. 39, no. 5, p. 689-704.

Ganti, V., Lamb, M. P., and McElroy, B., 2014, Quantitative bounds on morphodynamics and implications for reading the sedimentary record: Nature Communications, v. 5.

Garzanti, E., Vermeesch, P., Vezzoli, G., Andò, S., Botti, E., Limonta, M., Dinis, P., Hahn, A., Baudet, D., De Grave, J., and Kitambala Yaya, N., 2019, Congo River sand and the equatorial quartz factory: Earth-Science Reviews, v. in press.

Goodbred, S. L., 2003, Response of the Ganges dispersal system to climate change: a source-to-sink view since the last interstade: Sedimentary Geology, v. 162, no. 1-2, p. 83-104.

Guerit, L., Metivier, F., Devauchelle, O., Lajeunesse, E., and Barrier, L., 2014, Laboratory alluvial fans in one dimension: Physical Review E, v. 90, no. 2.

Gupta, S., Cowie, P. A., Dawers, N. H., and Underhill, J. R., 1998, A mechanism to explain rift-basin subsidence and stratigraphic patterns through fault-array evolution: Geology, v. 26, no. 7, p. 595-598.

Hajek, E. A., Heller, P. L., and Schur, E. L., 2012, Field test of autogenic control on alluvial stratigraphy (Ferris Formation, Upper Cretaceous-Paleogene, Wyoming): Geological Society of America Bulletin, v. 124, no. 11-12, p. 1898-1912.

Hajek, E. A., Heller, P. L., and Sheets, B. A., 2010, Significance of channel-belt clustering in alluvial basins: Geology, v. 38, no. 6, p. 535-538.

Hajek, E. A., and Straub, K. M., 2017, Autogenic Sedimentation in Clastic Stratigraphy: Annual Review of Earth and Planetary Sciences, Vol 45, v. 45, p. 681-709.

Hampson, G. J., 2016, Towards a sequence stratigraphic solution set for autogenic processes and allogenic controls: Upper Cretaceous strata, Book Cliffs, Utah, USA: Journal of the Geological Society, v. 173, no. 5, p. 817-836.

Hampson, G. J., Duller, R. A., Petter, A. L., Robinson, R. A., and Allen, P. A., 2014, Mass-balance constraints on stratigraphic interpretation of linked alluvial–coastal–shelfal deposits from source to sink: example from Cretaceous Western Interior Basin, Utah and Colorado, USA: Journal of Sedimentary Research, v. 84, no. 11, p. 935-960.

Heller, P. L., Paola, C., Hwang, I. G., John, B., and Steel, R., 2001, Geomorphology and sequence stratigraphy due to slow and rapid base-level changes in an experimental subsiding basin (XES 96-1): Aapg Bulletin, v. 85, no. 5, p. 817-838.

Hickson, T. A., Sheets, B. A., Paola, C., and Kelberer, M., 2005, Experimental test of tectonic controls on three-dimensional alluvial facies architecture: Journal of Sedimentary Research, v. 75, no. 4, p. 710-722.

Hidy, A. J., Gosse, J. C., Blum, M. D., and Gibling, M. R., 2014, Glacial-interglacial variation in denudation rates from interior Texas, USA, established with cosmogenic nuclides: Earth and Planetary Science Letters, v. 390, p. 209-221.

Hilgen, F. J., Hinnov, L. A., Aziz, H. A., Abels, H. A., Batenburg, S., Bosmans, J. H. C., De Boer, B., Husing, S. K., Kuiper, K. F., Lourens, L. J., Rivera, T., Tuenter, E., Van de Wal, R. S. W., Wotzlaw, J. F., and Zeeden, C., 2015, Stratigraphic continuity and fragmentary sedimentation: the success of cyclostratigraphy as part of integrated stratigraphy: Strata and Time: Probing the Gaps in Our Understanding. Geological Society London, Special Publications, v. 404, p. 157-197.

Hillgartner, H., and Strasser, A., 2003, Quantification of high-frequency sea-level fluctuations in shallow-water carbonates: an example from the Berriasian-Valanginian (French Jura): Palaeogeography Palaeoclimatology Palaeoecology, v. 200, no. 1-4, p. 43-63.

Hoffmann, T., 2015, Sediment residence time and connectivity in non-equilibrium and transient geomorphic systems: Earth-Science Reviews, v. 150, p. 609-627.

Hooke, R. L., 1968, Model geology: prototype and laboratory streams: discussion: Geological Society of America Bulletin, v. 79, p. 391-394.

Horton, B. K., Constenius, K. N., and DeCelles, P. G., 2004, Tectonic control on coarse-grained foreland-basin sequences: An example from the Cordilleran foreland basin, Utah: Geology, v. 32, no. 7, p. 637-640.

Hoyal, D. C. J. D., and Sheets, B. A., 2009, Morphodynamic evolution of experimental cohesive deltas: Journal of Geophysical Research-Earth Surface, v. 114.

Hudson, P. F., and Kesel, R. H., 2000, Channel migration and meander-bend curvature in the lower Mississippi River prior to major human modification: Geology, v. 28, no. 6, p. 531-534.

Humphrey, N. F., and Heller, P. L., 1995, Natural Oscillations in Coupled Geomorphic Systems - an Alternative Origin for Cyclic Sedimentation: Geology, v. 23, no. 6, p. 499-502.

Jerolmack, D. J., 2011, Causes and Effects of Noise in Landscape Dynamics: Eos, v. 92, no. 44, p. 385-396.

Jerolmack, D. J., and Mohrig, D., 2007, Conditions for branching in depositional rivers: Geology, v. 35, no. 5, p. 463-466.

Jerolmack, D. J., and Paola, C., 2010, Shredding of environmental signals by sediment transport: Geophysical Research Letters, v. 37.

Jerolmack, D. J., and Sadler, P., 2007, Transience and persistence in the depositional record of continental margins: Journal of Geophysical Research-Earth Surface, v. 112, no. F3.

Jervey, M. T., 1988, Quantitative geological modelling of siliciclastic rock sequences and their seismic expression, *in* Wilgus, C. K., Hastings, B. S., Kendall, C. G. S. C., Posamentier, H. W., Ross, C. A., and Van Wagoner, J. C., eds., Sea-Level Changes: An Integrated Approach: SEPM Special Publication, Volume 42, p. 47-69.

Karamitopoulos, P., Weltje, G. J., and Dalman, R. A. F., 2014, Allogenic controls on autogenic variability in fluvio-deltaic systems: inferences from analysis of synthetic stratigraphy: Basin Research, v. 26, no. 6, p. 767-779.

Kehrl, L., Conway, H., Holschuh, N., Campbell, S., Kurbatov, A. V., and Spaulding, N. E., 2018, Evaluating the Duration and Continuity of Potential Climate Records From the Allan Hills Blue Ice Area, East Antarctica: Geophysical Research Letters, v. 45, no. 9, p. 4096-4104.

Kim, W., and Jerolmack, D. J., 2008, The pulse of calm fan deltas: Journal of Geology, v. 116, no. 4, p. 315-330.

Kim, W., and Paola, C., 2007, Long-period cyclic sedimentation with constant tectonic forcing in an experimental relay ramp: Geology, v. 35, no. 4, p. 331-334.

Kim, W., Paola, C., Voller, V. R., and Swenson, J. B., 2006, Experimental measurement of the relative importance of controls on shoreline migration: Journal of Sedimentary Research, v. 76, no. 1-2, p. 270-283.

Kim, W., Petter, A., Straub, K., and Mohrig, D., 2014, Investigating the autogenic process response to allogenic forcing: experimental geomorphology and stratigraphy: From Depositional Systems to Sedimentary Successions on the Norwegian Continental Margin, v. 46, p. 127-138.

Klausen, T. G., Nyberg, B., and Helland-Hansen, W., 2019, The largest delta plain in Earth's history: Geology, v. 47, no. 5, p. 470-474.

Kleinhans, M. G., van Dijk, W. M., de Lageweg, W. I. V., Hoyal, D. C. J. D., Markies, H., van Maarseveen, M., Roosendaal, C., van Weesep, W., van Breemen, D., Hoendervoogt, R., and Cheshier, N., 2014, Quantifiable effectiveness of experimental scaling of river-and delta morphodynamics and stratigraphy: Earth-Science Reviews, v. 133, p. 43-61.

Knight, J., and Harrison, S., 2013, The impacts of climate change on terrestrial Earth surface systems: Nature Climate Change, v. 3, no. 1, p. 24-29.

Labourdette, R., 2011, Stratigraphy and static connectivity of braided fluvial deposits of the lower Escanilla Formation, south central Pyrenees, Spain: AAPG Bulletin, v. 95, no. 4, p. 585-617.

Lai, J., Wang, G. W., Wang, S., Cao, J. T., Li, M., Pang, X. J., Zhou, Z. L., Fan, X. Q., Dai, Q. Q., Yang, L., He, Z. B., and Qin, Z. Q., 2018, Review of diagenetic facies in tight sandstones: Diagenesis, diagenetic minerals, and prediction via well logs: Earth-Science Reviews, v. 185, p. 234-258.

Lambeck, K., and Chappell, J., 2001, Sea level change through the last glacial cycle: Science, v. 292, no. 5517, p. 679-686.

Lauer, J. W., and Parker, G., 2008, Net local removal of floodplain sediment by river meander migration: Geomorphology, v. 96, no. 1-2, p. 123-149.

Lazarus, E. D., Harley, M. D., Blenkinsopp, C. E., and Turner, I. L., 2019, Environmental signal shredding on sandy coastlines: Earth Surface Dynamics, v. 7, no. 1, p. 77-86.

Leeder, M. R., 1978, A quantitative stratigraphic model for alluvium, with spatial reference to channel deposit density and interconnectedness, *in* Miall, A. D., ed., Fluvial Sedimentology, Volume 5: Calgary, Can. Soc. of Pet. Geol. Mem.

-, 2011, Tectonic sedimentology: sediment systems deciphering global to local tectonics: Sedimentology, v. 58, no. 1, p. 2-56.

Li, Q., Benson, W. M., Harlan, M., Robichaux, P., Sha, X. Y., Xu, K. H., and Straub, K. M., 2017, Influence of Sediment Cohesion on Deltaic Morphodynamics and Stratigraphy Over Basin-Filling Time Scales: Journal of Geophysical Research-Earth Surface, v. 122, no. 10, p. 1808-1826.

Li, Q., Gasparini, N. M., and Straub, K. M., 2018, Some signals are not the same as they appear: How do erosional landscapes transform tectonic history into sediment flux records?: Geology, v. 46, no. 5, p. 407-410.

Li, Q., and Straub, K. M., 2017a, TDB_12_1: SEAD.

-, 2017b, TDB_13_1: SEAD.

Li, Q., Yu, L. Z., and Straub, K. M., 2016, Storage thresholds for relative sea-level signals in the stratigraphic record: Geology, v. 44, no. 3, p. 179-182.

Lopez-Blanco, M., Marzo, M., Burbank, D. W., Verges, J., Roca, E., Anadon, P., and Pina, J., 2000, Tectonic and climatic controls on the development of foreland fan deltas: Montserrat and Sant Llorenc del Munt systems (Middle Eocene, Ebro Basin, NE Spain): Sedimentary Geology, v. 138, no. 1-4, p. 17-39.

Lu, H., Moran, C. J., and Sivapalan, M., 2005, A theoretical exploration of catchment-scale sediment delivery: Water Resources Research, v. 41, no. 9.

Lyons, W. J., 2004, Quantifying channelized submarine depositional systems from bed to basin scalePhD]: Massachusetts Institute of Technology, 252 p.

Ma, H. B., Nittrouer, J. A., Naito, K., Fu, X. D., Zhang, Y. F., Moodie, A. J., Wang, Y. J., Wu, B. S., and Parker, G., 2017, The exceptional sediment load of fine-grained dispersal systems: Example of the Yellow River, China: Science Advances, v. 3, no. 5.

Mackey, S. D., and Bridge, J. S., 1995, 3-Dimensional Model of Alluvial Stratigraphy - Theory and Application: Journal of Sedimentary Research Section B-Stratigraphy and Global Studies, v. 65, no. 1, p. 7-31.

Malatesta, L. C., Avouac, J. P., Brown, N. D., Breitenbach, S. F. M., Pan, J. W., Chevalier, M. L., Rhodes, E., Saint-Carlier, D., Zhang, W. J., Charreau, J., Lave, J., and Blard, P. H., 2018, Lag and mixing during sediment transfer across the Tian Shan piedmont caused by climate-driven aggradation-incision cycles: Basin Research, v. 30, no. 4, p. 613-635.

Marr, J. G., Swenson, J. B., Paola, C., and Voller, V. R., 2000, A two-diffusion model of fluvial stratigraphy in closed depositional basins: Basin Research, v. 12, no. 3-4, p. 381-398.

Martin, J., Paola, C., Abreu, V., Neal, J., and Sheets, B., 2009a, Sequence stratigraphy of experimental strata under known conditions of differential subsidence and variable base level: AAPG Bulletin, v. 93, no. 4, p. 503-533.

Martin, J., Sheets, B., Paola, C., and Hoyal, D., 2009b, Influence of steady base-level rise on channel mobility, shoreline migration, and scaling properties of a cohesive experimental delta: Journal of Geophysical Research-Earth Surface, v. 114.

Mason, C. C., and Romans, B. W., 2018, Climate-driven unsteady denudation and sediment flux in a high-relief unglaciated catchment-fan using Al-26 and Be-10: Panamint Valley, California: Earth and Planetary Science Letters, v. 492, p. 130-143.

McNeill, L. C., Shillington, D. J., Carter, G. D. O., Everest, J. D., Gawthorpe, R. L., Miller, C., Phillips, M. P., Collier, R. E. L., Cvetkoska, A., Gelder, G. D., Diz, P., Doan, M.-l., Ford, M., Geraga, M., Gillespie, J., Hemelsdaël, R., Herrero-Bervera, E., Ismaiel, M., Janikian, L., Kouli, K., Le Ber, E., Li, S., Maffione, M., Mahoney, C., Machlus, M. L., Michas, G., Nixon, C. W., Asli Oflaz, S., Omale, A. P., Panagiotopoulos, K., Pechlivanidou, S., Sauer, S., Sequin, J., Sergiou, S., Zakharova, N., and Green, S., 2019, High-resolution record reveals climate-driven environmental and sedimentary changes in an active rift: Nature Scientific Reports, v. 9, no. 3116

Metivier, F., 1999, Diffusivelike buffering and saturation of large rivers: Physical Review E, v. 60, no. 5, p. 5827-5832.

Metivier, F., and Gaudemer, Y., 1999, Stability of output fluxes of large rivers in South and East Asia during the last 2 million years: implications on floodplain processes: Basin Research, v. 11, no. 4, p. 293-303.

Miall, A. D., 2015, Stratigraphy: a modern synthesis, Springer, 454 p.:

Michael, N. A., Whittaker, A. C., Carter, A., and Allen, P. A., 2014, Volumetric budget and grain-size fractionation of a geological sediment routing system: Eocene Escanilla Formation, south-central Pyrenees: Geological Society of America Bulletin, v. 126, no. 3-4, p. 585-599.

Mikes, D., ten Veen, J. H., Postma, G., and Steel, R., 2015, Inferring autogenically induced depositional discontinuities from observations on experimental deltaic shoreline trajectories: Terra Nova, v. 27, no. 6, p. 442-448.

Miller, K. G., Kominz, M. A., Browning, J. V., Wright, J. D., Mountain, G. S., Katz, M. E., Sugarman, P. J., Cramer, B. S., Christie-Blick, N., and Pekar, S. F., 2005, The phanerozoic record of global sea-level change: Science, v. 310, no. 5752, p. 1293-1298.

Milliken, R. E., Grotzinger, J. P., and Thomson, B. J., 2010, Paleoclimate of Mars as captured by the stratigraphic record in Gale Crater: Geophysical Research Letters, v. 37.

Mohrig, D., Heller, P. L., Paola, C., and Lyons, W. J., 2000, Interpreting avulsion process from ancient alluvial sequences: Guadalope-Matarranya system (northern Spain) and Wasatch Formation (western Colorado): Geological Society of America Bulletin, v. 112, no. 12, p. 1787-1803.

Mudd, S. M., 2017, Detection of transience in eroding landscapes: Earth Surface Processes and Landforms, v. 42, no. 1, p. 24-41.

Muto, T., 2001, Shoreline autoretreat substantiated in flume experiments: Journal of Sedimentary Research, v. 71, no. 2, p. 246-254.

Muto, T., and Steel, R. J., 1992, Retreat of the Front in a Prograding Delta: Geology, v. 20, no. 11, p. 967-970.

Muto, T., and Steel, R. J., 1997, Principles of regression and transgression: the nature of the interplay between accommodation and sediment supply: perspectives: Journal of Sedimentary Research, v. 67, no. 6.

Muto, T., Steel, R. J., and Burgess, P. M., 2016, Contributions to sequence stratigraphy from analogue and numerical experiments: Journal of the Geological Society, v. 173, no. 5, p. 837-844.

Muto, T., Steel, R. J., and Swenson, J. B., 2007, Autostratigraphy: A framework norm for genetic stratigraphy: Journal of Sedimentary Research, v. 77, no. 1-2, p. 2-12.

Nicholas, A. P., Smith, G. H. S., Amsler, M. L., Ashworth, P. J., Best, J. L., Hardy, R. J., Lane, S. N., Orfeo, O., Parsons, D. R., Reesink, A. J. H., Sandbach, S. D., Simpson, C. J., and Szupiany, R. N., 2016, The role of discharge variability in determining alluvial stratigraphy: Geology, v. 44, no. 1, p. 3-6.

Nutman, A. P., Mojzsis, S. J., and Friend, C. R. L., 1997, Recognition of >=3850 Ma water-lain sediments in West Greenland and their significance for the early Archaean Earth: Geochimica Et Cosmochimica Acta, v. 61, no. 12, p. 2475-2484.

Otsu, N., 1979, Threshold Selection Method from Gray-Level Histograms: Ieee Transactions on Systems Man and Cybernetics, v. 9, no. 1, p. 62-66.

Overeem, I., Weltje, G. J., Bishop-Kay, C., and Kroonenberg, S. B., 2001, The Late Cenozoic Eridanos delta system in the Southern North Sea Basin: a climate signal in sediment supply?: Basin Research, v. 13, no. 3, p. 293-312.

Paola, C., 2000, Quantitative models of sedimentary basin filling: Sedimentology, v. 47, p. 121-178.

-, 2016, A Mind of Their Own: Recent Advances in Autogenic Dynamics in Rivers and Deltas: Autogenic Dynamics and Self-Organization in Sedimentary Systems, SEPM Special Pubilication, v. 106, p. 5-17.

Paola, C., and Foufoula-Georgiou, E., 2001, Statistical geometry and dynamics of braided rivers: Gravel-Bed Rivers, p. 47-71.

Paola, C., Ganti, V., Mohrig, D., Runkel, A. C., and Straub, K. M., 2018, Time Not Our Time: Physical Controls on the Preservation and Measurement of Geologic Time: Annual Review of Earth and Planetary Sciences, Vol 46, v. 46, p. 409-438.

Paola, C., Heller, P. L., and Angevine, C. L., 1992, The large-scale dynamics of grain-size variation in alluvial basins, 1: Theory: Basin Research, v. 4, no. 2, p. 73-90.

Paola, C., and Martin, J. M., 2012, Mass-Balance Effects in Depositional Systems: Journal of Sedimentary Research, v. 82, no. 5-6, p. 435-450.

Paola, C., Straub, K., Mohrig, D., and Reinhardt, L., 2009, The "unreasonable effectiveness" of stratigraphic and geomorphic experiments: Earth-Science Reviews, v. 97, no. 1-4, p. 1-43.

Paola, C., and Voller, V. R., 2005, A generalized Exner equation for sediment mass balance: Journal of Geophysical Research-Earth Surface, v. 110, no. F4.

Parker, G., Paola, C., Whipple, K. X., and Mohrig, D., 1998, Alluvial fans formed by channelized fluvial and sheet flow. I: Theory: Journal of Hydraulic Engineering-Asce, v. 124, no. 10, p. 985-995.

Peakall, J., Ashworth, P. J., and Best, J., 1996, Physical modelling in fluvial geomorphology: Principles, Applications and Unresolved Issues, *in* Rhoads, B. L., and Thorn, C. E., eds., The scientific nature of geomorphology: Chichester, John Wiley & Sons, p. 221-253.

Peper, T., and Cloetingh, S., 1995, Autocyclic Perturbations of Orbitally Forced Signals in the Sedimentary Record: Geology, v. 23, no. 10, p. 937-940.

Phillips, C. B., and Jerolmack, D. J., 2016, Self-organization of river channels as a critical filter on climate signals: Science, v. 352, no. 6286, p. 694-697.

Picot, M., Marsset, T., Droz, L., Dennielou, B., Baudin, F., Hermoso, M., de Rafelis, M., Sionneau, T., Cremer, M., Laurent, D., and Bez, M., 2019, Monsoon control on channel

avulsions in the Late Quaternary Congo Fan: Quaternary Science Reviews, v. 204, p. 149-171.
Pizzuto, J., Keeler, J., Skalak, K., and Karwan, D., 2017, Storage filters upland suspended sediment signals delivered from watersheds: Geology, v. 45, no. 2, p. 151-154.
Porebski, S. J., and Steel, R. J., 2003, Shelf-margin deltas: their stratigraphic significance and relation to deepwater sands: Earth-Science Reviews, v. 62, no. 3-4, p. 283-326.
Posamentier, H. W., and Allen, G. P., 1993, Variability of the Sequence Stratigraphic Model - Effects of Local Basin Factors: Sedimentary Geology, v. 86, no. 1-2, p. 91-109.
Posamentier, H. W., Allen, G. P., and Sepm, 1999, Siliciclastic sequence stratigraphy : concepts and applications, Concepts in sedimentology and paleontology no. 7.
Postma, G., 2014, Generic autogenic behaviour in fluvial systems: lessons from experimental studies: From Depositional Systems to Sedimentary Successions on the Norwegian Continental Margin, v. 46, p. 1-18.
Postma, G., Kleinhans, M. G., Meijer, P. T., and Eggenhuisen, J. T., 2008, Sediment transport in analogue flume models compared with real-world sedimentary systems: a new look at scaling evolution of sedimentary systems in a flume: Sedimentology, v. 55, no. 6, p. 1541-1557.
Prelat, A., Covault, J. A., Hodgson, D. M., Fildani, A., and Flint, S. S., 2010, Intrinsic controls on the range of volumes, morphologies, and dimensions of submarine lobes: Sedimentary Geology, v. 232, no. 1-2, p. 66-76.
Reitz, M. D., and Jerolmack, D. J., 2012, Experimental alluvial fan evolution: Channel dynamics, slope controls, and shoreline growth: Journal of Geophysical Research-Earth Surface, v. 117.
Reitz, M. D., Jerolmack, D. J., and Swenson, J. B., 2010, Flooding and flow path selection on alluvial fans and deltas: Geophysical Research Letters, v. 37.
Ritchie, B. D., Gawthorpe, R. L., and Hardy, S., 2004, Three-dimensional numerical modeling of deltaic depositional sequences 1: Influence of the rate and magnitude of sea-level change: Journal of Sedimentary Research, v. 74, no. 2, p. 203-220.
Rodriguez-Tovar, F. J., and Pardo-Iguzquiza, E., 2003, Strong evidence of high-frequency (sub-Milankovitch) orbital forcing by amplitude modulation of Milankovitch signals: Earth and Planetary Science Letters, v. 210, no. 1-2, p. 179-189.
Romans, B. W., Castelltort, S., Covault, J. A., Fildani, A., and Walsh, J. P., 2016, Environmental signal propagation in sedimentary systems across timescales: Earth-Science Reviews, v. 153, p. 7-29.
Rygel, M. C., and Gibling, M. R., 2006, Natural geomorphic variability recorded in a high-accommodation setting: Fluvial architecture of the Pennsylvanian Joggins Formation of Atlantic Canada: Journal of Sedimentary Research, v. 76, no. 11-12, p. 1230-1251.
Sadler, P. M., 1981, Sediment Accumulation Rates and the Completeness of Stratigraphic Sections: Journal of Geology, v. 89, no. 5, p. 569-584.
Sadler, P. M., and Strauss, D. J., 1990a, Estimation of Completeness of Stratigraphical Sections Using Empirical-Data and Theoretical-Models: Journal of the Geological Society, v. 147, p. 471-485.
-, 1990b, Estimation of completeness of stratigraphical sections using empirical data and theoretical-models: Geological Society of London, Journal, v. 147, p. 471-485.
Schlager, W., 1993, Accommodation and Supply - a Dual Control on Stratigraphic Sequences: Sedimentary Geology, v. 86, no. 1-2, p. 111-136.
Schlunegger, F., and Kissling, E., 2015, Slab rollback orogeny in the Alps and evolution of the Swiss Molasse basin: Nature Communications, v. 6.

Schumer, R., Jerolmack, D., and McElroy, B., 2011, The stratigraphic filter and bias in measurement of geologic rates: Geophysical Research Letters, v. 38.

Schumer, R., and Jerolmack, D. J., 2009, Real and apparent changes in sediment deposition rates through time: Journal of Geophysical Research-Earth Surface, v. 114.

Schumm, S. A., Mosley, M. P., and Weaver, W. E., 1987, Experimental fluvial geomorphology, New York, John Wiley.

Scotchman, J. I., Pickering, K. T., Sutcliffe, C., Dakin, N., and Armstrong, E., 2015, Milankovitch cyclicity within the middle Eocene deep-marine Guaso System, Ainsa Basin, Spanish Pyrenees: Earth-Science Reviews, v. 144, p. 107-121.

Sheets, B. A., Hickson, T. A., and Paola, C., 2002, Assembling the stratigraphic record: depositional patterns and time-scales in an experimental alluvial basin: Basin Research, v. 14, no. 3, p. 287-301.

Shen, Z. X., Tornqvist, T. E., Mauz, B., Chamberlain, E. L., Nijhuis, A. G., and Sandoval, L., 2015, Episodic overbank deposition as a dominant mechanism of floodplain and delta-plain aggradation: Geology, v. 43, no. 10, p. 875-878.

Simpson, G., and Castelltort, S., 2012, Model shows that rivers transmit high-frequency climate cycles to the sedimentary record: Geology, v. 40, no. 12, p. 1131-1134.

Slingerland, R., and Smith, N. D., 2004, River avulsions and their deposits: Annual Review of Earth and Planetary Sciences, v. 32, p. 257-285.

Somme, T. O., Helland-Hansen, W., Martinsen, O. J., and Thurmond, J. B., 2009, Relationships between morphological and sedimentological parameters in source-to-sink systems: a basis for predicting semi-quantitative characteristics in subsurface systems: Basin Research, v. 21, no. 4, p. 361-387.

Stouthamer, E., and Berendsen, H. J. A., 2007, Avulsion: The relative roles of autogenic and allogenic processes: Sedimentary Geology, v. 198, no. 3-4, p. 309-325.

Straub, K. M., and Esposito, C. R., 2013, Influence of water and sediment supply on the stratigraphic record of alluvial fans and deltas: Process controls on stratigraphic completeness: Journal of Geophysical Research-Earth Surface, v. 118, no. 2, p. 625-637.

Straub, K. M., and Foreman, B. Z., 2018, Geomorphic stasis and spatiotemporal scales of stratigraphic completeness: Geology, v. 46, no. 4, p. 311-314.

Straub, K. M., Li, Q., and Benson, M., 2015, Influence of sediment cohesion on deltaic shoreline dynamics and bulk sediment retention: A laboratory study: Geophysical Research Letters, v. 42, no. 22, p. 9808-9815.

Straub, K. M., Paola, C., Mohrig, D., Wolinsky, M. A., and George, T., 2009, Compensational Stacking of Channelized Sedimentary Deposits: Journal of Sedimentary Research, v. 79, no. 9-10, p. 673-688.

Straub, K. M., and Wang, Y. A., 2013, Influence of water and sediment supply on the long-term evolution of alluvial fans and deltas: Statistical characterization of basin-filling sedimentation patterns: Journal of Geophysical Research-Earth Surface, v. 118, no. 3, p. 1602-1616.

Strong, N., Sheets, B. A., Hickson, T. A., and Paola, C., A mass-balance framework for quantifying downstream changes in fluvial architecture, *in* Proceedings Fluvial Sedimentology VII2005, Volume 35, International Association of Sedimentologists, Special Publication.

Sun, T., Paola, C., Parker, G., and Meakin, P., 2002, Fluvial fan deltas: Linking channel processes with large-scale morphodynamics: Water Resources Research, v. 38, no. 8, p. 1151.

Syvitski, J. P. M., and Kettner, A., 2011, Sediment flux and the Anthropocene: Philosophical Transactions of the Royal Society a-Mathematical Physical and Engineering Sciences, v. 369, no. 1938, p. 957-975.
Syvitski, J. P. M., and Milliman, J. D., 2007, Geology, geography, and humans battle for dominance over the delivery of fluvial sediment to the coastal ocean: Journal of Geology, v. 115, no. 1, p. 1-19.
Tipper, J. C., 2015, The importance of doing nothing: stasis in sedimentation systems and its stratigraphic effects: Strata and Time: Probing the Gaps in Our Understanding, v. 404, p. 105-122.
-, 2016, Measured rates of sedimentation: What exactly are we estimating, and why?: Sedimentary Geology, v. 339, p. 151-171.
Toby, S. C., Duller, R. A., De Angelis, S., and Straub, K. M., 2019a, A stratigraphic framework for the preservation and shredding of environmental signals: Geophysical Research Letters, v. 46, no. 11, p. 5837-5845.
Toby, S. C., and Straub, K. M., 2019a, TDB_16_1: SEAD.
-, 2019b, TDB_16_2: SEAD.
Toby, S. C., Straub, K. M., Dutt, R., and Akintomide, A., 2019b, TDB_16_3: SEAD.
Tornqvist, T. E., 1994, Middle and Late Holocene Avulsion History of the River Rhine (Rhine-Meuse Delta, Netherlands): Geology, v. 22, no. 8, p. 711-714.
Trampush, S. M., and Hajek, E. A., 2017, Preserving proxy records in dynamic landscapes: Modeling and examples from the Paleocene-Eocene Thermal Maximum: Geology, v. 45, no. 11, p. 967-970.
Trampush, S. M., Hajek, E. A., Straub, K. M., and Chamberlin, E. P., 2017, Identifying autogenic sedimentation in fluvial-deltaic stratigraphy: Evaluating the effect of outcrop-quality data on the compensation statistic: Journal of Geophysical Research-Earth Surface, v. 122, no. 1, p. 91-113.
Trower, E. J., Ganti, V., Fischer, W. W., and Lamb, M. P., 2018, Erosional surfaces in the Upper Cretaceous Castlegate Sandstone (Utah, USA): Sequence boundaries or autogenic scour from backwater hydrodynamics?: Geology, v. 46, no. 8, p. 707-710.
Tucker, G. E., and Slingerland, R., 1997, Drainage basin responses to climate change: Water Resources Research, v. 33, no. 8, p. 2031-2047.
Vail, P. R., Mitchum, R. M., and Thompson III, B. J., 1977, Seismic stratigraphy and global changes of sea level, part 4: global cycles of relative changes of sea-level., *in* Payton, C. E., ed., Seismic Stratigraphy - Application to Hydrocarbon Exploration, Volume 26, Am. Assoc. Petrol. Geol. Mem., p. 83-97.
Van De Wiel, M. J., and Coulthard, T. J., 2010, Self-organized criticality in river basins: Challenging sedimentary records of environmental change: Geology, v. 38, no. 1, p. 87-90.
Van Den Berg Van Saparoea, A. P. H., and Postma, G., 2008, Control of Climate Change on the Yield of River Systems: Recent Advances in Models of Siliciclastic Shallow-Marine Stratigraphy. SEPM Special Publication, v. 90, p. 15-33.
van Dijk, M., Postma, G., and Kleinhans, M. G., 2008, Autogenic cycles of sheet and channelised flow on fluvial fan-deltas: River, Coastal and Estuarine Morphodynamics: Rcem 2007, Vols 1 and 2, p. 823-828.
-, 2009, Autocyclic behaviour of fan deltas: an analogue experimental study: Sedimentology, v. 56, no. 5, p. 1569-1589.
Van Dijk, W. M., Densmore, A. L., Singh, A., Gupta, S., Sinha, R., Mason, P. J., Joshi, S. K., Nayak, N., Kumar, M., Shekhar, S., Kumar, D., and Rai, S. P., 2016, Linking the morphology of fluvial fan systems to aquifer stratigraphy in the Sutlej-Yamuna plain of

northwest India: Journal of Geophysical Research-Earth Surface, v. 121, no. 2, p. 201-222.

van Heijst, M. W. I. M., and Postma, G., 2001, Fluvial response to sea-level changes: a quantitative analogue, experimental approach: Basin Research, v. 13, no. 3, p. 269-292.

Van Wagoner, J. C., Posamentier, H. W., Mitchum, R. M., Vail, P. R., Sarg, J. F., Loutit, T. S., and Hardenbol, J., 1988, An overview of the fundamentals of sequence stratigraphy and key definitions, *in* Wilgus, C. K., Hastings, B. S., Kendall, C. G. S. C., Posamentier, H. W., Ross, C. A., and Van Wagoner, J. C., eds., Sea-Level Changes: an Intergrated Approach, Volume 42, p. 39-45.

Vaughan, S., Bailey, R. J., and Smith, D. G., 2011, Detecting cycles in stratigraphic data: Spectral analysis in the presence of red noise: Paleoceanography, v. 26.

Ventra, D., and Nichols, G. J., 2014, Autogenic dynamics of alluvial fans in endorheic basins: Outcrop examples and stratigraphic significance: Sedimentology, v. 61, no. 3, p. 767-791.

Vincent, S. J., 1993, Fluvial palaeovalleys in mountain belts: an example from the south central Pyrenees [PhD PhD thesis]: University of Liverpool.

von der Heydt, A., Grossmann, S., and Lohse, D., 2003, Response maxima in modulated turbulence. II. Numerical simulations: Physical Review E, v. 68, no. 6, p. 066302.

von Eynatten, H., and Dunkl, I., 2012, Assessing the sediment factory: The role of single grain analysis: Earth-Science Reviews, v. 115, no. 1-2, p. 97-120.

Wang, Y. A., Straub, K. M., and Hajek, E. A., 2011, Scale-dependent compensational stacking: An estimate of autogenic time scales in channelized sedimentary deposits: Geology, v. 39, no. 9, p. 811-814.

Watkins, S. E., Whittaker, A. C., Bell, R. E., McNeill, L. C., Gawthorpe, R. L., Brooke, S. A. S., and Nixon, C. W., 2018, Are landscapes buffered to high-frequency climate change? A comparison of sediment fluxes and depositional volumes in the Corinth Rift, central Greece, over the past 130 k.y.: Geological Society of America Bulletin, v. 131, p. 372-388.

West, A. J., Galy, A., and Bickle, M., 2005, Tectonic and climatic controls on silicate weathering: Earth and Planetary Science Letters, v. 235, no. 1-2, p. 211-228.

Whipple, K. X., Parker, G., Paola, C., and Mohrig, D., 1998, Channel dynamics, sediment transport, and the slope of alluvial fans: Experimental study: Journal of Geology, v. 106, no. 6, p. 677-693.

Whipple, K. X., and Tucker, G. E., 1999, Dynamics of the stream-power river incision model: Implications for height limits of mountain ranges, landscape response timescales, and research needs: Journal of Geophysical Research-Solid Earth, v. 104, no. B8, p. 17661-17674.

-, 2002, Implications of sediment-flux-dependent river incision models for landscape evolution: Journal of Geophysical Research-Solid Earth, v. 107, no. B2.

Whittaker, A. C., Duller, R. A., Springett, J., Smithells, R. A., Whitchurch, A. L., and Allen, P. A., 2011, Decoding downstream trends in stratigraphic grain size as a function of tectonic subsidence and sediment supply: Geological Society of America Bulletin, v. 123, no. 7-8, p. 1363-1382.

Wickert, A. D., Martin, J. M., Tal, M., Kim, W., Sheets, B., and Paola, C., 2013, River channel lateral mobility: metrics, time scales, and controls: Journal of Geophysical Research-Earth Surface, v. 118, no. 2, p. 396-412.

Wilkinson, B. H., McElroy, B. J., Kesler, S. E., Peters, S. E., and Rothman, E. D., 2009, Global geologic maps are tectonic speedometers-Rates of rock cycling from area-age frequencies: Geological Society of America Bulletin, v. 121, no. 5-6, p. 760-779.

Wulf, H., Bookhagen, B., and Scherler, D., 2010, Seasonal precipitation gradients and their impact on fluvial sediment flux in the Northwest Himalaya: Geomorphology, v. 118, no. 1-2, p. 13-21.

Yalin, M. S., 1971, Theory of hydraulic models, London, MacMillan.

Yu, L. Z., Li, Q., and Straub, K. M., 2017, Scaling the Response of Deltas to Relative-Sea-Level Cycles by Autogenic Space and Time Scales: A Laboratory Study: Journal of Sedimentary Research, v. 87, no. 8, p. 817-837.

Zeebe, R. E., Ridgwell, A., and Zachos, J. C., 2016, Anthropogenic carbon release rate unprecedented during the past 66 million years: Nature Geoscience, v. 9, no. 4, p. 325.